UNIVERSITY OF SOUTHAMPTON

FACULTY OF ENGINEERING, SCIENCE & MATHEMATICS

OPTOELECTRONICS RESEARCH CENTRE

Novel Study of Design for Miniature Correlation Spectroscopy Handheld Gas Sensor for Methane (CH_4) Using 2.3 μm Wavelength Band

by

Raja Kamarulzaman Raja Ibrahim

Thesis submitted for the degree of Master of Philosophy

August 2005

DECLARATION OF AUTHORSHIP

I, **Raja Kamarulzaman Raja Ibrahim**,

declare that the thesis entitled

Novel Study of Design for Miniature Correlation Spectroscopy Handheld Gas Sensor for Methane (CH_4) Using 2.3 µm Wavelength Band

and the work presented in it are my own. I confirm that:

- this work was done wholly or mainly while in candidature for a research degree at this University;
- where any part of this thesis has previously been submitted for a degree or any other qualification at this University or any other institution, this has been clearly stated;
- where I have consulted the published work of others, this is always clearly attributed;
- where I have quoted from the work of others, the source is always given. With the exception of such quotations, this thesis is entirely my own work;
- I have acknowledged all main sources of help;
- where the thesis is based on work done by myself jointly with others, I have made clear exactly what was done by others and what I have contributed myself;
- none of this work has been published before submission

Signed: .....

Date: .....

To

Raja Ibrahim Raja Awang

&

Jarah Ishak

UNIVERSITY OF SOUTHAMPTON

ABSTRACT

Faculty of Engineering, Science and Mathematics

Optoelectronics Research Centre

Master of Philosophy

Novel Study of Design for Miniature Correlation Spectroscopy Handheld Gas Sensor for Methane (CH_4) Using 2.3 μm Wavelength Band

by Raja Kamarulzaman Raja Ibrahim

A highly selective methane gas sensor, using the correlation spectroscopy technique, has been constructed. This sensor is handheld and has a compact folded cell arrangement; it operates with 2.3 μm switched LED sources. The selected methane absorption band at 2.3 μm is relatively strong, even over a short path length (10 cm), yet this wavelength still allows the use of commercial glass lenses and optical windows, a simple 45° silicon wafer slice as a beam splitter and low noise InGaAs detectors. A noise-limited detection sensitivity of 0.21% by volume with a measurement time constant of 0.1 s was achieved.

CONTENTS

LIST OF FIGURES

LIST OF TABLES

ACKNOWLEDGMENTS

This page is dedicated to the numerous individuals who assisted me with my research and in completing this thesis. In particular, I am deeply indebted to Professor J. P. Dakin for the opportunity to be involved in his research group. His guidance and patience has been paramount. I am also greatly appreciative of Dr. Ed Austin and Dr. Paul Chambers for their generous technical support, fruitful discussions and constructive criticisms. I thank my colleagues Mr. Everado Vargas-Rodriguez, Mr. Faisal Rafiq Mahamd Adikan, Dr. Mohd. Ridzuan Mokhtar, Mr. Rodrigo Amezcua, and Dr. Stuart Russell for their part. A special thanks to Dr. Eleanor Tarbox for her enormous help, advice and constructive comments regarding this thesis. I am also indebted to Mrs. Eve Smith, Mrs. Janet Mansour, Mrs. Jane Britt and Mrs. Wendy White for their friendly and efficient administrative support throughout my study. I humbly acknowledge the significant help provided by Professor Harvey Rutt and Professor Peter Smith. Not to forget, everybody within the Optoelectronics Research Centre who has helped me with my study - directly or indirectly. Thanks also to my housemates Maria Susana Avila Garcia, Andriy Kharechko and Jorge Sanchez, my fellow UTM colleagues and the whole Malaysian community for making my stay in Southampton a memorable one. I acknowledge the support of UTM for their studentship and for granting my study leave. Last but not least, my utmost gratitude to my parents and all my siblings for their love and support.

ABBREVIATIONS

AC	Alternating current
cm	centimetre
cm^{-1}	Wavenumber
CoSM	Complementary source modulation
CoSp	Correlation spectroscopy
dB	Decibel
DC	Direct current
DNA	Deoxyribonucleic acid
FWHM	Full width at half maximum
HITRAN	High-resolution transmission molecular absorption
Hz	Hertz
IDHL	Immediately dangerous for health of life
LED	Light emitting diode
LEL	Lower explosive limit
m	modulation index
mbar	millibar
ml	millilitre
mm	millimetre
MMF	Multimode fibre
NIR	Near-infrared
PBFs	Photonic band gap fibres

PC	Personal computer
ppm	parts per million
SNR	Signal-to-noise ratio
UV	Ultraviolet
VIS	Visible
vol	volume
μm	Micrometer

CHAPTER 1
INTRODUCTION

1.1 TALKING WITH LIGHT

The creation of light is one of the wonderful and fascinating 'gifts' from our Creator. It not only gives brightness to human life, but has also created a great revolution in telecommunication's technology, as well as scientific applications. The use of light as a sensing means opens many new dimensions for applications such as medical diagnosis, surgery, military, industry, biotechnology, DNA and tissue cell characterization. Gas sensing is one of the fields that has benefited and this is the subject of this thesis.

1.2 GAS SENSOR

In an industrial setting, the detection of potentially explosive, flammable, or toxic gases is a moral, and often legal, requirement to help protect personnel and equipment from an unpredictable event. Even in the case of inert gases, safety aspects are important due to a lack of awareness about the possible dangers of asphyxiation. The presence of nitrogen which is a non-toxic, non-explosive and non-flammable gas, for example in a closed space, is still dangerous because it will reduce the level of oxygen, resulting in suffocation and possible death. In another example, even oxygen, the gas which supports life, can be hazardous as the enhancement of oxygen can dramatically increase flammability. Obviously, safety is a crucial key in the development of a gas sensor.

In the last few decades, pellistor-based detectors and flame ionisation detectors were widely used to measure gas concentration. These technologies expressed the concentration of gas in either parts per million (ppm) by volume, as a percentage of the

lower explosion limit (LEL) of the gas mixture, or % volume. Sensitivity is a parameter which is often used to describe the performance of a gas sensor and is expressed in both ppm and LEL units. A pellistor-based sensor uses techniques which operate by oxidising the gas mixture on a heated catalyst bead and can be used in both the LEL and ppm ranges. Flame ionisation sensors are based on directly burning the gas sample in a hydrogen flame. Basically, both sensors show a high sensitivity and, for example, the flame ionisation technique can detect natural gas at concentrations as low as a few ppm.

Besides sensitivity, selectivity is another term which is often used in describing the performance of gas sensors. In general, a good sensor should show a high selectivity in detecting only the gas of interest. Cross-sensitivity is a parameter used to measure the presence of other contaminant gases which might perturb the actual gas measurement. This perturbation will affect the reliability of the gas measurement as the actual measurement needs to consider an error in a particular range in that measurement. Basically, the ability of a kind of gas sensor to measure cross-sensitivity means that the sensor is susceptible to the contaminant gases and this affects the reliability of that sensor. A significant disadvantage of pellistor and electrochemical sensors is that they show fairly poor selectivity for the gas of interest.

Recently, an interest in optical based sensors has become more significant, benefiting from the boost in photonic technology. The development of advanced optical sources and optical detectors gives a bright future for the gas sensor based on optical techniques. One optical technique is also known as molecular spectroscopy as this is the basis of an optical technique where some kind of interaction process occurs between light radiation and matter. Basically, there are two optical processes in that interaction which are scattering and absorption processes. The latter is more important because the gas absorption spectrum has unique or specific characteristics, thus it gives a 'finger print' for detection of the gas of interest.

The absorption spectroscopic technique is also known as infrared spectroscopy due to the fact that many of the common industrial and pollutant gases possess an absorption spectrum within the range of the infrared region. This technique has numerous advantages such as long term stability, it can be designed as a self referencing system,

and it is immune to electromagnetic interference and is able to be used in monitoring systems when the gas sensor is associated with optical fibres particularly in environmental pollution evaluation. It is a low power technique and, unlike the pellistor, it cannot be poisoned. In recent years, there has been an increase in the interest of the infrared optical gas sensor because this technique is able to measure the cross-sensitivity of the contaminant gases.

Previously, we discussed about the possibility of contaminant gases influencing the gas measurement, in the case where the gas sensor is able to give a cross-sensitivity measurement. Actually, in some cases the ability of a gas sensor to measure the cross-sensitivity is an advantage, depending upon the type of gases to be detected. The measurement of toxic gases for example, often uses electrochemical methods which offer a method with poor selectivity for the target gas, but with sensitivity in the lower ppm range. Fortunately, cross-sensitivity is often less importance when using this method. However, when dealing with the presence of explosive and flammable gases in a given environment, the cross-sensitivity measurement is able to give an initial warning about the possibility of other gases being present instead of only the gas of interest.

However, of course, the cross-sensitivity measurement should not give a significant influence on the measurement of the actual gas of interest. This is only a minor problem to the optical technique method as, by using a different approach and sensing technique, and compromising between a few parameters the selectivity and also the sensitivity of the measurement can be tailored depending on the requirements of the measurement.

1.3 AIM OF RESEARCH

In the research and development of devices or instruments for gas sensing the reliability and accuracy of those systems is very important. At this stage, scientific measurement data obtained from laboratory work is usually satisfactory, but insufficiently robust selectivity and sensitivity of any chemical sensor technologies, after miniaturization, is a common limitation that is faced by any practical instrumentation system.

The greatest challenges are to re-engineer experimental apparatus to be more compact and inexpensive but still retain a sufficiently good measurement performance. In the gas sensor, miniaturization often causes problems such as an increase in the presence of noise in the measurement. The need for a long optical path length to achieve sufficient sensitivity of measurement is the main practical problem when producing a handheld gas sensor. This requirement can be compromised by designing an optical system working at the fundamental absorption of the gas of interest or at a stronger absorption band and also by using a suitable technique.

The first aim of the work presented in this thesis is to evaluate the most convenient methane absorption band as we need a stronger absorption band and, at the same time, a practical band in terms of the availability of the optical components to construct the optical system working in that region with sufficient optical transmission. This is important as the sensor sensitivity can be increased by working at a strong absorption band.

The second aim of this work is to design a miniature of the correlation spectroscopy based sensor to be more compact, at a reasonable cost, while still able to give a highly selective technique and appreciable sensitivity in detecting methane gas. To realize this, a simple optical system to operate with correlation spectroscopy is designed. The simple optical system is considered as a more complicated design will result in increasing the number of optical components, thus increasing the cost of the sensor. Then, data from the HITRAN database [1] is used to build a theoretical model for predicting the sensor performance. Finally, the performance of the gas sensor is evaluated to calculate the sensitivity and the selectivity of that sensor.

1.4 ORGANISATION OF THESIS

The project effectively had two aims; the study of design for a miniature correlation spectroscopy handheld gas sensor for methane and analysis of the most convenient of the methane absorption bands to obtain a highly selective gas sensor with an appreciable sensitivity at reasonable cost. As such, the following chapters will discuss about the

theoretical aspects of a gas and the aspects associated with the handheld gas sensor design.

Chapter 2 briefly discusses the theoretical aspects of the gas absorption spectrum. The aim of this chapter is to describe the characteristics of the gas absorption shape which gives the uniqueness or 'finger print' and can be used to identify a particular gas species. The gas spectrum characteristics are important to understand as they will influence the selection of the optical components which will be used to construct an optical absorption sensor.

Chapter 3 gives the overall idea and important concepts needed to construct a handheld sensor design based on an optical absorption process. This is described by the Beer-Lambert's law. Then, the basic requirements of the gas sensor performance are given as: - fast response, high selectivity and sensitivity. This is followed by the discussion on the issues to improve the sensor performance. This chapter also reviews the previous work and discusses the two main techniques in the optical absorption based sensor which are laser spectroscopy and the use of a broadband light source in the correlation spectroscopy technique.

The correlation spectroscopy, as introduced in Chapter 3, is discussed in detail in Chapter 4. Firstly, the basic principles of the correlation spectroscopy technique are discussed. Then, the matched optical filter is used to illustrate correlation spectroscopy as a highly selective technique. This is followed by the illustration of the schematic diagram of the correlation spectroscopy system. From that diagram the received signal in the detection system is graphically described. From that, the theoretical formula of the sensor response is derived by using a numerical analysis technique.

In Chapter 5, the basic idea of the optical design is briefly discussed. Then, our basic idea of the miniaturization correlation spectroscopy handheld sensor is presented. This is followed by a deeper discussion on the absorption band of methane. The discussion is focussed on the selection of the most convenient methane absorption band and the issues associated with that selection such as the practical limitation to construct an optical system working in the mid-infrared region. The selection of the absorption band of

methane is important as the selected band will determine the wavelength region of the optical system which needs to be designed. Then, the selection of the suitable optical components to work in the selected absorption band will be discussed. Finally, the design of our correlation spectroscopy handheld methane gas sensor is presented in detail and the principles of the operation of our sensor are described.

Chapter 6 is about the evaluation of the optical system performance before the sensor can be used to measure methane gas. The first evaluation is on the polarization and multiple reflections effect on the correlation spectroscopy system and their effects on the sensor response. The second evaluation is made on the optical transmission performance. It is carried out to evaluate the transmission performance of the light beam in the optical system, as a sufficient level of light transmission can influence the performance of the sensor measurement.

In Chapter 7 the experimental setup of the sensing system is presented to describe the process of the experiments that will be carried out. Then, a theoretical model to predict the sensor response is constructed and the results from theoretical calculations are plotted into a graph to describe the relation between the sensor response and the concentration of the methane sample. Then, the results from experiments are presented and the comparison between both results will be discussed, covering the performance of the sensor, the selectivity and its sensitivity.

The thesis is concluded in Chapter 8, summarising the theoretical model and the improvement of the sensor to obtain better performance. A few possible studies of the theoretical model and the correlation spectroscopy handheld sensor design are suggested as possible future developments for the project.

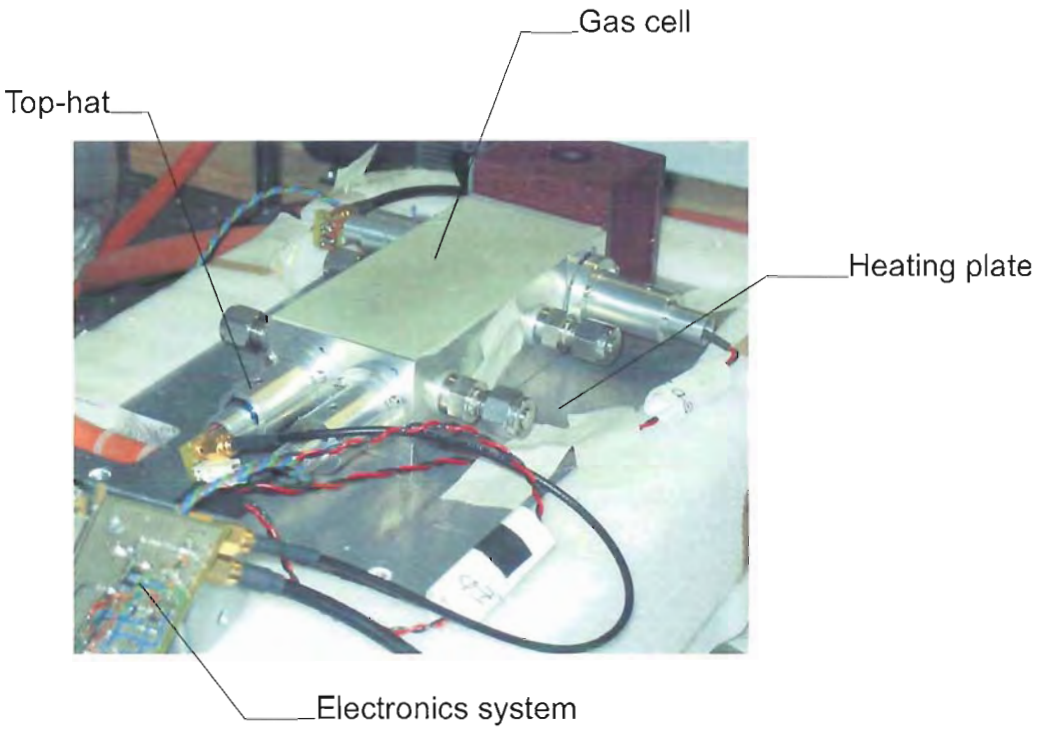

FIGURE 1.1: The prototype of the correlation spectroscopy handheld sensor.

CHAPTER 2
THEORETICAL ASPECTS OF GASEOUS ABSORPTION SPECTRA

2.1 INTRODUCTION

In this chapter, the basic theory of gaseous absorption spectra, which covers the interaction between electromagnetic radiation and matter, will be discussed. The interaction between electromagnetic radiation and matter can only take place under certain circumstances (allowed transition). These interactions must arise from, or produce, respectively, some electromagnetic effect in order to be able to observe an emission or an absorption spectrum [2]. There are some mechanisms that result from the changes of a nuclear, molecular, or electronic configuration and these changes are influenced by the electric or magnetic fields of the light radiation.

2.2 THE INTERACTION OF ELECTROMAGNETIC RADIATION WITH GAS

Many molecules have their fundamental absorption bands in the mid-infrared region between 2.5 μm – 25μm and the visible-to-UV range (0.7 μm – 0.25μm) [3]. Absorption in these regions is produced by vibrational-rotational energy transition levels in the gas molecules [2]. The absorption spectrum produced has a set of rotational absorption lines, which form a band structure known as an absorption band. The absorption band is uniquely characterized [2] while the absorption features such as line position, line strength and the band intensity are molecule specific. To understand the complexity of the gas absorption spectrum, the study of the vibrating and rotating molecule becomes

important. The well-known Schrödinger equation is used to solve the rotational and vibrational energy levels and selection rules of the gas molecules [4].

The following section heavily borrows from the references listed below. A theoretical knowledge on interaction between molecular gas and light radiation is pertinent in optical gas sensing technique. A few text books which are 'Fundamentals of molecular spectroscopy' by C.N. Banwell et al., 'Modern spectroscopy' by J.M Hollas, 'Molecular spectra and molecular structure' by G. Herzberg, 'Introduction to molecular spectroscopy' by G.M Barrow, and 'Air monitoring by spectroscopic techniques' edited by M.W Sigist have been referred to in order to discuss the theoretical aspects of interaction between light radiation and gas in this chapter.

2.3 THE VIBRATING MOLECULE

The discussion of the vibrating molecules is based on the appearance of elasticity characteristics of the molecular bond. This characteristic concerns the fact that atoms in a molecule vibrate about some mean position. This vibration can be treated by using the simple harmonic oscillator and an anharmonic oscillator model.

2.3.1 THE SIMPLE HARMONIC OSCILLATOR

The solution of the Schrödinger equation for a one-dimensional harmonic oscillator dictates that the allowed transition vibrational energy E_v of the gas molecules is given by [5]:-

$$E_\upsilon = h\omega\left(\upsilon + \frac{1}{2}\right) \text{Joules} \qquad (2.1)$$

where h is Planck's constant, ν is the vibrational quantum number, and ω refers to the classical vibration frequency. This classical vibration frequency is given as:-

$$\omega = \frac{1}{2\pi}\left(\frac{k}{\mu}\right)^{\frac{1}{2}} \text{ Hz} \tag{2.2}$$

Equations (2.1) and (2.2) show that the vibrational energy transition is in turn proportional to the frequency of vibration and this frequency is in turn proportional to the force constant k and inversely proportional to the reduced mass μ of the molecule. The unique characteristics of k and μ for a particular molecule give the specific value of the vibrational energy level for that molecule.

Equation (2.1) expressed the vibrational energy in units of Joules. This equation can be more simply expressed in wavenumbers as:-

$$\nu_\upsilon = \frac{E_\upsilon}{hc} = \left(\upsilon + \frac{1}{2}\right)\varpi \text{ cm}^{-1} \tag{2.3}$$

where ϖ is the expression for oscillation frequency in units cm^{-1}.

The solution of the Schrödinger equation for the simple harmonic oscillator also gives the selection rule for the vibrational transition which gives the transitions of the energy levels that can only take place as [5]:-

$$\Delta\upsilon = \pm 1$$

By applying the selection rule for two neighbouring energy levels, the separation between two energy levels can be obtained and it is given by:-

$$\nu_{\upsilon+1\to\upsilon} = \left(\upsilon+1+\frac{1}{2}\right)\varpi - \left(\upsilon+\frac{1}{2}\right)\varpi = \varpi \text{ cm}^{-1} \tag{2.4}$$

Equation (2.4) shows that the separation energy between two neighbouring levels is equal to ϖ. However, in the real measurement, it is found that many gases do not show that equal energy separation pattern in their bands.

2.3.2 THE ANHARMONIC OSCILLATOR

The molecular bond is not perfectly elastic, particularly at the higher ν, due to the fact that at some point of vibration, the bond may be dissociated. The force constant becomes weaker as ν increases and the vibrational energies become closer. Equation (2.3) needs to be modified to consider the anharmonicity effect in the molecular vibration. This correction is given as [5]:-

$$\nu_{\nu} = \left(\upsilon+\frac{1}{2}\right)\varpi_e - \left(\upsilon+\frac{1}{2}\right)^2 \varpi_e\chi_e \text{ cm}^{-1} \tag{2.6}$$

where ϖ_e is an equilibrium oscillation frequency of the anharmonic system and χ_e is the corresponding anharmonicity constant. The correction part of Equation (2.6) shows that the separation of vibrational energy levels at higher ν becomes closer. Equation (2.6) can be re-written to be simpler as:-

$$\nu_v = \varpi_e \left\{1 - \chi_e \left(\upsilon + \frac{1}{2}\right)\right\}\left(\upsilon + \frac{1}{2}\right) \text{ cm}^{-1} \qquad (2.7)$$

The selection rules of the anharmonicity oscillator are similar to the harmonic oscillator but with the additional possibility of larger transitions. This gives the selection rules for the anharmonic oscillator to be [5]:-

$$\Delta\upsilon = \pm 1, \pm 2, \pm 3 \ldots$$

Commonly, only the lines of $\Delta\upsilon = \pm 1, \pm 2, \pm 3 \ldots$ are considered to have an observable intensity at room temperature (20°C). The transition at $\nu = 1$ or 2 or 3... to higher levels can be neglected because of the fact that the initial population at $\nu = 1$ is only 0.01 percent of the ground state [6].

2.3.3 The Fundamental, Overtone, Combination, and Hot Bands Absorption

The classification of the band absorption is divided into a few categories depending on the origin of that absorption band. These are the fundamental, overtone, combination, and the hot bands. Fundamental absorption refers to the absorption band arising from the transitions $\nu = 0$ to $\nu = 1$. Overtones band refers to the larger jump of energy transitions ($\nu = 0$ to $\nu = 2$, $\upsilon = 0$ to $\nu = 3 \ldots$) which arises at frequencies near $2\nu_1$, $3\nu_1 \ldots$, $2\nu_2$, and $3\nu_2 \ldots$ $2\nu_3$.....and etc. where ν_i is the fundamental mode. A combination band (or difference band) arises when one photon excites two different vibrations simultaneously. The photon which causes this transition has a frequency approximately equal to the sum (or the difference) of the two frequencies (or more) needed to excite the two vibrations

separately. The sum of those frequencies can be the addition of two or more fundamental frequencies or overtones, for example $v_1 + v_4$, $2v_3 + v_2$, and etc. A hot band refers to a band arising from the transition $v = 1$ to the higher levels. Although, as mentioned in the section 2.3.2, the transition from $v = 1$ to the higher levels is neglected, according to the Boltzmann distribution at high temperatures the population at $v = 1$ will increase. This gives the probability that the spectrum can be observed, as temperature increases its absorption intensity.

2.4 THE ROTATING GAS MOLECULE

The discussion of the rotating molecule can be introduced by using a simple system of linear molecular theory. This theory can be applied to the linear polyatomic molecules [7]. There are two models that can be used to describe the rotational energy levels of the rotating molecule; the rigid rotor and the non-rigid rotor approximation.

2.4.1 THE RIGID ROTOR APPROXIMATION

The rigid rotor model, which was introduced previously in section 2.4, assumes that the bond joining the nuclei is a rigid weightless rod. The Schrödinger solution for that model then gives the rotational energy level allowed for its rotating molecule as [8]:-

$$E_r = \frac{h^2}{8\pi^2 I} J(J+1) \text{ Joules} \qquad (2.8)$$

This equation expresses the energy in Joules. For practical reasons, the electromagnetic spectrum is often measured in terms of frequency (Hz) or in the form of wave-number (cm^{-1}), thus equation (2.8) can be re-written as:-

$$\nu_J = \frac{h}{8\pi^2 Ic} J(J+1) \text{ cm}^{-1} \tag{2.9}$$

where c is the velocity of light, J rotational quantum number, h is the Planck's constant, and I refers to the moment of inertia of the rotating molecule. The constant part, $h/8\pi^2Ic$, can be reduced to be a single parameter B and it is known as the rotational constant for the particular molecule and is given as:-

$$B = \frac{h}{8\pi^2 Ic} \tag{2.10}$$

For the diatomic molecule, the moment of inertia is expressed as I_B which refers to the moment of inertia about an axis perpendicular to the internuclear axis and going through the centre of mass. It is given as [8]:-

$$I_B = \mu r^2 \tag{2.11}$$

where μ is the reduced mass and given as m_1m_2/m_1+m_2. Substituting (2.10) into (2.9), the energy level for a rigid rotor can be expressed by:-

$$\nu_J = BJ(J+1) \text{cm}^{-1} \tag{2.12}$$

There are some conditions that need to be fulfilled in order for the absorption spectrum to be observed from the rotating molecules. The first one, which was discussed in

section 2.1, where the periodically permanent dipole moment changes in response to the electromagnetic radiation that can be interacted with the matter. The second one is where each transition of the rotational energy is restricted under the selection rule in which only changes of J by one unit are allowed. This is given as [8];

$$\Delta J = \pm 1$$

Using the expression for the energy levels given in (2.12) and taking the selection rule $\Delta J = \pm 1$, and neglecting the presence of a magnetic field, the frequencies of the rotational transitions are given by [8];

$$\nu_{J \to J+1} = B(J+1)(J+2) - BJ(J+1) = 2B(J+1)\,\mathrm{cm}^{-1} \qquad (2.13)$$

Since J can take a value of 0, 1, 2, 3... the associated energy of a given J is equal to $\pm 2B$, $\pm 4B$, $\pm 6B$, $\pm 8B$... respectively. Therefore, the absorption spectrum will have a set of equally spaced rotational lines [8] as shown in the Figure 2.1.

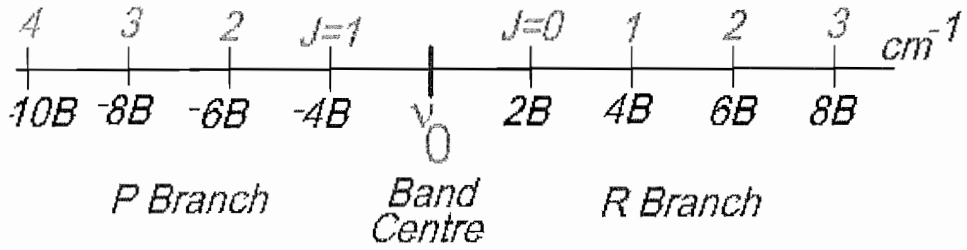

FIGURE 2.1: The rotational-vibrational spectrum of a diatomic molecule illustrates that all the rotational lines are observed at equally spaced intervals with a separation transition energy equal to 2B.

In this figure, the lower frequencies side is indicated as the *P* branch and the higher side is expressed as the *R* branch. For example, this pattern can be found in the few rotational lines of carbon monoxide, CO, as shown in the Figure 2.2.

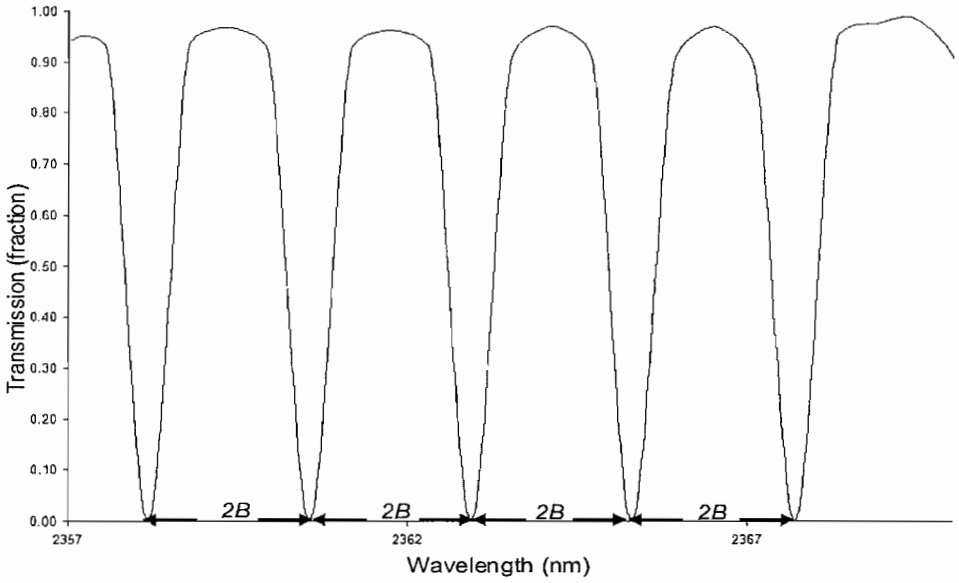

FIGURE 2.2: A section of the rotational-vibrational spectrum of a carbon monoxide molecule (CO) and the observed equally spaced rotational transitions with separation equal to *2B*. This graph is obtained by using HITRAN 2000 for 50% CO concentration with a path length of 1 m, at 1.013 bar and 296 K.

2.4.2 THE NON-RIGID ROTOR

The rotational energy separation for each transition is found to be not equally spaced, but it becomes closer as the J number increases. This pattern can be observed in the numerous gas spectra such as hydrogen fluoride (see Figure 2.3). Therefore, the separation rotational energy level which has been predicted as *2B* in the previous section is no longer true and some modifications to equation (2.12) are required. The non-rigid rotator is a better model which can be used to explain this phenomenon.

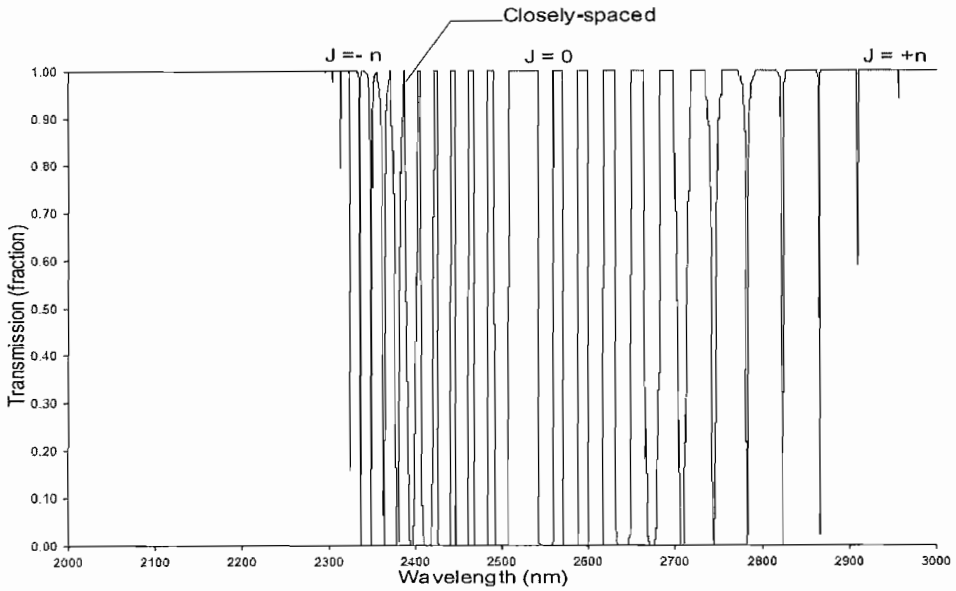

FIGURE 2.3: The graph shows an absorption spectrum of HF at the 2.55 μm band. The P branch of this spectrum shows non-equalized rotational lines; instead they become closer together at high J level. This graph is obtained by using HITRAN 2000 for 100% of HF concentration with a path length of 1 m, at 1.013 bar and 296 K.

The non-rigid rotator can be illustrated as a diatomic molecule with its nuclei connected by a spring. As with a metal spring, the bond of a molecule can be compressed or stretched periodically, thus producing vibrational energy with a particular fundamental frequency dependent upon the masses of the atoms and the elasticity force k of the bond. Apparently, the bond of the molecule is not rigid but appears to have an elastic character which has an effect on the value of B as J is increased.

It is found that, as the speed of rotation increases, J increases, more quickly as the diatomic molecule rotates. It produces a greater centrifugal force which tends to move the atoms apart. This means that as the spring is stretched the bond of the molecule will expand its length. By using equation (2.11), an increment in the molecular bond length

will result in a greater value of I_B and, from (2.10), it is clear that B is proportional to $1/I_B$. Therefore, decrements in B will decrease the separation of the rotational energy level.

Due to the apparent elasticity, equation (2.12) can be slightly modified to consider the effect of centrifugal force, giving [8]:-

$$\nu_J = BJ(J+1) - DJ^2(J+1)^2 \text{ cm}^{-1} \tag{2.14}$$

where D is centrifugal distortion and it is expressed as;

$$D = \frac{4B^3}{\omega^2} \tag{2.15}$$

Therefore, the rotational transitions for the non-rigid rotor, which are given in equation (2.15), can be modified to be:-

$$\nu_{J\to J+1} = 2B(J+1) - D[(J+1)^2(J+2)^2 - J^2(J+1)^2] \text{ cm}^{-1} \tag{2.16}$$

or can be reduced as:-

$$\nu_{J\to J+1} = 2B(J+1) - DJ^2(J+1)^2 \text{ cm}^{-1} \tag{2.17}$$

Data from experimental studies shows that the value of B is of the order 10 cm^{-1} and the value of D of the order 10^{-3} cm^{-1}[9]. Equation (2.17) is only applied to a simple harmonic force field. Actually, in most of the cases a few more spectroscopic constants are required to predict correctly the allowed rotational transitions and it is given as [8]:-

$$\nu_J = BJ(J+1) - DJ^2(J+1)^2 + HJ^3(J+1)^3 + KJ^4(J+1)^4 + .. \text{cm}^{-1} \qquad (2.16)$$

here H, K... are very small constants which are dependent upon the geometry of the specific molecule .

2.5 THE VIBRATIONAL - ROTATIONAL SPECTRUM

The gas spectrum that appears in the infrared region has a complex band because of the presence of the rotational lines associated with its vibrational band. According to the Born-Oppenheimer approximation [10], for the diatomic molecules the rotational-vibrational energy ν_{total} is given as the sum of the separate energies:-

$$\nu_{total} = \nu_{rotational} + \nu_{vibrational} \text{ cm}^{-1} \qquad (2.17)$$

By substituting Equation (2.7) and (2.12) into (2.17), the ν_{total} can be expressed as:-

$$\nu_{total} = BJ(J+1) + \varpi_e \left\{1 - \chi_e\left(\upsilon + \frac{1}{2}\right)\right\}\left(\upsilon + \frac{1}{2}\right) \text{ cm}^{-1} \qquad (2.18)$$

The selection rules for the combined motions; rotational-vibrational are the same as those for each separately and given as:-

$$\Delta J = \pm 1, \quad \Delta\upsilon = \pm 1, \pm 2, \pm 3.$$

The separation of the two neighbouring levels can be illustrated by applying the selection rules to the energy levels in Equation (2.18), for example the transition $\nu = 0$ to $\nu = 1$ is found to be [5]:-

$$\Delta\nu_{J,\upsilon} = \varpi_0 + B(J' - J'')(J' + J'' + 1) \text{ cm}^{-1} \qquad (2.19)$$

where ϖ_0 is the brevity of $\varpi(1 - 2\chi_e)$, J' and J'' are the rotational at upper and lower level, respectively. Equation (2.19) can be separated into two parts as the selection rules for the rotational have a $\Delta J+$ and $\Delta J-$:-

$$\text{For } \Delta J = +1,\ \Delta\nu_{J,\upsilon} = \varpi_0 + 2B(J'' + 1) \text{ cm}^{-1}, \quad J'' = 0,1,2... \qquad (2.20)$$

$$\text{For } \Delta J = -1,\ \Delta\nu_{J,\upsilon} = \varpi_0 - 2B(J' + 1) \text{ cm}^{-1}, \quad J' = 0,1,2... \qquad (2.21)$$

where ϖ is the band centre [11]. Both equations can be combined to be a simpler form as [5]:-

$$\Delta\nu_{J,\upsilon} = \varpi_0 + 2Bm \text{ cm}^{-1}, \quad m = \pm1,\pm2... \tag{2.22}$$

where m is $(J' + 1)$ or $(J'' + 1)$. In Equation (2.22), as $m \neq 0$ the line at ϖ_0 $(\Delta J = 0)$ does not appear and is known as the Q branch [11]. Due to $m = \pm1, \pm2...$the lines will arise at equally spaced intervals for both increasing and decreasing frequencies. The lines arising at the low frequencies, corresponding to m negative, are known as P branch whereas at the high frequencies side (m positive) is known as R branch. The other branches that can be observed are where the ΔJ can be ±2 and so on.

In Equation (2.22) the effect of centrifugal distortion D is neglected as it is considered that its contribution is very small compared with B. However, the anharmonicity factor needs to be considered as this constant is important to explain the occurrences of the overtones by extending the selection rules of $\Delta\upsilon = \pm2, \pm3$ and also to explain the appearance of an overtones band having an identical rotational structure.

2.6 ROTATIONAL LINES INTENSITIES

Previously, the discussion about the selection rule rotational energy transitions is given by $\Delta J = \pm1$. In that sense, the allowed transition will be $J = 0$ to $J = 1$, J = 1 to $J = 2$, and so on. Theoretically, there is no limit to the numbers of J but of course at some degree of the rotating velocity, the molecular bond will split apart. Every transition produces the rotational lines which have a form of nearly equally spaced structure with each other. However, all the rotational lines appear different in their intensity strength.

The strength of the line intensity is proportional to the initial numbers of the molecules in each level. At each level, the number of molecules depends on two factors. The first one is the Boltzmann distribution and the second factor is the possibility of degeneracy to occur in each energy level. The Boltzmann distribution gives the population at a particular energy level as [5]:-

$$\frac{n_J}{n_0} = \exp\left(-\frac{BhcJ(J+1)}{kT}\right) \tag{2.23}$$

where k is the Bolztmann's constant, h is Planck's constant, T is temperature in Kelvin, n_J and n_0 are the numbers of the molecular populations at the initial level and the upper level, respectively. From this equation, the calculation shows that n_J/n_0 decreases as J increases.

The strength of the rotational lines' intensity increases with J until a maximum value and then diminishes. The lines' intensity pattern can be expressed mathematically as [5]:-

$$\frac{n_J}{n_0} = (2J+1)\exp\left(-\frac{BhcJ(J+1)}{kT}\right) \tag{2.24}$$

The presence of $(2J+1)$ in this equation is due to the degeneracy, as mentioned previously. By integration of equation (2.24), it is can be found that the most intense line occurs at the nearest J given by:-

$$J_{\max} = \sqrt{\frac{kT}{2hcB}} - \frac{1}{2} \tag{2.25}$$

whereas the lower and higher J have relatively weaker line intensities. Figure 2.4 illustrates the band strength as a function of J.

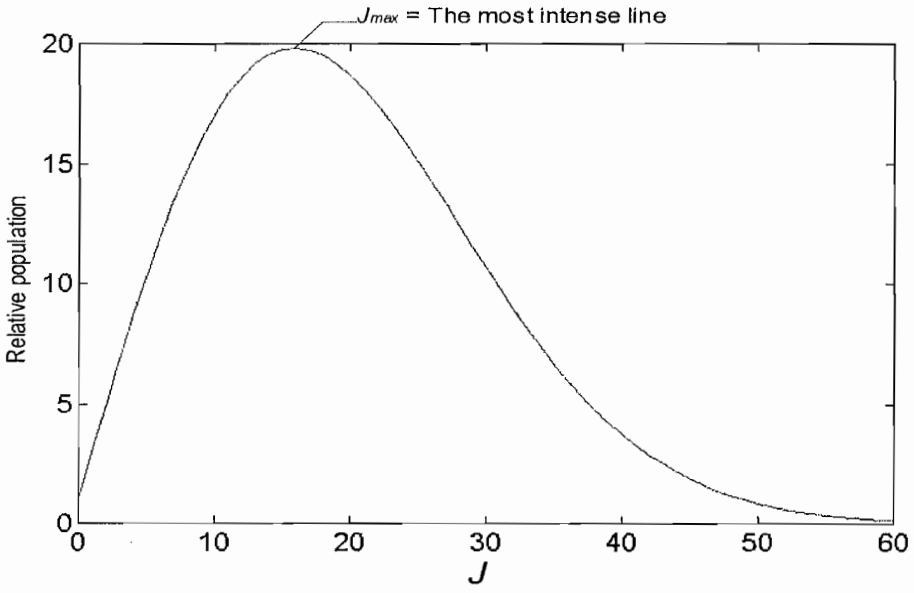

FIGURE 2.4: Relative population of rotational energy levels for a linear molecule. The most intense rotational line is indicated as J_{max}.

2.7 METHANE SPECTRUM

The characteristics of the gas spectrum which were discussed previously are not completely useful to explain the characteristics of methane. Methane is classified as a

spherical top molecule which has all three principal moments of inertia equal [12], $I_A = I_B = I_C$. This means that methane will have three species of degenerate vibrational levels which are indicated as A_1, E, and F_2 [13] as shown in Figure 2.5.

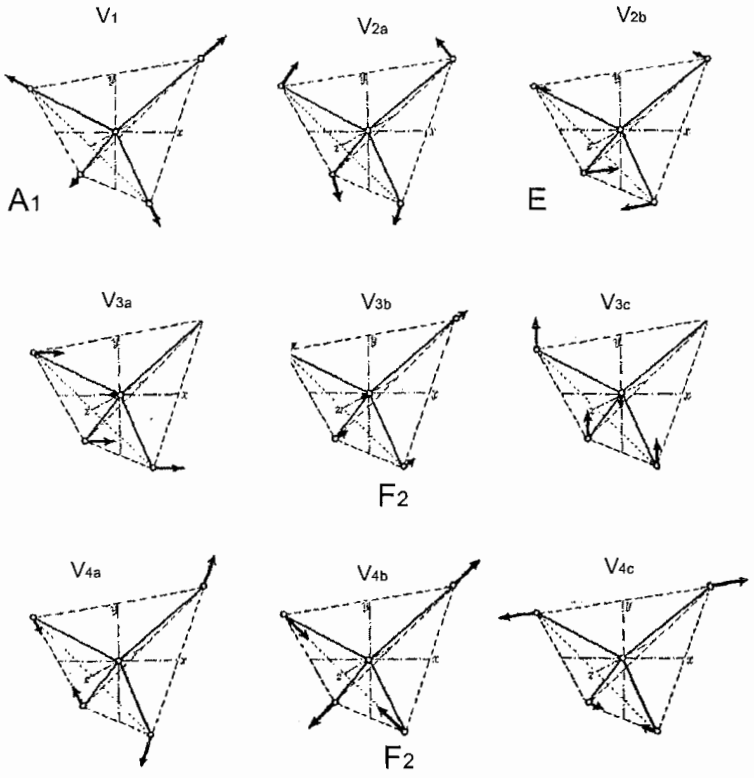

FIGURE 2.5: Three degenerate species of methane are indicated as A_1, E, and F_2.

SOURCE: Herzberg, G. (1966). *Molecular Spectra and Molecular Structure*, D. Van Nostrand Company, Inc., Princeton, pp. 100.

The existance of triply degenerate vibrational levels of methane will allow the perturbation of coriolis to occur [14]. Then, the effect of the coriolis coupling between rotation and vibration in the upper degenerate vibrational level [15] will change the band spacing of methane. In other words, the spacing of every methane band does not

appear in a particular spacing as predicted by Equation (2.4). The absorption bands of methane will be discussed in more detail in Chapter 5 (section 5.5.1).

2.8 CONCLUSION

The theoretical aspects of the gas spectrum are presented and there gave an overview of the real observable gas spectrum. There are a few important pieces of information that can be extracted from the characteristics of the observable gas spectrum. These are:-

1. The simultaneous motions of the rotational-vibrational produced a complex gas spectrum which for every vibrational band, has associated simultaneously rotational lines. These rotational lines formed an absorption band in which the band centre is given by the vibrational transition.

2. The absorption band of gas formed a 'wing' shape due to the rotational lines appearing at different intensity strengths.

3. The occurrences of a lot of gas absorption bands for a certain gas are due to the appearances of the overtones, combination bands, as well as hot bands.

4. The fundamental band has stronger absorption intensity than the overtones, combination bands, and the hot bands.

5. Methane shows different characteristics in its absorption spectrum which is caused by the effect of coriolis perturbation in its upper degenerate vibrational level.

Familiarity with the gas absorption band characteristics is important to better understand the concept of gas sensor based on an optical absorption spectroscopy which will be discussed in the following chapter.

CHAPTER 3

BASIC DESIGN ASPECTS OF PROPOSED ABSORPTION GAS SENSOR

3.1 INTRODUCTION

In this chapter the desired design features of the gas sensor will be introduced. The Beer-Lambert's law will be discussed as the fundamental explanation of the optical absorption processes. Then, a few issues concerning the effect of miniaturizing the gas sensors, based on optical absorption, on the detection sensitivity and the approach to improve the detection sensitivity will be reviewed.

The implementation of the optical absorption method in the gas sensors will be discussed, which covers the use of laser spectroscopy as a selective technique and the poor selectivity performance of the sensing system based on the use of a broadband source will be briefly discussed. Finally, the complementary source modulation (CoSM), which is a variant of the correlation spectroscopy (CoSp) technique, will be discussed as a highly selective technique with the ability to offer an appreciable sensitivity even when the broadband source is employed.

3.2 THE FIGURES OF MERIT OF THE GAS SENSORS

Safety aspects become an important key in developing a gas sensor as the presence of many industrial and pollution gas species, even at a lower concentration, can be classified as hazardous. Therefore, it is important to design and develop such a sensor with the ability to give a rapid response with a high sensitivity and selectivity [16]. The rapid response of the gas sensor becomes crucial considering that many of the gases of interest are poisonous, toxic, flammable, explosive, and can cause asphyxiation. The presence of an explosive gas for instance, just in a few percent of its concentration in the air is enough to cause an explosion.

Lower explosive limit (LEL) [17] is defined to indicate the lowest concentration of the explosive gases present in the air which can start an explosion when the source of ignition is introduced. For methane for instance, its LEL is set at 5% [18] which is equal to 50,000 ppm (parts per million) in the air. Table 3.1 lists a few selected gases and their LEL.

From Table 3.1, all figures clearly show the requirements to develop a gas sensor offering a high sensitivity or at least able to detect gas under its LEL when safety reasons are under consideration. Sensitivity can be defined as the lowest level of gas concentration that can be detected or referred to the smallest increment of concentration that can be detected in the sensing environment [19]. The smaller the gas concentration that can be detected means the better the sensitivity of a particular gas sensor.

TABLE 3.1: A few selected gases and their lower explosive limit (LEL). The LELs concentration is given by unit percentage by volume in air at 20°C and atmospheric pressure.

SOURCE: Gases-explosive and flammability concentration limits. Retrieved from World Wide Web: www.engineeringtoolbox.com/ explosive-concentration-limits-9_423.html

Substances / gases	LEL (% by volume in air)
acetone	2.6
acetylene	2.2
gasoline	1.4
kerosene	0.7
octane	1.0
propane	2.1
butane	1.8
methane	5.0

Selectivity is another parameter that needs to be considered, as high sensitivity of a gas measurement is not enough, it must also be associated with a reliable measurement of the desired gas with no interference from other gases. Selectivity refers to the ratio of the sensor's ability to detect what is of interest over the sensor's ability to detect what is not of interest (the interferences) [19]. To be reliable, the gas under measurement needs a proper identification for only a particular gas species and should not be influenced by other gases which are present as contaminants in the measurement. These three parameters become the challenges to design and develop a handheld gas sensor which is required to be compact and robust, and able to give high selectivity and sensitivity.

3.3 OPTICAL ABSORPTION PROCESS

Absorption processes are the most important tools for the spectroscopic detection of the various gas species. This is because many of the common industrial and pollutant gases exhibit a strong optical absorption in a wide region of the infrared region and the visible-to-ultraviolet (UV) range [20]. The characteristics of the gas absorption band, as discussed previously in Chapter 2, have a 'finger print' due to its absorption features and intensity strengths are molecule specific [20]. Thus, any gas species can be reliably identified by examining the differences of its optical absorption characteristics when the light radiation is passed through a sample of that gas.

The well known absorption equation; Beer-Lambert's law [21] is used mathematically to explain the process of optical absorption. The Beer-Lambert's law can be described by a simple experiment as illustrated in Figure 3.1. This figure shows a light radiation with intensity I_o passing through a gas chamber which contains the gas of interest and emerging at the other side with intensity I.

It is found that the intensity I detected at the optical detector is less than the intensity of the incident light I_o. This is because the energy of the light radiation was absorbed by the gas molecules at a frequency coincident with the vibrational frequency ω [22] of that gas. The Beer-Lambert's law gives the relation between I_o and I as a function of wavelength λ as [21]:-

$$I_0(\lambda) = I(\lambda)\exp^{[-\alpha(\lambda)c.L]} \tag{3.1}$$

where $\alpha(\lambda)$ is the common absorption coefficient (cm^{-1}), c the concentration of absorbing gas (molecule cm^{-3}) and L (cm) represents the effective interaction length or the length of the gas cell.

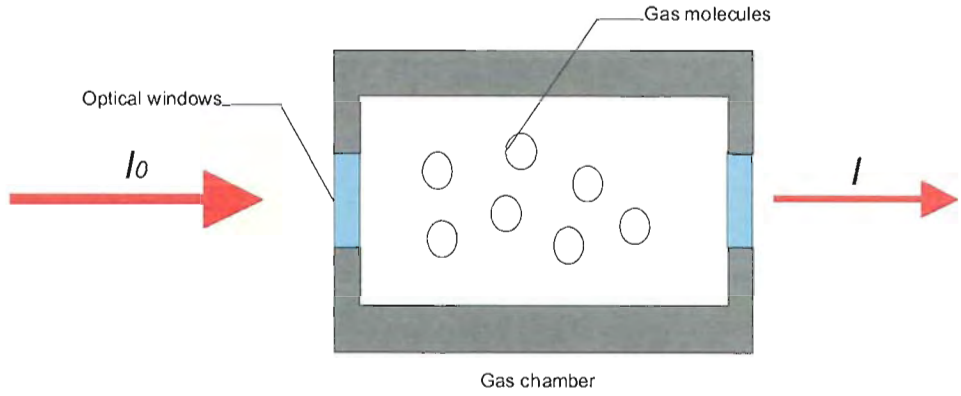

FIGURE 3.1: The process of optical absorption is described by the Beer-Lambert's law. Attenuation of the incident light radiation with intensity I_o to become I after passing through the gas chamber is mathematically described by the Beer- Lambert's law as given in equation (3.1).

Equation 3.1 illustrates a single absorption of the monochromatic source at a specific frequency or can be written in a form of wavelength λ as both parameters are related. This equation demonstrates the relationship between radiation absorbed with the path length of the interaction region and the concentration of the gas sample. It is shown that the greater the path length interaction, and the higher the gas concentration, the greater the chances of the gas molecules absorbing the light radiation. In other words, more light will be absorbed by the gas molecules.

This equation can be re-written in other forms as:-

$$A = \log_{10}\left(\frac{I_0}{I}\right) \tag{3.2}$$

where A (normalized unit) is absorbance. This equation is written in the form of a ratio, thus it can be applied to determine the absorption of a gas by a broadband source.

3.4 GAS SENSORS BASED ON OPTICAL ABSORPTION SPECTROSCOPY

Gas sensors based on optical absorption spectroscopy have a great advantage particularly regarding their ability to give a fast measurement response. This is because in the optical absorption method, the light radiation absorbed by the gas molecules is directly detected by the optical detector without the need to have any physical or chemical changes in giving the measurement response. The sensitivity and selectivity of the optical absorption sensor is relatively excellent and can be improved depending upon the optical systems and techniques which are used in the sensing systems. In sections 3.4.1 and 3.4.2, the sensitivity and selectivity of the optical absorption sensors will be reviewed and discussed.

3.4.1 THE ISSUES OF HANDHELD SENSOR SENSITIVITY

Commonly, sensitivity and selectivity for this kind of sensor are related to the spectral brightness of the radiation source and the responsivity of the optical detector [23] used in the detection system. However, both of those parameters still can be improved and for instance, the sensitivity of the gas measurement can be improved by employing a long gas cell and a high selectivity can be achieved by using appropriate techniques which will be discussed later.

Theoretically the sensitivity of the gas detection can be improved by using a long gas cell as explained previously by Beer-Lambert's law. The long gas cell allows more gas molecules to interact with the light radiation and results in a greater light energy being absorbed by the gas molecules. In this way, the intensity of the light emerging after the interaction, I, will significantly reduce compared with the incident light, I_o, as illustrated previously by a simple absorption experiment in the Figure 3.1. The more I reduces the better the optical contrast that is detected at the optical detector. The better contrast

can result in the better ability of the optical detector to differentiate between the actual received signal (I) and the presence of the unwanted noise signals received by the optical detector. The better ability of the sensing system to differentiate between actual signal and the unwanted signal means a higher sensitivity of the gas measurement can be achieved.

However, there are still big challenges when a handheld gas sensor is considered to be developed. Of course, the first limitation comes from the size of the sensor itself. Miniaturization of the sensor size often results in insufficiently robust selectivity and sensitivity and generates an increase in noise [20]. The present of noise is another problem which will reduce the signal-to-noise ratio (SNR) and thus decreases the sensitivity of the sensor.

To overcome these problems a multi-pass gas cell can be employed. In this way, the short length of the gas cell can be retained and the long path length can be achieved. The multiple reflection gas cells can be developed by using a set of reflectors such as a plane mirror or a corner-cube retro reflector [24]. Figure 3.2 shows a few examples of the reflectors' arrangement in the multiple reflection gas cells.

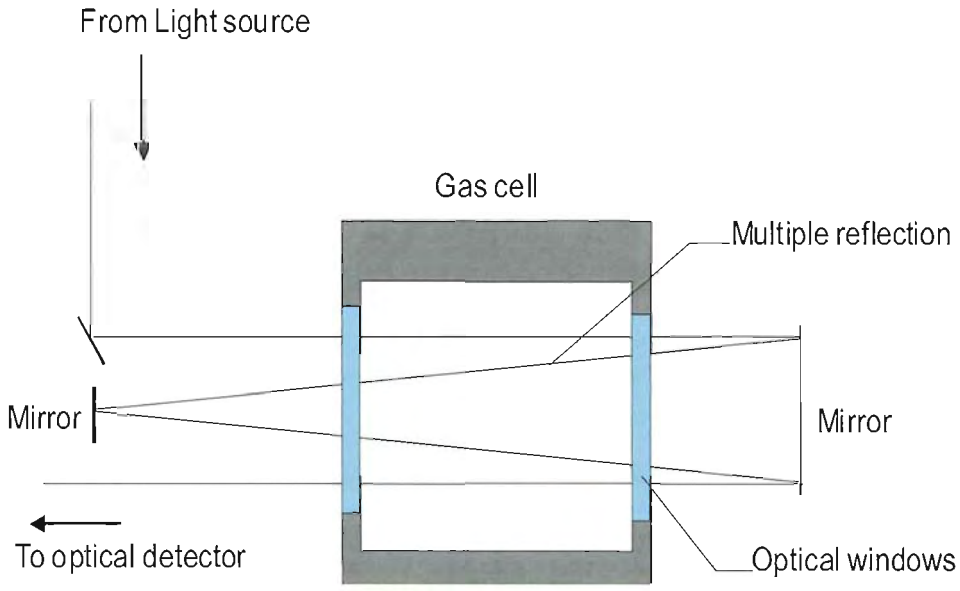

(a)

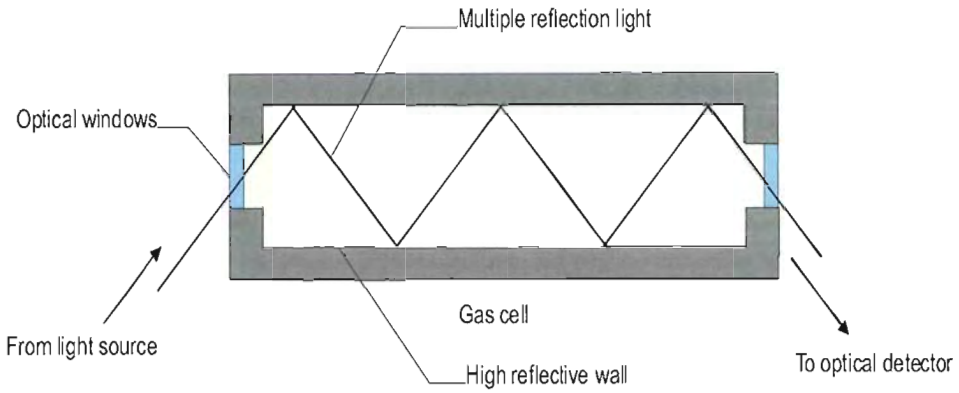

(b)

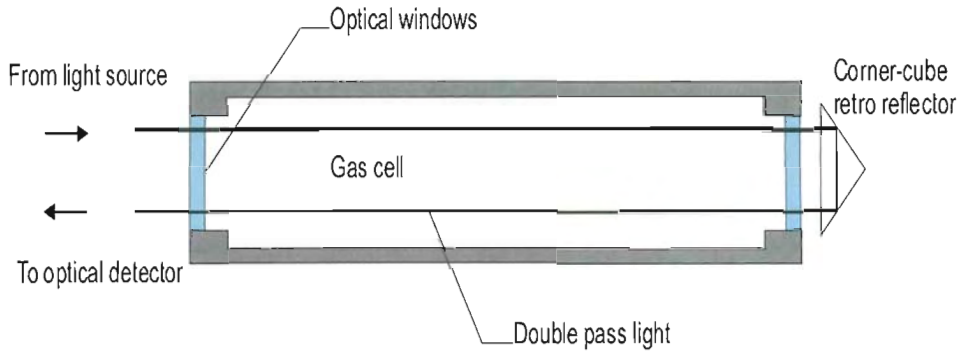

(c)

FIGURE 3.2: The figures show, (a) two high reflective mirrors at 0° to the incident light beam are used to obtain the multiple reflections of the light beam whereas in (b) the wall of the gas cell is made of a highly reflective material to reflect the light beam along the gas cell and in (c) a corner-cube retro reflector is used to give a double path of the light beam.

Figure 3.2 (a) shows that, two highly reflective mirrors can be arranged in parallel and the gas cell is located at the middle to allow a few reflections of the light beam passing through the gas cell via a pair of optical windows. This arrangement is used by

Anderson et al. [25] to measure nitric oxide by using an ultraviolet diode-laser-based optical source. By this arrangement, 20 cm path length is achieved or equivalent to four passes of the 5 cm gas cell length. It was reported that this sensor achieved 0.21% in its detection sensitivity.

The use of a highly reflective gas cell's wall to produce a multiple reflection of the light beam is demonstrated by Hennig et al. [26] in their handheld sensor for simultaneously detecting ethane and methane. The multiple reflection of the light beam in that gas cell is obtained by launching the light source at a certain angle to allow the beam to hit the gas cell wall then reflect the light beam for several passes prior to being received at the detector. With that type of gas cell, it was reported that 19.8 cm in the overall length of the path was obtained. However, the length of that gas cell is not given.

A corner-cube retro reflector can be used to double the path length as illustrated in the Figure 3.2 (c). This arrangement was used by Dakin et al. [27] in their work to detect oxygen gas in pure dry nitrogen. The 0.8 m gas cell was used and by using a corner-cube retro reflector the 1.6 m effective path length was obtained. By doubling the light beam, it was reported that the response of the sensor was doubled, thus increasing the optical contrast of the measurement.

A White cell [28] is the standard and most readily available multiple reflection gas cell that can be used to increase the path length. This design produces 600 cm [29] of path length and can be tailored depending upon the particular design of the gas cell. Galle et al. [30] for instance used a White cell with a 560 cm path length and it was found that the use of long optical path length (the path length 50 – 1000 cm) can result in sensitivities down-to-mixing ratios of a few ppb (parts per billion) for simultaneous detection of a few gases.

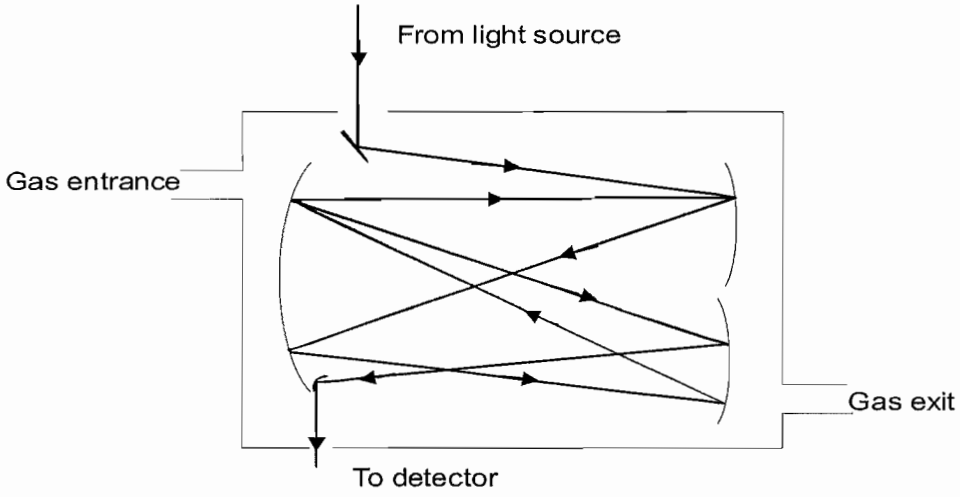

FIGURE 3.3: A schematic diagram of the White cell.

There are some other examples of the gas sensors which use a White cell to increase the path length and these can be referred to in a few more references [29, 31, and 32]. However, more information on the White cell design is not covered in this thesis and for further reading it is helpful to refer to these references [28, 33]. The other similar versions of the White cell are Heriot cell [34], Horn-Pimentel [35], and the gas absorption cell model 5611 based on a parabolic mirror [36] manufactured by New-Focus Inc. which can be used for the same purpose.

The advantages of the multiple reflection gas cell are not only for improving the sensitivity of the gas detection but also, indirectly, the interaction of the light radiation and the gas molecules that can be more homogeneous [24] as the light beam is passing through in the different paths. On the other hand, not all of the multiple reflection cells are suitable to match with a handheld gas sensor because this kind of gas cell is relatively weighty due to the bulk optical components used in their optical arrangement. Furthermore, the optical design of the multiple reflection cells is more complicated and needs to have a high reflectivity surface; this is often a limitation in using the multiple reflection cells. In addition, a high intensity optical source is required to avoid insufficient received intensity light power at the optical detector. This is because the

light power will decrease due to an increase in reflection loss [37] as the number of reflections increases, thus a weak optical signal will be received at the measurement detector.

An integrating sphere is a device which is used to spatially integrate radiant flux [38]. It is designed and constructed for the measurement of multiple optical properties, such as to measure transmittance, reflectance, and absorbance of specular samples [39]. The integrating sphere can be used as well to detect and measure the concentration of a gas by functioning as a multiple reflection gas cell. The gas cell based on the integrating sphere model is another interesting technology which is capable of detecting low-concentration traces in a gas mixture. Tranchart et al. [38] has presented an experiment and a theoretical model of the gas sensor based on the integrating sphere model. The theoretical model developed by Tranchart illustrates the relationship between the total fluxes exiting the detector port without the absorbing gas $\phi_e(0)$ and the fraction of flux changes when the sample gas is introduced $\Delta\phi$ as:-

$$\Delta\phi / \phi_e(0) = \left[\sigma(\nu) L_{eff}\right] / \left\{1 - \rho\left[1 - \sigma(\nu) L_{eff}\right](1-h)\right\} \tag{3.3}$$

where $\sigma(\nu)$ is the absorption coefficient of the gas, L_{eff} is an effective path length, ρ is the wall reflectance, and h refers to the ratio of the sum of all port areas to the area of the sphere. In the case of the sphere, which has a very small aperture ($h << 1$) and is filled with a sample gas characterized by a very small absorption coefficient ([$\sigma(\nu) L_{eff} << 1$]), the fractional absorption is enhanced by a factor of $1/(1-\rho)$, and the equivalent absorption path length of the integrating sphere L_{eq} is of order of [38]:-

$$L_{eq} = L_{eff} / (1-\rho) = 2/3D/(1-\rho) \tag{3.4}$$

By using this equation, a 10 cm diameter integrating sphere made of Spectralon ($0.989 < \rho < 0.992$ for $0.4 < \lambda < .8$ μm) can achieve several meters of path length [38]. By using this integrating sphere as the gas cell and using a differential absorption technique, it was reported that a concentration of 1.8% butane in atmosphere (the lower flammability butane is given as 1.8%) can be easily detectable. This sensor uses a diode as an optical source centred at 1.18 μm and an integrating sphere 10 cm in diameter and thus offers a possibility to develop a compact gas sensor.

At this stage, a multi-pass reflection cell is found as an important design regarding its ability to enhance the sensitivity of the gas detection. Nevertheless, a single-pass light beam is relatively easier to develop and its optical system is simpler than the arrangement of a reflection mirror which is found in the multi-pass reflection cell. In some cases, the use of multiple reflection gas cells can reduce the sensitivity of gas detection due the presence of etalon interference fringes [40]. This phenomenon arises due to a multiple reflection between parallel surfaces in the optical system such as from two parallel optical windows.

On the other hand, using a single-pass light beam needs a long gas cell to obtain a better sensitivity and this factor is often a limitation in developing a compact and handheld gas sensor. The other options such as the use of special optical fibres or developing an optical system working at a stronger gas absorption band or using special modulation signal techniques can be taken to overcome this limitation.

Previously, in numerous works, conventional and infrared fibre optics were used in the gas sensing system to convey the transmission light beam [31, 42- 47] to the gas cell or to the interaction area. There are a number of advantages to integrate fibre optics as a medium to convey the light beam in the sensing system. This is because of the immunity of the optical signal carried by fibre optics from electromagnetic interference, fibre optic links allow the gas cell to be located many kilometres from the monitoring station and the low power optical techniques [48] inherently offer a safe detection system particularly for detecting gas in the hazardous and high risk environments. Currently, the invention of photonic band gap fibres (PBFs), sometimes known as microstructure optical fibres, opens a new dimension into the gas sensing areas [41].

The application of photonic band gap fibres totally changes the function of fibre optics in the sensing system but still retains its advantages. This is due to the ability of PBFs to be functioned to be compact, light, and offering a long gas cell. Ritari et al. [49] demonstrated this in their work to detect acetylene and methane at 1.5 μm and 1.3 μm absorption bands, respectively. A 1-meter long PBF was used to detect acetylene and the experiment was conducted at 10 mbar. It was reported that the signal-to-noise ratio obtained from this experiment was 20 dB. This result shows the potential of PBFs for high sensitivity gas detection. The measurement for methane is conducted by using a 10 m long piece of PBF and the experiment is done at 630 mbar. The reason for using a long PBF and at higher pressure is because the absorption band of methane at 1.3 μm is very weak. However, no figure concerning the detection sensitivity of methane is given. Figure 3.4 shows the setup for both the experiments.

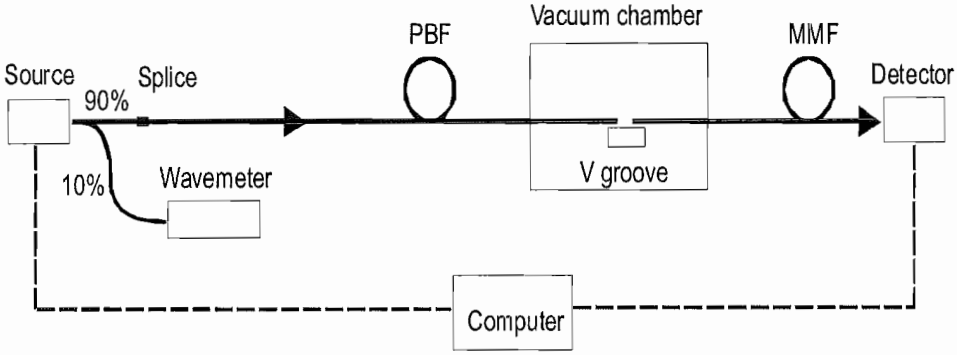

FIGURE 3.4: The diagram shows the experimental setup for measuring acetylene and methane in which PBF acts as the gas cell. The gas sample is filled into the PBFs by applying a high pressure in the gas chamber. The notation of the MMF in this diagram is referred to multimode fiber optics.

The long gas cell and the high insensitivity to bending offered by PBFs [50] allows the more compact gas sensor to be constructed as a gas cell. In addition, theoretically, PBFs can offer the wide range of the transmission window as the light beam is transmitted via

a hollow air core and thus gives a possibility for detection to be done at a stronger absorption band (in the mid-infrared region). Currently, the development of PBFs in the range 0.4 μm to 2.55 μm [49] has been achieved with varying losses and the transmission up to the mid-infrared region that was reported can be constructed by using special compound glasses [51].

However, the use of PBFs as the gas cell is restricted by the needs of the high pressure condition to fill gas into the small diameter of PBF's core. This factor results in slowing the gas detection response as time is consumed to fill the gas sample into the small core of the PBFs, which is typically around a few seconds [49] and depends upon the gas chamber pressure and the length of PBFs. For a similar reason, to evacuate the gas from PBFs can take up to 30 minutes [49]. Further more, this technology can be considered to be new and thus the availability of suitable PBFs is still questioned.

The operation of the gas sensor at a stronger absorption band is the other option that can be taken to improve the sensitivity of the gas detection. The stronger absorption bands of gases come from their fundamental absorption bands. Commonly, the fundamental absorption of many gas species appear as a strong absorption band coincident in the mid-infrared region at around 3 μm to 7 μm [39] and for a few species at around 0.25 μm to 0.7 μm. The overtone and combination bands have two orders weaker absorption bands and usually occur in the near-infrared region [26] at around 1 μm to 2 μm.

Carbon dioxide (CO_2) for example has a strong absorption band at 4.2 μm [52], Ammonia (NH_3) appears as strong bands at 6.14 μm, 3 μm, 2.93 μm [53], and acetylene (C_2H_2) has a strong band absorption at 3.04 μm [54] in the mid-infrared regions. Nitrogen dioxide (NO_2) is one example of the gas species having a strong absorption band in the visible region at around 0.49 μm [31]. Typically, the line strengths of the overtone is two orders of magnitude weaker than the line strengths at the fundamental. Methane for example, has line strengths of order 10^{-21} cm molecule^{-1} at 1.665 μm which is approximately 2 orders weaker than the 3.3 μm band [17] of its fundamental. Apparently, the fundamentals can offer absorption that is much more effective, or stronger, than the overtones.

However, due to practicality reasons the development of gas sensors working at mid-infrared regions is not a preferred option. The lack of optical sources for working in the mid-infrared regions is one of the reasons for the near-infrared regions being a priority in developing the optical system of the gas sensors. This is true when considering developing a compact and handheld gas detection system which operates at room temperature. It is because the compact optical sources for the mid-infrared region in the gas sensor applications often are laser based, such as the tunable diode laser or semiconductor laser. The tunable diode laser for instance, is available only over a range of wavelengths extending from about 0.63 μm in the visible range to just about 2.2 μm in the near-infrared region [55] for operating at room temperature. While, semiconductor based p-n junction lasers can be available in the range 2 – 3 μm for operation at room temperature [16].

The presence of strong water vapour absorption in the mid-infrared region is another factor needing to be taken into account because of the tendency of its absorption spectrum to overlap with the gas spectrum of interest. Furthermore, most of the standard optical components available are limited for use over the visible regions and only extend to the near-infrared regions. Normally, optical components to be used in the infrared regions need to be custom ordered and require special anti-reflection coating because infrared material often appears high in its index of refraction, thus making it relatively expensive. Both of these aspects, the presence of water vapour in the infrared region and the discussion on the optical components to be used in the infrared region will be discussed in Chapter 5.

3.4.2 LASER SPECTROSCOPY TECHNIQUE

As mentioned earlier, optical sources play an important factor in determining the sensitivity and as well as the selectivity of the gas sensors' performance. Laser spectroscopy (referred to the laser as the optical source) is ideal to use for gas detection since it combines high sensitivity (as the laser has high spectral brightness), is able to

give fast response [56], and shows high selectivity since the laser has a very narrow wavelength spread of the light emission [21].

Laser systems can occasionally be cross sensitive to water vapour because of the significant presence of water vapour over the infrared regions. However, a very narrow emission bandwidth of laser emission can minimize the possibility of interference between the contamination from water vapour and other gases regarding the absorption line of the gas of interest. This can be achieved by choosing the absorption line of the gas of interest coincident at the centre of the laser emission wavelength or, by tuning the laser spectrum to match the strongest absorption line of the gas of interest as depicted in Figure 3.5.

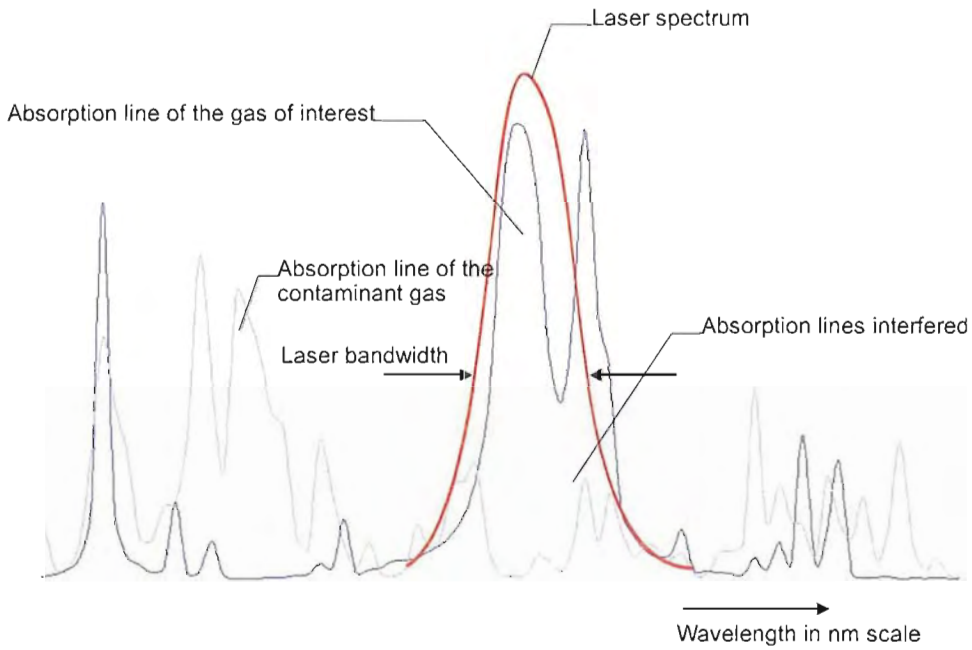

FIGURE 3.5: The strongest absorption line is matched with the narrow bandwidth of the laser spectrum. The presence of other gases spectra as contaminants can be minimized as laser has a narrow spectrum bandwidth.

A tunable diode laser [55, 57] is the most common laser source which is used in the absorption spectroscopy. The most useful feature of tunable diode lasers is their wavelength tunability [57]. This feature allows many different gas species to be detected as the suitable laser at a particular wavelength can be tuned to coincide with the strongest, or selected, absorption line of a particular gas species. In addition, a compact size and low cost of the tunable diode laser can match with the requirement to develop a handheld gas sensor. The implementation of a tunable diode laser in the absorption spectroscopy sensor can be referred to in a few references [21, 25, 26, 58, and 59]. The disadvantages of using laser are that any single absorption line might be duplicated. This duplication can result from a number of sources such as gas impurities, interference fringes due to multiple reflections or inter-mode interference in optical fibre.

3.4.3 CORRELATION SPECTROSCOPY AS A HIGHLY SELECTIVE GAS SENSOR TECHNIQUE

Generally, the use of a broadband source in the gas detection system will result in a poor selectivity [60] as it could increase the susceptibility of contaminants' absorption spectra to other gases and water vapour. The presence of such contaminant will increase the crosstalk in the measurement and thus result in the inaccuracy of the gas detection. Nevertheless, the use of a broadband source in the correlation spectroscopy technique can offer a high selectivity and an appreciable sensitivity of the gas measurement.

Correlation Spectroscopy (CoSp) [27, 43, 44, 60 - 68] is one of the techniques used in gas sensing based on optical absorption. This technique was reported as early as 1967 by Goody [60] and further works by Taylor [61], for application in planetary spectra, the gas mixture in the atmosphere, and may also be used for industrial gas analysis. In the correlation spectroscopy, the high selectivity of the gas measurement can be achieved by exploiting the multiple gas absorption lines which show specific features for a particular gas [64]. This is one of the advantages of this technique as all the

absorption lines within the bandwidth of the broadband source are used rather than just a single line (in the laser spectroscopy) as shown in the Figure 3.6. In that figure, the dashed line illustrates the area over which the absorption lines of the gas of interest will have interaction with the light radiation.

The general approach of CoSp is to use a gas sample as a matched optical filter then, using that information for selectively detecting similar absorption spectra of the same gas in a measurement cell which contains an unknown percentage of its concentration. Thus, the existence of any contamination spectra such as water vapour or any gases with non-matching properties with the gas sample spectra in the reference cell does not affect the gas measurement.

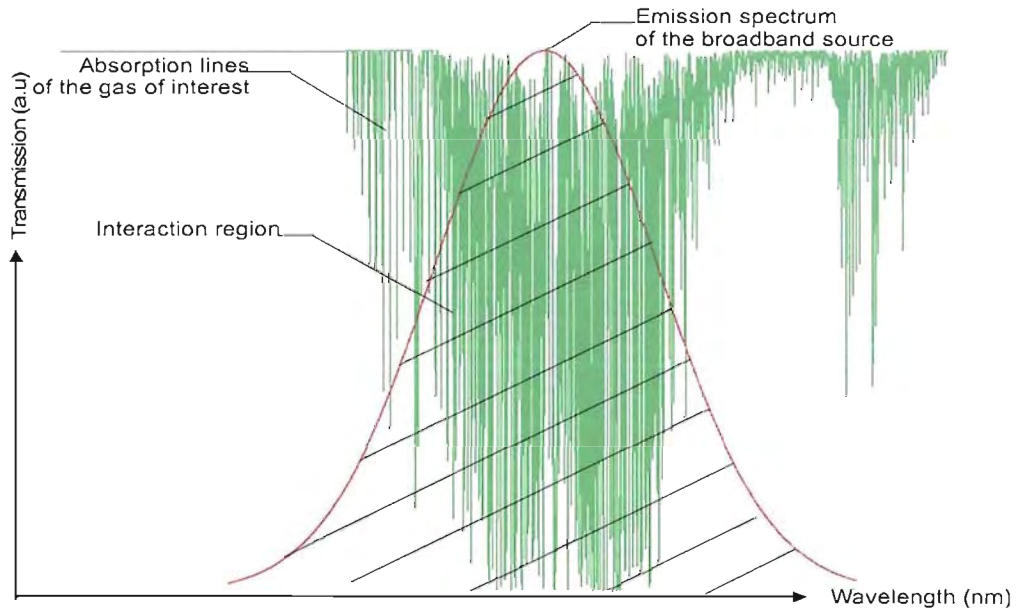

FIGURE 3.6: The dashed area is indicated as the region in which the interaction between light radiation and gas molecules can occur. The light radiation is only absorbed in this area within the bandwidth of the broadband source.

There are several methods to modulate the received signal, using correlation spectroscopy, which are Stark modulation [63, 64], pressure modulation, gas correlation detection [44] and complementary source modulation [27, 65, 66, and 67]. Complementary source modulation (CoSM) is a generic variant of the CoSp which has a more attractive technique that can be used to modulate the detected optical signal.

The implementation of the CoSM in the CoSp technique is carried out by using two gas cells which are the reference and measurement cell, two optical broadband sources and two optical detectors. Two white light sources can be employed in this system, as demonstrated by Dakin et al. [64]. However, light emitting diodes (LEDs) can replace the thermal source because the LED can offer better characteristics for the gas sensing purposes. Recently, the more advanced technology in the development of the LED offers a more powerful output power at room temperature. It can be available at the range which coincides with the absorption bands of the common gas species; for instance, Krier and Sherstnesv [69] have demonstrated powerful light emitting diodes for methane gas detection which exhibit more than 3.5 mW of output power at room temperature. This LED has a peak emission centred at 3.28 μm which can be used for methane detection at its v_3 fundamental absorption band, centred at around 3.3 μm. There are a few manufacturers [70, 71] which offer a variety of LEDs for operating in the infrared regions.

Furthermore, there are advantages in the compact size of the LEDs and their relatively narrow bandwidth compared with the emission spectrum of the white light, which can be matched with the absorption band of the gas species of interest. This is different when the thermal source is used because of the need for a rotating chopper disc for selecting the desired wavelength range [72]. In addition, an optical filter can be used to limit the bandwidth of the LED thus minimizing the interference from contaminant gases.

3.5 CONCLUSION

The optical absorption gas sensor is the most important spectroscopic technique as its detection performance can give a fast response. Sensitivity of this kind of sensor can be improved by using a long gas cell to obtain a long path length or this can be achieved by designing a multiple reflection cell in order to produce a handheld gas sensor. The use of a stronger gas absorption band is another option that can be taken as the compromise of a short gas cell can be made without significantly reducing the sensitivity of the gas measurement. An excellent selectivity often can be obtained in the laser spectroscopy and a poor selectivity results from the use of broadband source in that sensing technique. However, the use of a broadband source in the correlation spectroscopy technique will result in a highly selective sensing performance. The correlation spectroscopy technique will be deeply discussed in the following chapter.

CHAPTER 4
CORRELATION SPECTROSCOPY

4.1 INTRODUCTION

In this chapter the idea of correlation spectroscopy, as introduced in Chapter 3, is discussed in more detail. This chapter covers the basic principles of correlation spectroscopy, the idea of using a matched optical filter to perform the selective sensing technique, the characteristics of the detection signal in correlation spectroscopy and the derivation of modulation index which represents the sensor response. Then, the understanding of all correlation spectroscopy aspects can be used to simulate the prediction for the experimental value of the handheld correlation spectroscopy sensor, which will discuss in the next chapter.

4.2 BASIC PRINCIPLES OF CORRELATION SPECTROSCOPY

The general approach of correlation spectroscopy is undertaken using 100% concentration of the gas of interest in the reference cell, as a matched optical filter, and then using that filtered information to selectively detect similar absorption spectra of the same gas in the measurement cell, which is filled with an unknown concentration of the same gas. By that means, this technique can offer a highly selective method even when using a broadband source. The use of a broadband source is required to take advantage of this technique and is employed to overlap all gas absorption lines that form the absorption band of the gas.

In general, the correlation spectroscopy system consists of two gas cells; reference and measurement cell, two identical broadband sources, and two identical optical detectors

which are used as reference and measurement detectors. These components form the complementary source modulation (CoSM) setup, the variant of correlation spectroscopy to modulate the received signal at the optical detector. Basically, the light beam from the first source (namely S_1) will pass through the reference cell containing the sample gas of interest. This partially absorbed light beam (the light beam of S_1 was absorbed by gas molecules in the reference cell) will combine with another unaffected source (namely S_2) in such proportion to give zero net intensity. The appropriate proportion can be achieved by equalization of the optical power of S_1 and S_2 at the reference detector. Then, the combined beam can be used to probe the target gas in the measurement cell.

As the beam component, which has passed through the reference cell has less available optical energy lying within the narrow spectral region of the gas of interest's absorption lines; a net intensity modulation of the equalized combined beam will be re-established when it passes through a measurement cell which contains the unknown % concentration of the gas of interest. This induced intensity modulation is proportional to the gas of interest's absorption level as a differential absorption between the two beam components; S_1 and S_2.

The use of a reference detector to equalize the received combined signal and reset the sensing system to be zero inherently offers a self referencing technique in which the sensing system is always reset to zero prior to probing the target gas in the measurement cell. By this means, the various factors that might cause optical intensity changes do not affect the received signal at the measurement detector.

4.2.1 THE MATCHED OPTICAL FILTER AS A SELECTIVE TECHNIQUE

The idea of a reference cell as a matched optical filter, as introduced in section 4.2 is described in this section. In Figure 4.1 (a), the absorption spectrum of 100% (methane) target gas in the reference cell is illustrated in the form of a transmission spectrum and

the light radiation passed through the gas cell is assumed to have a Gaussian shape. The absorbed light radiation by molecules is limited by the bandwidth of the broadband source, thus the selected gas absorption lines are only in the area which is under the Gaussian shape. By that means, the absorption lines of the target gas are filtered because the light radiation acts as a filter. Now, the filtered absorption lines from the target gas in the reference cell will be used to detect and select the similar absorption gas lines in the measurement cell.

Figure 4.1 (b) shows the absorption spectrum of a similar gas with unknown concentration (< 100%) represented as blue lines. Due to the absorption band of the particular gas being uniquely characterized or having a 'fingerprint', all absorption lines of the target gas in the reference cell match the absorption lines of a similar gas in the measurement cell. According to the Beer-Lambert's law, the absorption of light radiation by molecules is proportional to the concentration of the gas present. The gas absorption lines of the unknown % gas in the measurement cell will be less absorbed and formed as weaker lines (blue lines) relative to the absorption by 100% gas in the reference cell (green lines), as shown in Figure 4.1 (b).

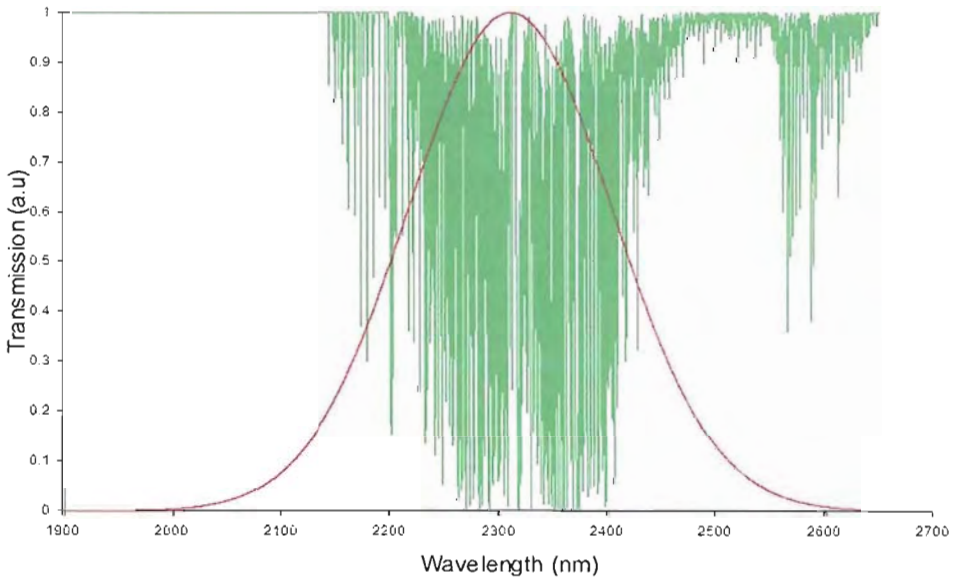

(a)

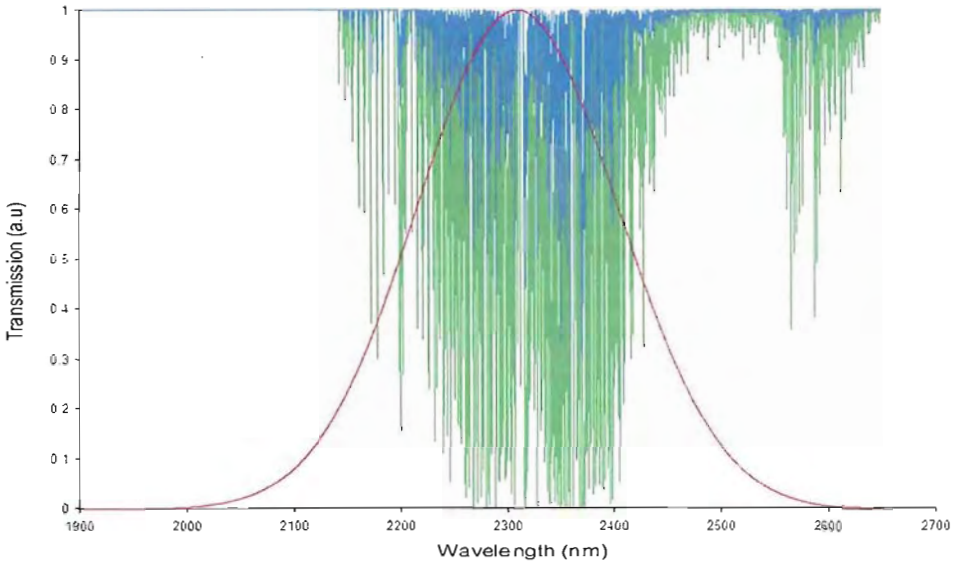

(b)

FIGURE 4.1: (a) The absorption spectrum of methane in the region of transmission and the Gaussian shape broadband source. The area under the Gaussian shape is referred to as the optical matched filter, as introduced in section 4.2, and (b) absorption band of present gas in the measurement cell has similar absorption characteristics but is weaker than the absorption from 100% gas concentration. Both reference cell and measurement cell are assumed to have the same effective path length, temperature, and pressure. The example of the gas spectrum is obtained from HITRAN.

4.3 SIGNAL DETECTION IN CORRELATION SPECTROSCOPY

There are two different optical system arrangements that can be used in correlation spectroscopy associated with complementary source modulation (CoSM). These arrangements are either for a bulk optical component based, or an arrangement for a fibre optics based, sensing system. Both types of arrangement of the optical system are shown in Figure 4.2 (a) and (b).

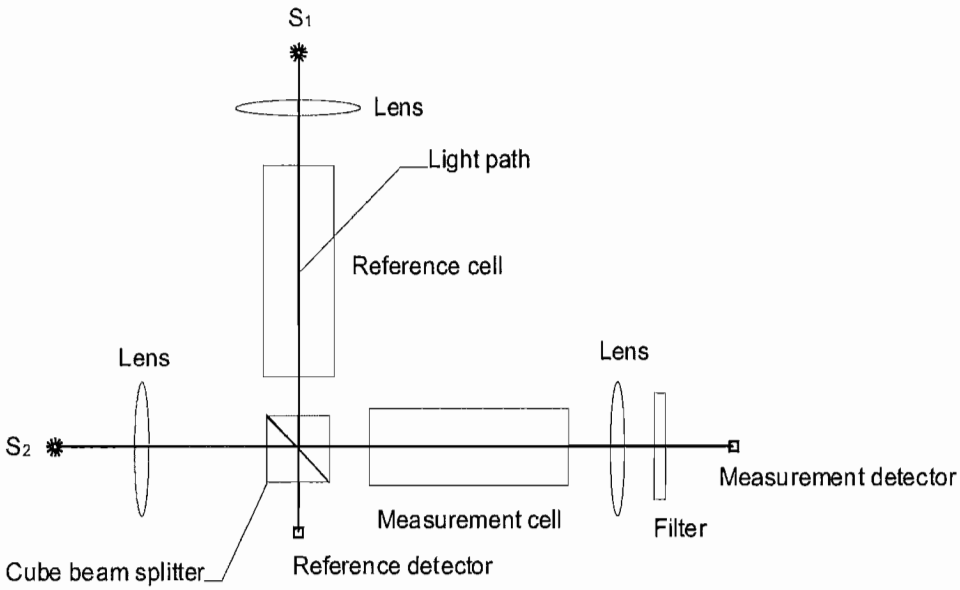

(a)

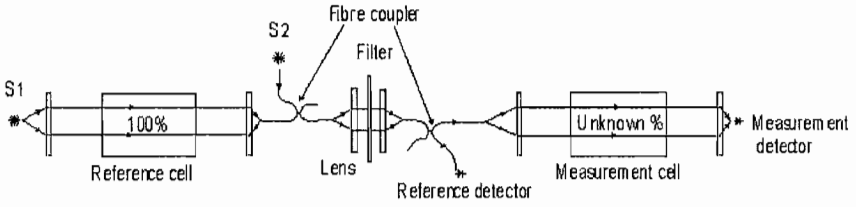

(b)

FIGURE 4.2: (a) Optical components arrangement for a correlation spectroscopy sensing system based on fibre optics and (b) arrangement for bulk optical components based.

For both arrangements, the CoSM's approach involves the manipulating of two light sources to modulate the received optical signal at the measurement detector. This 'manipulation' is done by alternating on / off switching of two light sources, thus producing alternately received optical signals 180° out of phase with each other. The alternating received optical signal is described in terms of intensity with time, as illustrated in Figure 4.3 where S_1 and S_2 represent the intensity of source one and source two, respectively.

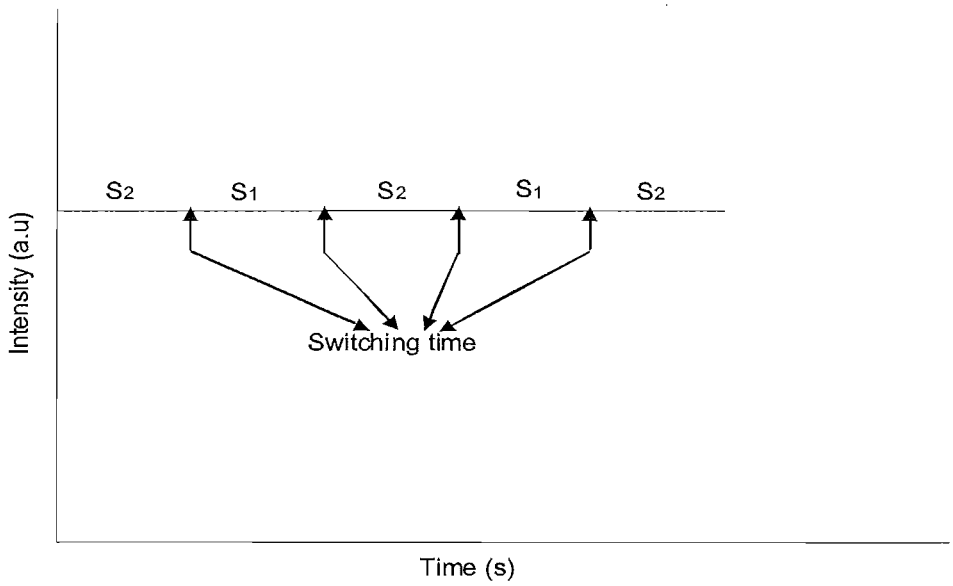

FIGURE 4.3: (a) An alternating on / off switching of two light sources 180° out of phase with each other.

Principally, the mechanism of detection for both arrangements is similar and involves the equalization of received signal levels at a reference detector and then, measuring the optical signal contrast at the measurement detector. To equalize the received signal, two sources are arranged in conditions such that only S_1 will pass through the reference cell containing 100% of the target gas. The intensity of S_1 was reduced due to absorption by gas molecules in the reference cell. Then, the fraction of absorbed light beam is combined with unaffected light beam from S_2. At this point, the intensity of the received

optical signal from the combined beam at the measurement detector is described in Figure 4.4.

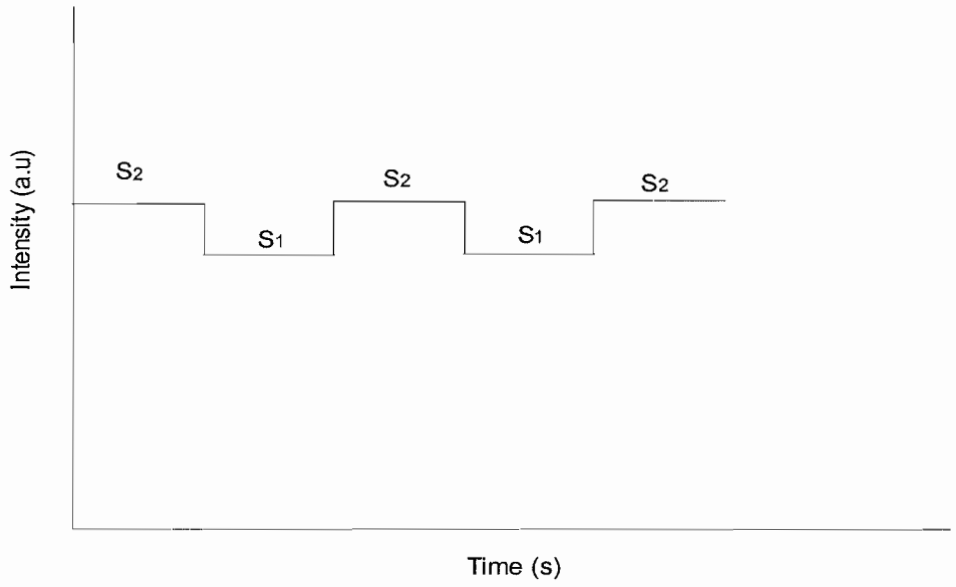

FIGURE 4.4: S_1 is illustrated as having a lower intensity due to absorption by gas molecules in the reference cell and S_2 does not pass through the reference cell so is unaffected and its intensity remains at the same level, as described previously in Figure 4.3 (a).

The received optical signal, as described in Figure 4.4, is needed to set their optical energy in such a proportion to achieve zero net intensity. This is can be done by adjusting the relative strength of sources S_1 and S_2. This process equalizes the intensities of S1 and S_2 and can be monitored at the reference detector. In this condition, the sensing system is set to zero.

The production of zero net intensity is described in the graph in Figure 4.5. The graph (a) shows S_1 having a slightly higher intensity relative to S_2 with the dashed area indicating the reduction of optical energy due to absorption of the light beam of S_1 by gas molecules in the reference cell. However, the average intensity of S_1 and S_2 is similar

due to the higher level of S_1 balancing the lower energy in that dashed area, as shown in graph (b).

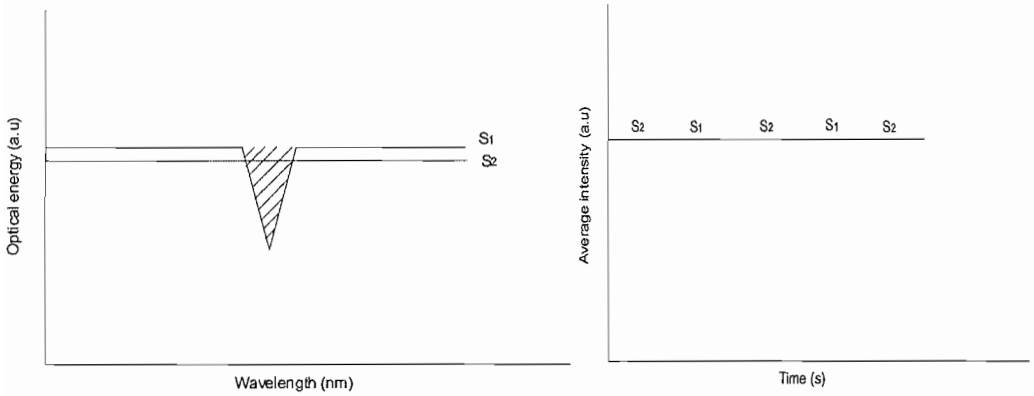

(a) (b)

FIGURE 4.5: (a) The level of S_1 illustrated has a higher level than S_2 in its optical energy. The dashed area is represented as a very narrow region which is optical energy that was absorbed by gas molecules and (b) both sources are illustrated remaining similar in their average intensity.

Now, the equalized signal intensity of the combined beam can be used to interrogate the presence of an unknown target gas concentration in the measurement cell. In the case when the measurement cell is not filled with the target gas, the two light beam sources are similarly in a condition of zero net intensity. There is no change in their relative intensities. In the presence of an unknown concentration of the target gas, the fraction of the unaffected light beam (S_2) will experience greater attenuation due to absorption by gas molecules which match with the absorption lines in the reference cell. This produces a net intensity modulation which is proportional to the absorption level of the target gas in the measurement cell. A higher gas concentration will result in a higher absorption level. The light beam component which has passed through the reference cell

is less absorbed by gas molecules because it has less available energy overlapping the comparable gas absorption lines so its intensity level is not so strongly reduced.

The optical signal intensities received at the measurement detector can be illustrated, as shown in Figure 4.6, in which the intensity of S_2 is lower than S_1. This is the final light intensity detected by the measurement detector which is the valuable output signal to determine the concentration of unknown gas present in the measurement cell. Modulation index, which is the sensor response, can be derived from the final intensity output received at the measurement detector.

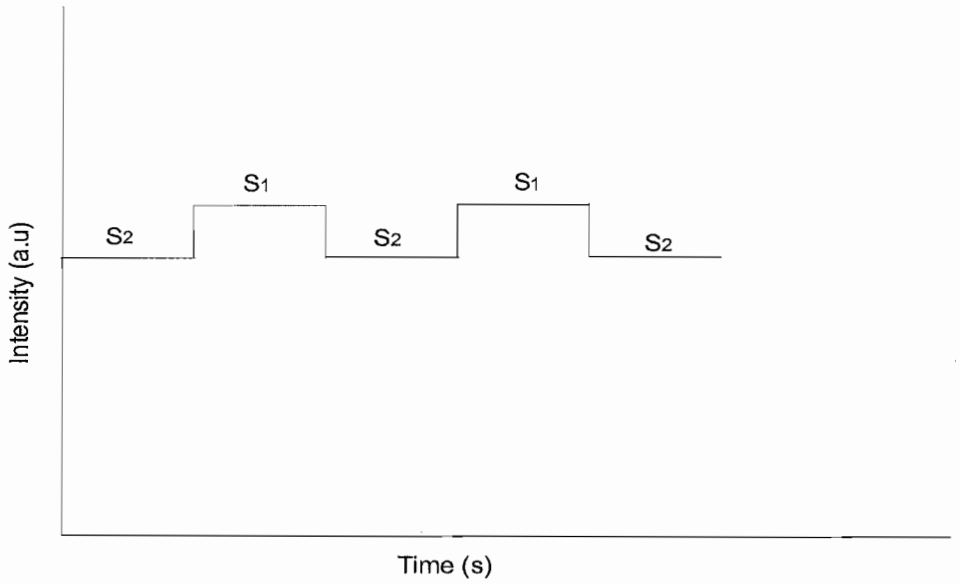

FIGURE 4.6: The final intensity output shows S_2 lower than S_1 after the combined beam passed through the measurement cell. The intensity of S_1 remains similar, as shown previously in Figure 4.5 (b).

4.4 DERIVATION OF MODULATION INDEX

Modulation index is defined as an alternating current signal (AC signal) received at the measurement detector and divided by means of the direct current (DC) level. The AC signal is referred to as the peak to peak alternately on / off modulated signal levels of S_1 and S_2 when the target gas is introduced into the measurement cell. This peak to peak signal level is shown in Figure 4.7 and can be expressed as:-

$$AC = I_{m1} - I_{m2} \tag{4.1}$$

where Im_1 and Im_2 refer to the photocurrent developed at the measurement detector and received from S_1 and S_2, respectively.

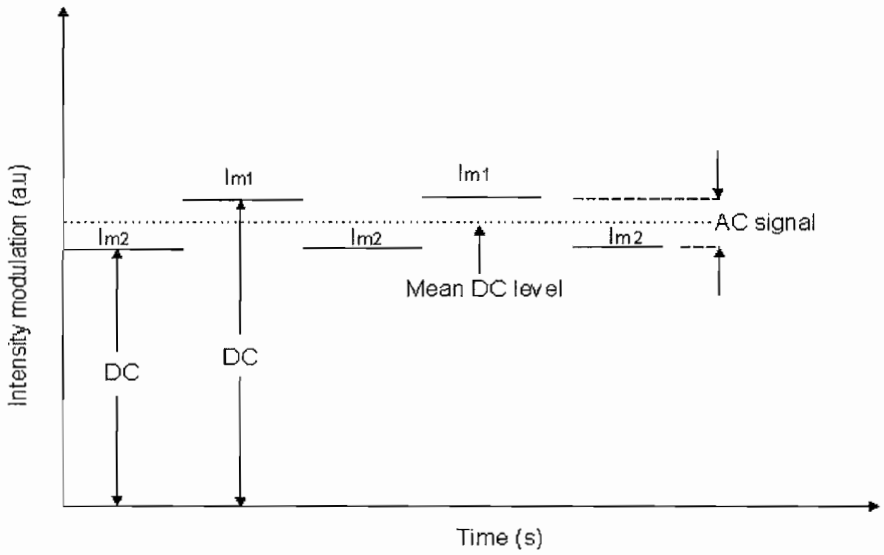

FIGURE 4.7: The AC signal is shown as the peak to peak of alternately received optical signal at the measurement detector. The DC signal is referred to as the mean value of two optical signal levels received at measurement detector.

The DC signal referred to as the mean of the DC current level at the measurement detector, is given as:-

$$DC = \frac{I_{m1} + I_{m2}}{2} \tag{4.2}$$

By that, modulation index m can be expressed as:-

$$m = 2\left(\frac{I_{m1} - I_{m2}}{I_{m1} + I_{m2}}\right) \tag{4.3}$$

The photocurrent developed at the measurement detector Im_1 and Im_2 can be described mathematically by using numerical analysis on to the optical transmission as a function of wavelength, which is passed through the optical system and received by optical detectors, as described in section 4.4. This numerical analysis is done first to the received optical signal at the reference detector to investigate the zero net intensity condition.

By using numerical analysis, the photocurrent developed at the reference detector during alternate on / off switching S_1 and S_2, as shown in Figure 4.2, can be expressed as:-

$$I_{R1} = \int S_1(\lambda).T_r(\lambda).R_r(\lambda).d\lambda \tag{4.4}$$

$$I_{R2} = \int S_2(\lambda).R_r(\lambda).d\lambda \tag{4.5}$$

where is I_{R1} and I_{R2} are represented as the photocurrent developed at the reference detector due to the received optical signal from the S_1 and S_2 path, respectively. In equation (4.4) and (4.5), $S_1(\lambda)$ and $S_2(\lambda)$ are the optical spectral powers generated at optical sources S_1 and S_2, T_r is the optical transmission spectrum of the gas in the reference cell, and $R_r(\lambda)$ represents the spectral responsivity of the reference detector.

Zero net intensity is achieved by equalizing the two alternate signals of photocurrent developed by S_1 and S_2. This is the first approximation to derive the modulation index and mathematically can be represented by equalized I_{R1} and I_{R2}, giving:-

$$\int S_1(\lambda).T_r(\lambda).R_r(\lambda).d\lambda = k\int S_2(\lambda).R_r(\lambda).d\lambda \tag{4.6}$$

where is k is the factor to modify S_2 to convene this feedback condition. This equation is made by assuming the linear changes of the spectral output of both the light beam sources. Equation (4.6) can be re-written as:-

$$k = \frac{\int S_1(\lambda).T_r(\lambda).R_r(\lambda).d\lambda}{\int S_2(\lambda).R_r(\lambda).d\lambda} \tag{4.7}$$

Zero net intensity is the pre-measurement condition to setup a correlation spectroscopy sensing system at zero or equal to 0% concentration of the target gas in the measurement cell.

The photocurrents developed at the measurement detector I_{m1} and I_{m2} are expressed in the following equations as:-

$$I_{m1} = \int S_1(\lambda).T_r(\lambda).T_m(\lambda).R_m(\lambda).d\lambda \tag{4.8}$$

$$I_{m2} = k\int S_2(\lambda).T_m(\lambda)R_m(\lambda).d\lambda \tag{4.9}$$

where $T_m(\lambda)$ is the optical transmission spectrum of the target gas in the measurement cell and $R_m(\lambda)$ is the spectral responsivity of the measurement detector. Both $R_r(\lambda)$ and $R_m(\lambda)$ are considered as constant and these parameters can be neglected. This is because both optical detectors are assumed to have a flat spectral responsivity lying much broader than the transmission spectrum of the target gas region. The final equation which represents modulation index, *m*, is obtained by substituting equation (4.8) and (4.9) into equation (4.3), giving:-

$$m = 2\left\{\frac{\int S_1(\lambda).T_r(\lambda).T_m(\lambda).d\lambda - k\int S_2(\lambda).T_m(\lambda).d\lambda}{\int S_1(\lambda).T_r(\lambda).T_m(\lambda).d\lambda + k\int S_2(\lambda).T_m(\lambda).d\lambda}\right\} \tag{4.10}$$

This is the final equation which is used to quantify the sensor response and is known as modulation index.

4.5 CONCLUSION

In this chapter, the correlation spectroscopy was introduced as a highly selective gas sensing technique. The basic principles of the correlation spectroscopy technique were discussed and the schematic diagram of the correlation spectroscopy based sensor was presented. A mathematical formula was derived to give a modulation index as a sensor response. This chapter is important as foundation knowledge to design a handheld sensor based on the correlation spectroscopy technique.

CHAPTER 5

OPTICAL SYSTEM DESIGN OF THE HANDHELD METHANE GAS SENSOR

5.1 INTRODUCTION

In this chapter, the discussion will start with a brief review about the basic idea of the optical design. Then, since there are a few limitations to develop an optical system in the mid-infrared region, the problems associated with the optical system design in that region will be deeply discussed. Firstly, the discussion will cover the selection of absorption bands of methane and then secondly the selection of optical components suitable for the selected gas absorption band. From that, the optical design of the handheld methane sensor working with the correlation spectroscopy technique is presented.

5.2 THE OPTICAL SYSTEM

An optical system is a vital part of a gas detection system as it inherently influences the performance of the sensing system. 'Optical system' refers to optical sources, all optical components such as lenses, optical windows, etc., and optical detectors. Basically, the main purpose of the optical system is to collect as much light radiation as possible from the source; guiding that light, passing it through the interaction region (gas cells) and directing it onto the small active area surface of the optical detector.

This involves the process of focussing, collimating, reflecting, splitting and re-focusing the light beam where the final objective is to obtain a high intensity of signal received at the measurement detector. The high transmitted light beam received at the measurement detector is required to obtain the utmost sensitivity of the gas detection. In addition, an effective optical system means the well collimated light radiation. This can reduce the noise level caused by the multi-reflections of the stray light radiation received at the measurement detector.

Geometrical optics is an appropriate starting point that can be used to design any optical system [73]. This is because the imaging properties of a lens and mirror system will determine the flux distribution sensed by the optical detector. In geometrical optics, the imaging properties formed at the optical detector can be approximated graphically by using ray tracing [74].

The information from ray tracing can be used to design a well collimated and efficient light guidance of the optical system. This is achieved due to the ray tracing providing an idea of how to select a lens with a suitable focal length to match with the length of the gas cell. By that, a loss of optical energy and beam deviation can be minimized and the problems associated with stray light can be reduced.

5.2.1 OUR BASIC IDEA OF HANDHELD SENSOR DESIGN

In considering developing a handheld gas sensor which is operating based on CoSM of the CoSp technique, as previously discussed in chapter 4, a basic idea of the handheld gas sensor design will be presented. Figure 5.1 illustrates a rough sketch of our basic idea.

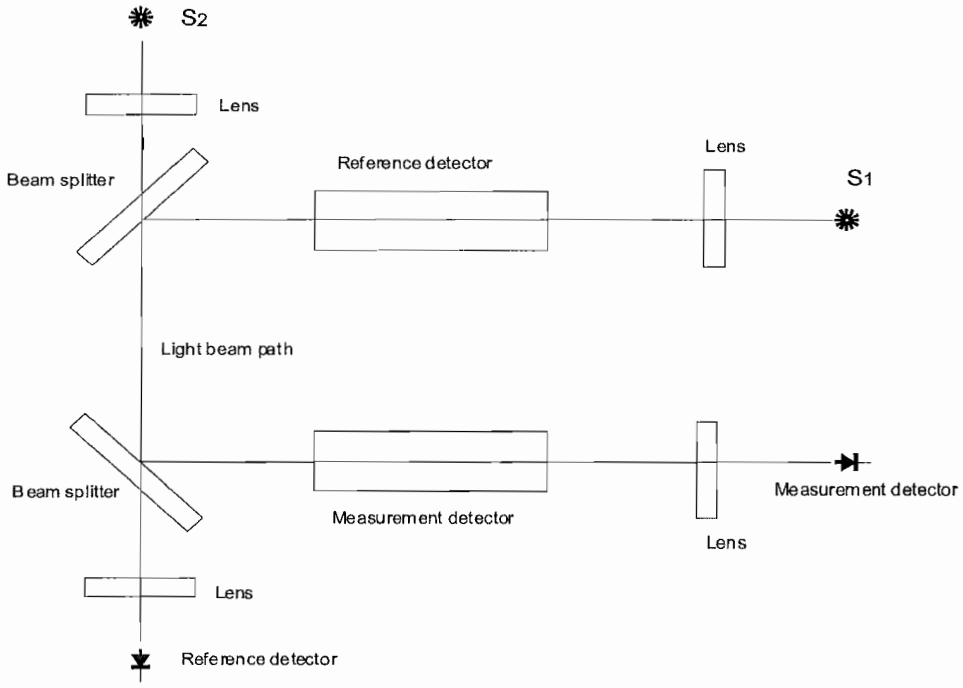

FIGURE 5.1: A sketch of our basic idea of handheld gas sensor design.

Briefly, the sketch shows that the handheld sensor can be constructed by using two LEDs, S_1 and S_2 a reference and measurement detector and two beam splitters. Besides, two gas cells need to be used; one gas cell for reference and the other gas cell is used for measuring the unknown methane concentration. Four lenses are expected to be used to collimate and focuss the light beam. Before this sensor can be designed, the study of methane absorption bands is required in order to choose the best wavelength region for this sensor to operate. Then, the availability of optical components to be matched to work in that region will be discussed.

5.3 MOST CONVENIENT SELECTION OF METHANE BAND

The sensitivity of the designated methane sensor depends upon the availability of optical components, the power of optical sources, the performance of the detectors, and the sensing system setup itself. However, it is important to emphasize that to achieve high gas detection sensitivity it is often desirable to work at the strongest possible absorption band of the gas [58], as discussed in Chapter 3. These requirements, after conflict and compromises, must be made in the design.

The use of a stronger gas absorption band can result in improved optical contrast detected at the measurement detector as discussed in Chapter 4. The improved optical contrast meant that better sensitivity could be achieved. Apparently, the study of a methane absorption band to select the most suitable absorption band is becoming important and will be deeply discussed in the section 5.3.1.

5.3.1 THE ABSORPTION BAND OF METHANE

Methane has four fundamental absorption bands which are ν_1 at 3.43 (2914.2 cm^{-1}) μm, ν_2 at 6.55 (1526 cm^{-1}) μm, ν_3 at 3.31μm (3020.3 cm^{-1}), and ν_4 at 7.65 μm (1306.2 cm^{-1}) [75]. Fundamental absorptions of ν_2 and ν_4 correspond to the two bending vibrational modes [76] and ν_1 and ν_3 are due to the stretching mode of the tetrahedron species (since CH_4 is in that class), whose centre is occupied by the C (carbon) atom.

The observation of the methane absorption spectrum is complex due to the association of the rotational energy transition simultaneously in the vibrational transition and also because of the presence of degenerate bands; overtone, combination band, and hot bands. Commonly, all the degenerate bands appear as relatively weaker absorption bands compared with the absorption of the fundamental bands.

The weaker methane absorption from overtones are $2\nu_2$ that occurs at 3.25 μm (3071.5 cm^{-1}), $2\nu_3$ at 1.66 μm (6006 cm^{-1}) and $2\nu_4$ at 3.84 μm (2600 cm^{-1}) [75]. There are a lot of combination bands which contribute to the complexity of the methane absorption spectrum. For instance, the combinations of $\nu_2 + 2\nu_4$, $\nu_1 + \nu_4$, $\nu_3 + \nu_4$, and $\nu_2 + \nu_3$ occur at 2.42 μm (4123 cm^{-1}), at 2.37 μm (4216.3 cm^{-1}), at 2.31 μm (4313.2 cm^{-1}), and at 2.2 μm (4546 cm^{-1}) respectively, forming a complex absorption band at around 2.3 μm. If the hot bands are considered, the complexity of the methane spectrum becomes difficult to analyse due to the overlapping of different absorption bands at the same wavelength region.

Basically, the absorption bands of methane lying over the near-infrared to the mid-infrared regions are shown in Figure 5.2, for the region from 1.5 μm to 9 μm. This spectrum is generated from the well characterized, and readily available, HITRAN software [1]. In this spectrum, only two fundamental methane spectra can be observed as the other two are infrared inactive. The two infrared active ones are ν_3 (3.3 μm band) and ν_4 (7.65 μm band) as indicated in the Figure 5.2. The other absorption bands of methane that are shown in the Figure 5.2 come from $2\nu_3$ at 1.66 μm and the combination of several bands at around 2.3 μm.

There are a few references [76 - 82] which are useful to study the various methane absorption bands as well as its characteristics. It is necessary to study the absorption band of methane as it is the foundation on which to build the optical sensing system. The selected absorption band of methane will determine the selection of optical sources, detectors, filters, and also the optical components.

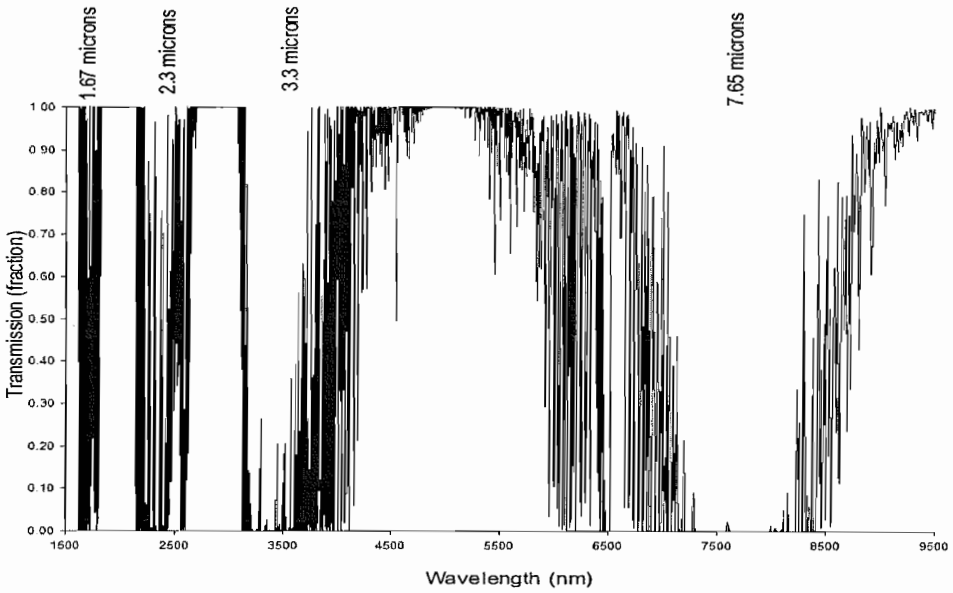

FIGURE 5.2: The absorption band of methane for the infrared region, from 1.5 μm to 9.5 μm. This graph is obtained by using HITRAN 2000 for 100% of methane concentration with a path length of 1 m, at 1.013 bar and 296 K.

5.3.2 THE ABSORPTION BAND SELECTION CRITERIA

In a number of previous studies [26, 30, 36, 40, 45 - 47, 58] it is shown that sensors developed for methane detection often work at around 1.67 μm in the near-infrared region. This region coincides with the transmission windows of many available optical components particularly those based on silica. Standard fibre optics for use in telecommunications can be used as well, as there appears to be sufficient light transmission in this region, thus it is straight forward to convey the light beam into the sensing system. Unfortunately for optical absorption spectroscopy purposes, operating in the near-infrared region decreases the detection sensitivity because weaker vibrational transitions are detected [21].

However, it is desirable to use as strong an absorption band as possible to obtain better sensitivity for the handheld gas sensor. Commonly, the strong absorption, which is due to the fundamental transition, appears in the mid-infrared regions and the transition due to overtones can be found in the near-infrared region. For example, the absorption band of methane at 1.67 μm comes from the first overtone $2\nu_3$ band [77]. This indicates that for methane the better wavelength regions for a sensing system should coincide with its fundamental transition which is at around 3.3 μm, or 7.65 μm in the mid-infrared region.

The other criteria to be considered are that the selected absorption band needs to be isolated [83] from interference with the absorption band of other gas species particularly water vapour. The concentration of water vapour in the air is so much higher than any other gases [84] and its spectrum can be found in the infrared region. Water vapour, H_2O, appears as two strong absorption bands at 6.27 μm (1595 cm^{-1}) and at 2.66 μm (3755.8 cm^{-1}) due to the fundamentals ν_2 and ν_3 respectively. A large number of water vapour overtones and combination bands also appear in the infrared region whereas the first overtones $2\nu_2$ and the combination $\nu_3 + \nu_4$ show fairly strong absorption bands [75] in the mid-infrared region. Obviously, the presence of water vapour in the mid-infrared is a big problem for the methane sensing as the tendency of their band to overlap with the methane bands is very high. This will contribute to an increase of the water crosstalk in the real methane measurement.

5.4 LIMITATIONS IN THE MID-INFRARED REGIONS

In considering the fundamental absorption band of the methane gas, mid-infrared is the better region which can offer a large gas absorption band cross section, as required to increase the sensitivity of the sensor. However, there are two main practical limitations to working in the mid-infrared region. The first one is the availability of the optical components to use in developing the optical system. The second one comes from the contamination from the water vapour and some other impurity gases which have a high probability to overlap with the methane absorption lines, thus resulting in increasing the crosstalk of the measurement. Figure 5.3 shows the presence of a water vapour

absorption band which interferes with absorption bands of a few selected methane absorption bands.

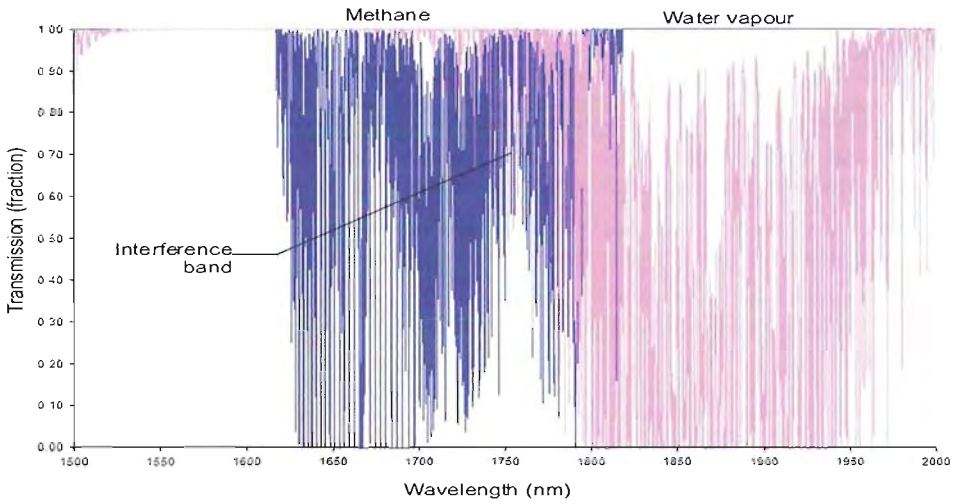

(a)

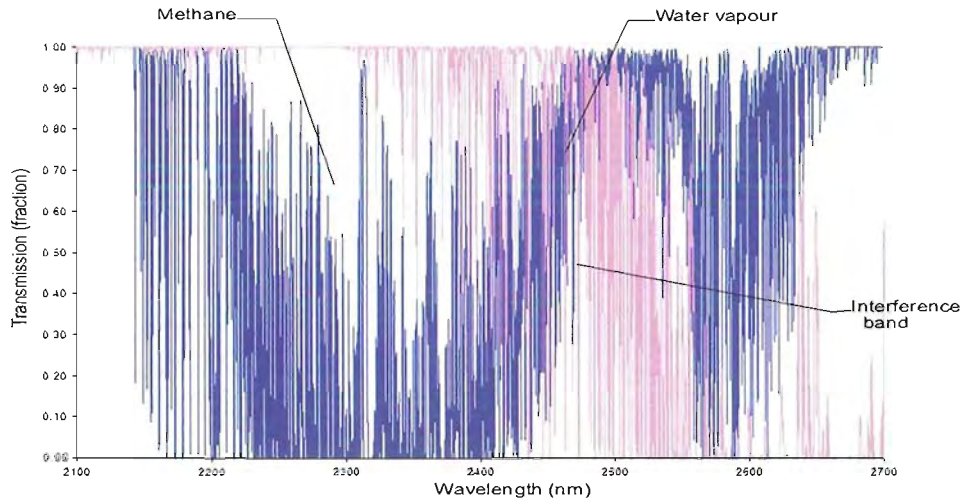

(b)

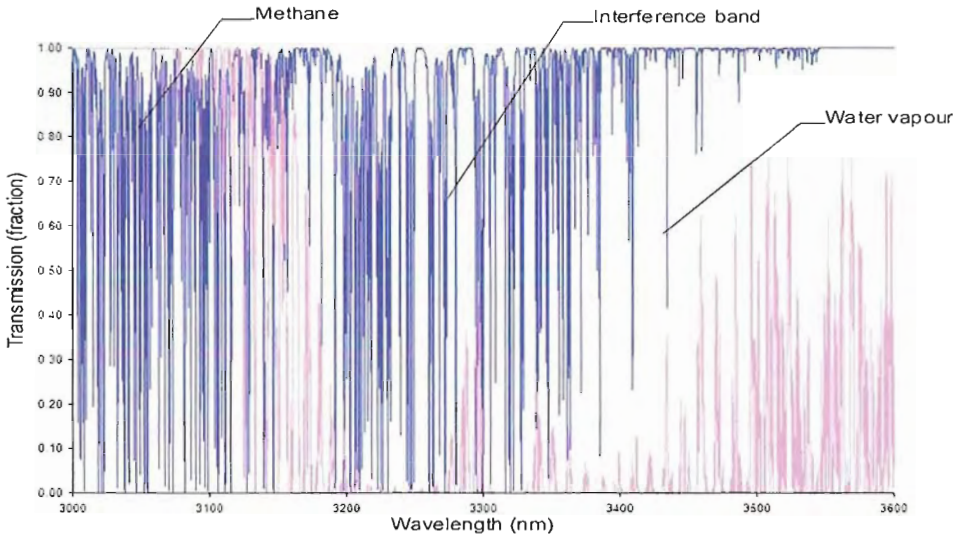

(c)

FIGURE 5.3: The water vapour band (pink lines) significantly interferes with the methane band (blue lines) at (a) 1.67 μm, (b) 2.3 μm, and (c) 3.3 μm. These graphs are obtained by using HITRAN 2000 for 100% concentration of methane and water vapour with a path length of 1 m, at 1.013 bar and 296 K.

5.5 THE SELECTED METHANE BAND

The 2.3 μm absorption band of methane is selected based on the 'exclusive' nature of its location near the mid-infrared region, as shown in the Figure 5.4.

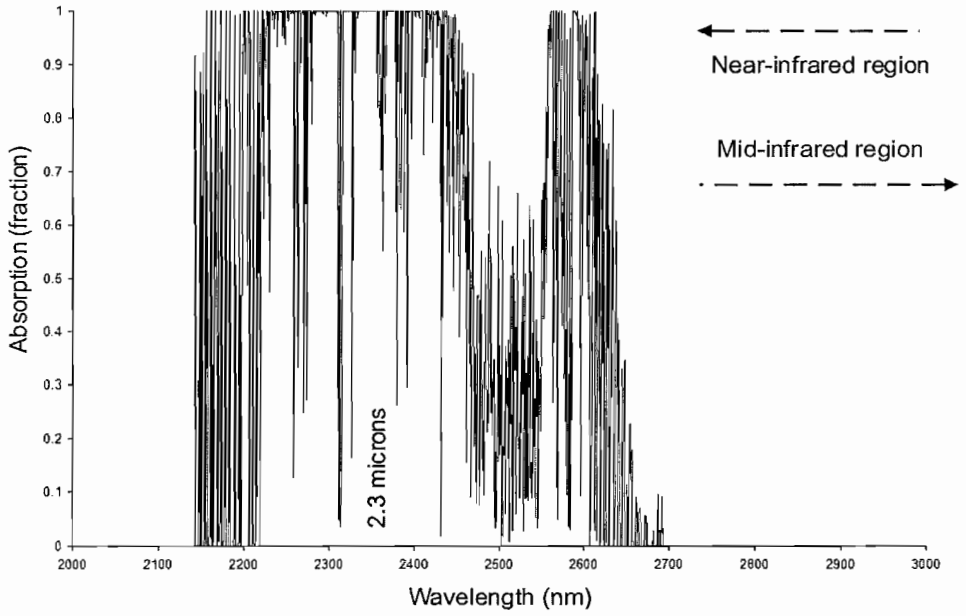

FIGURE 5.4: The location of the 2.3 μm absorption band of methane near the mid-infrared region. This graph is obtained by using HITRAN 2000 for 100% concentration of methane with a path length of 1 m, at 1.013 bar and 296 K.

There are two advantages in working in the 2.3 μm band. The first one is the availability of some common optical components (silica based material) which show sufficient transmission extending into this region. The second reason is that the absorption band of methane, centred at around 2.3 μm, visually appears approximately two and half times stronger in absorption than the absorption band centred at 1.67 μm.

5.5.1 ANALYSIS OF THE 2.3 μm BAND

This analysis is divided into three parts. The first part will concentrate on the identification of the various absorption bands of methane formed at around 2.3 μm. This is followed by comparison of the cross section absorption for 1.67 μm and 2.3 μm, and

the last part will cover the discussion on the effect of the water vapour and other gas present at the 2.3 μm band.

The 2.3 μm band is classified into an octad system [80] and is referred to as the region 2 μm to 3 μm. This band is composed of 8 vibrational bands split into 24 sub bands, as summarized in Table 5.1.

TABLE 5.1: Summary of the octad bands.

SOURCE: Hilico, J. C., Robert, O., et al. (2001). Analysis of the interacting octad system of $^{12}CH_4$. *Journal molecular spectroscopy*, 208, 1-13.

Band	**Subband symmetric**	**Centre (cm^{-1}) / (μm)**	**Sum intensity at 296 K (cm^{-2} / atm)**
$\nu_1 + \nu_2$	E	4435.1207 / 2.25	0.07
$\nu_1 + \nu_4$	F_2	4223.4615 / 2.37	6.27
$\nu_2 + \nu_3$	F_1	4537.5505 / 2.2038	1.78
	F_2	4543.7630 / 2.2008	
$\nu_3 + \nu_4$	A_1	4322.6890 / 2.3134	11.8
	E	4322.1978 / 2.3136	
	F_1	4322.5768 / 2.3134	
	F_2	4319.210 / 2.3152	
$3\nu_2$	A_1	4595.4597 / 2.1760	0.03
	A_2	4595.2799 / 2.1761	
	E	4592.0088 / 2.1777	
$3\nu_4$	A_1	3909.1898 / 2.5581	0.82
	F_1	3920.5235 / 2.5507	

	F_2	3870.4870 / 2.5837	
	F_2	3930.9210 / 2.5439	
$2\nu_2 + \nu_4$	F_1	4363.5917 / 2.2917	0.63
	F_2	4348.7078 / 2.2995	
	F_2	4378.9774 / 2.2836	
$\nu_2 + 2\nu_4$	A_1	4133.0236 / 2.4915	0.86
	A_2	4161.9081 / 2.4027	
	E	4104.6175 / 2.4363	
	E	4151.0043 / 2.4091	
	F_1	4128.7283 / 2.4421	
	F_2	4142.8629 / 2.4138	

There are eight interacting bands but only the three strongest bands [80] contribute significantly to the sum intensity at the 2.3 μm band. These three bands included $\nu_3 + \nu_4$, $\nu_1 + \nu_4$, and $\nu_2 + \nu_3$, with the sum of intensities 11.8, 6.27, and 1.78 respectively. All the positions and intensities of bands in the octad system can be referred to in the table.

The strongest combination band $\nu_3 + \nu_4$ fall at around 4319.2107 cm^{-1} to 4322.6890 cm^{-1}, which is equivalent to 2.3133 μm to 2.3152 μm. Absorption in this band is contributed to by the ground state transition A_1, and three other species of degenerate vibrational levels, which are indicated by E at 4322.1978 cm^{-1}, F_1 at 4322.1978 cm^{-1} and F_2 at 4319.2107 cm^{-1}. The combination bands of $\nu_1 + \nu_4$ fall at 4223.4615 cm^{-1} (2.3677 μm) due to the degeneracy of the F_2 transition. The band $\nu_2 + \nu_3$ at around 4322 cm^{-1} (around 2.2 μm) is contributed to by transitions of F_1 and F_2. There are a few references [84, 85] that can be referred to for the discussion of other bands in the octad system. Figure 5.5 shows three of the methane bands which form the stronger absorption at around 2.3 μm.

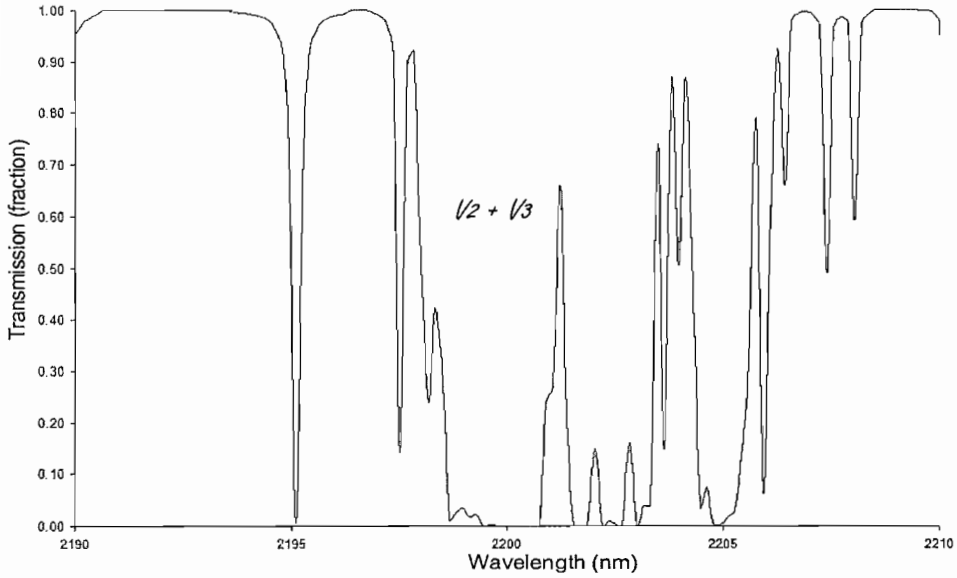
Transmission (fraction)
1.00
0.90
0.80
0.70
0.60
0.50
0.40
0.30
0.20
0.10
0.00
2190
2195
2200
2205
2210
Wavelength (nm)
V2 + V3

(a)

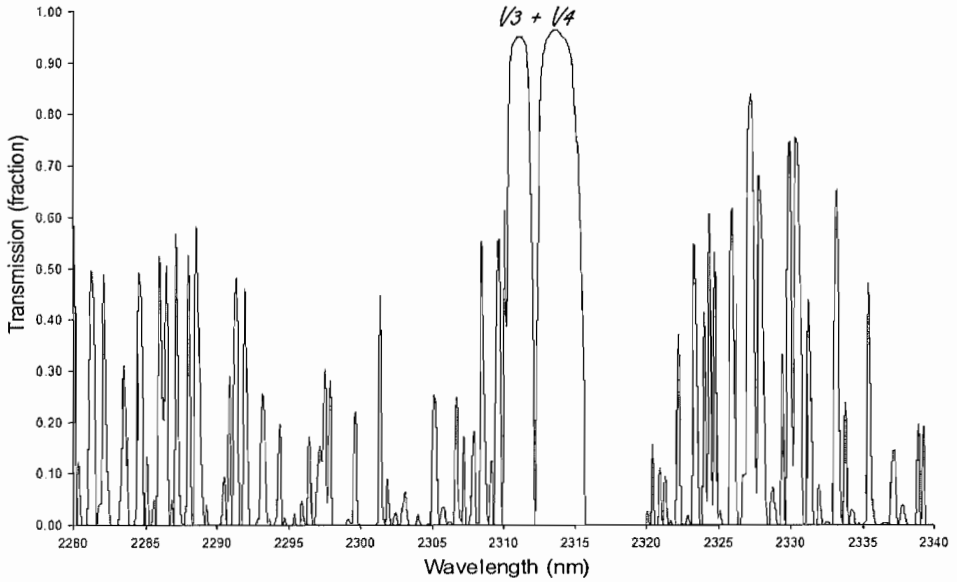
Transmission (fraction)
1.00
0.90
0.80
0.70
0.60
0.50
0.40
0.30
0.20
0.10
0.00
2280
2285
2290
2295
2300
2305
2310
2315
2320
2325
2330
2335
2340
Wavelength (nm)
V3 + V4

(b)

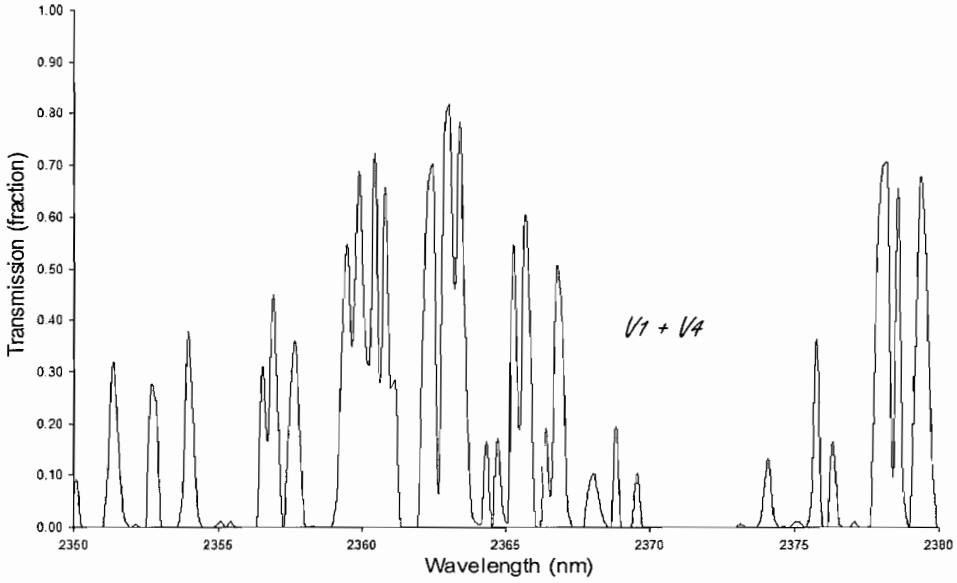

(c)

FIGURE 5.5: Three strongest absorption bands of methane, at around 2.3 μm, are represented by a) $\nu_2 + \nu_3$, b) $\nu_3 + \nu_4$, and c) $\nu_1 + \nu_4$. These graphs are obtained by using HITRAN 2000 for 100% concentration of methane and water vapour with a path length of 1 m, at 1.013 bar and 296 K.

The position of every rotational line associated with the vibrational energy transition is not too important to identify at their exact wavelength due to the fact that all lines are used in the correlation spectroscopy method. The most important thing is to determine the centre of the strongest absorption band and the absorption cross section for that band. In this way, the optical source with a suitable peak emission and bandwidth can be chosen to match the selected band.

The analysis of cross section absorption can be done by calculating the sum intensity of that band using the database provided by HITRAN 2000 [1]. The calculation of sum intensities for 1.67 μm is done by assuming that this band emerged in the range 1620 nm to 1820 nm and 2140 nm to 2700 nm for 2.3 μm. These absorption bands are generated from 100% methane concentration with one meter effective path length, at a

temperature equal to 296 K and pressure at 1 atmosphere. The absorption bands at 1.67 μm and 2.3 μm are shown in the Figure 5.6.

Visually, the cross section of the 2.3 μm band can be approximated at around two and a half times larger than the 1.67 μm band. This approximation is proved by calculation which shows that the sum intensity for the absorption band cross section of the 2.3 μm band is approximately 220% times larger than for the 1.67 μm band.

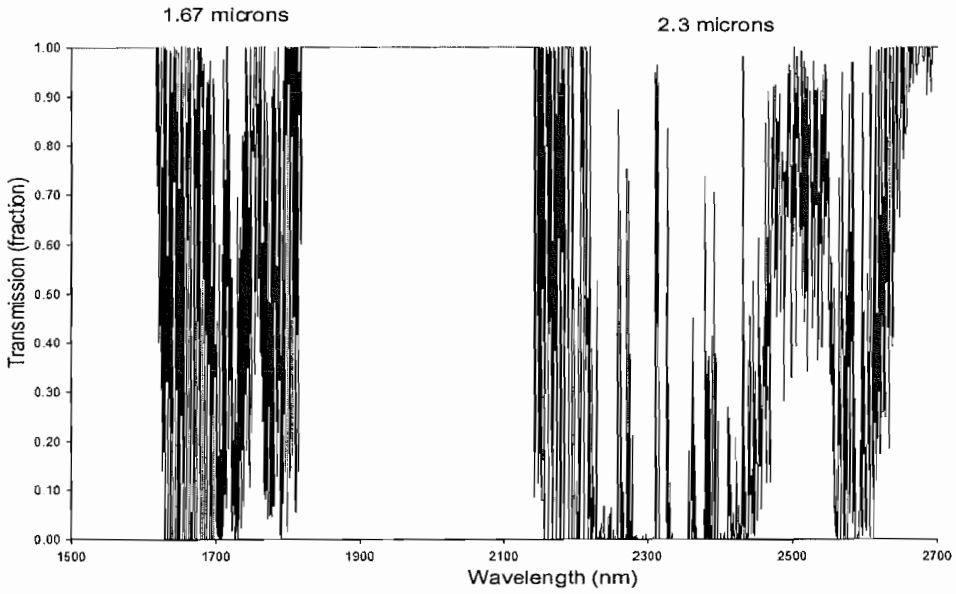

FIGURE 5.6: The cross section of the 2.3 μm band is around two and a half times larger than the cross section of the 1.67 μm band. These graphs are obtained by using HITRAN 2000 for 100% concentration of methane and water vapour with a path length of 1 m, at 1.013 bar and 296 K.

In a similar way, the isolation of the methane band from interference with water vapour can be examined by calculating its sum intensity and comparing this with the sum intensity of the water vapour for a comparable band range. It is found that the presence

of water vapour at the 3.3 μm band is comparatively, approximately, 41%, 22% at the 1.67 μm band, and 47% at the 2.3 μm. This analysis is done based on the assumption that the band at 3.3 μm exists in the range 3.00 μm to 3.50 μm, band 1.67 μm in the range 1.62 μm to 1.82 μm, and band 2.3 μm in the range 2.14 μm to 2.50 μm. The presence of water vapour at the methane absorption bands has been shown previously in Figure 5.3 (a), (b) and (c), and in Table 5.2 is given the summary of the percentage of water present in the 1.67 μm, 2.3 μm, and 3.3 μm bands.

TABLE 5.2: Summary of the percentage of water vapour present in the 1.67 μm, 2.3 μm, and 3.3 μm bands.

Band (μm)	**1.67**	**2.3**	**3.3**
Band range (μm)	1.62 – 1.82	2.14 – 2.50	3.00 – 3.50
Water Vapour (%)	22%	47%	41%

However, the comparison of sum intensity for examining the band cross section and the isolation of the methane band is only an approximation. The more accurate calculation should consider the optical source bandwidth as a factor that limits the absorbed lines. The accurate analysis of both parameters can be carried out by using numerical analysis and it will be discussed in detail for the 2.3 μm band in chapter 6.

5.6 OPTICAL COMPONENTS

The selection of optical components must give sufficient optical transmission at the interaction region of the light radiation and the gas. At the same time, it can function as a filter to suppress the wide radiation band of external background radiation particularly from environmental sources. In that way, the signal to noise ratio (SNR) of the detection signal at the measurement detector can be improved.

Since the absorption band of methane has been selected to be centred at 2.3 μm, the optical components selected must have sufficient transmission at that wavelength. Most of the common optical components which are silica based have a sufficient optical transmission curve, limited in the visible range and extending to the near-infrared region depending on their thickness. However, in many cases, silica based optical components appear to have either a sloping decrease or a drastic drop [86, 87] in their transmission curve in the region exceeding 2.1 μm due to band edge or absorption by hydroxyl ion (O-H). Thus, a reliable datasheet or the transmission curve of selected optical components is necessary to avoid insufficient transmission of the light radiation.

Optical components based on infrared material have an excellent optical transmission over a wide range of the infrared region [73, 88, and 89]. However, most of the infrared materials appear to be relatively high in their refractive index [90]. The high refractive index can result in a lowering of the external light transmission due to Fresnel reflection. The distribution of light power between the transmitted (τ) and reflected (r) light components is given by the Fresnel equation as;

$$\tau = \frac{4n_2 n_1}{(n_2 + n_1)^2} \tag{5.1}$$

$$r = \left(\frac{n_2 - n_1}{n_2 + n_1} \right)^2 \tag{5.2}$$

where τ is the fraction of transmittance, r is the fraction of reflectance and n_1 and n_2 represent the refractive index of air (or interface medium) and the optical components, respectively. These equations are derived with the assumption that there is no absorbance and that the incident light is at a small angle. The bigger difference in the refractive index at the interface of two mediums will result in more light power being reflected. The flux Φ (Watt) of transmitted light passing through the optical components, and reflected, is given by;

$$\Phi_{transmitted} = \Phi_{incident} \times \tau \tag{5.3}$$

$$\Phi_{reflected} = \Phi_{incident} \times r \tag{5.4}$$

The reflection of light can be reduced by coating the optical components with a special dielectric antireflection layer [73].

Although, the high transmission characteristic was the main consideration in selecting optical components, there are some other characteristics that need to be taken into account. The selected optical components should be resistant to the environmental conditions either physically or chemically. Solubility is an example of chemical properties which is described by the ability of water to dissolve the optical components. The higher value of the solubility means the higher volume of water that can be present

in the optical component and thus this increases the light absorbed by the water solute in that optical component.

The physical properties such as the toughness are a common factor to produce a more robust sensor. This is another disadvantage of optical components based on infrared material as many of them are crystalline which often possess weak properties [91] and as well as being brittle. For the special gas sensing application, the selection of optical components should consider the suitability and ability to work in the specific conditions for example, to work under high pressure or under thermal shock. In a more specific case, the use of germanium (Ge) and silicon (Si) should be avoided for high temperature applications since these materials become opaque at about 373 K and 673 K [73], respectively. This is due to an increased thermal activation of carriers from the valence band to the conduction band at high temperature. In addition, both materials are not efficient in transmitting light radiation because of having high index of refraction. Germanium and silicon have refractive indexes of 4.0 and 3.5 on average over the infrared region. Appendix A shows the refractive index for common infrared materials.

In conclusion, obviously the knowledge of material properties is really essential to select the most suitable optical components. It is found that there are a few restrictions associated with the use of infrared material. In addition, the cost of infrared based optical components is relatively expensive, thus it is often not an attractive option.

5.6.1 THE SELECTED OPTICAL COMPONENTS

There are a few materials based on silica that show a sufficient optical transmission extending to the near-mid infrared region depending on their thickness. Borosilicate glass with 1.75 mm thickness and AR-Glass with 1 mm thickness show more than 80% of the optical transmission across the visible and this extends up to 2.60 μm. This range covers the strongest band of methane centred at 2.3 μm and is wider than the bandwidth of light emitting diodes (LEDs) with the peak emission at 2.31 μm. Figure 5.7 shows the transmission curve of both selected optical components compared with the LED 20 #23

-1 ISBG Optoelectronics with 2.31 μm peak emission and LED23 Hamamatsu with 2.35 μm peak emission, and the transmission spectrum of methane centred at 2.3 μm.

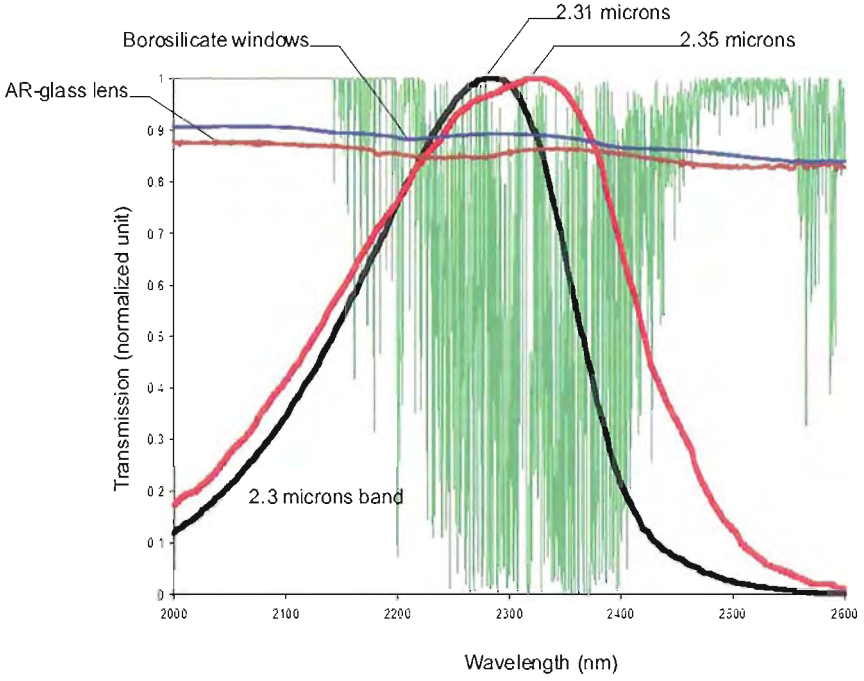

FIGURE 5.7: The selected optical windows (Borosilicate glass) and lenses (AR-Glass) shows the sufficient average transmission over the transmission spectrum of the methane centred at 2.3 μm and wide enough compared to the emission spectrum of the optical sources used in the sensing system.

The Borosilicate glass is selected for optical windows and AR-Glass for lenses due to their optical transmission being sufficient over the gas absorption lines with a band centred at 2.3 μm. Figure 5.8 (a) and (b) show the optical transmission of Borosilicate glass and AR-glass.

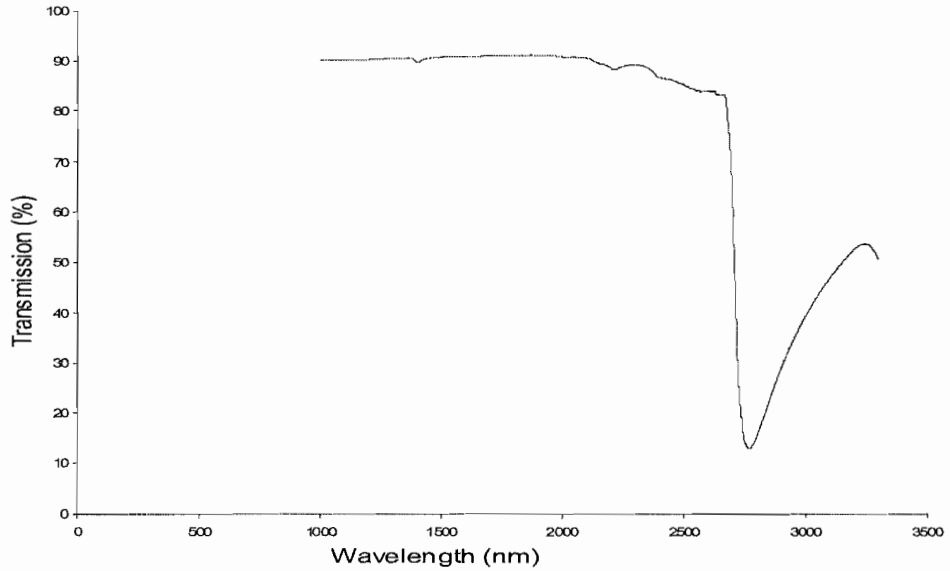

(a)

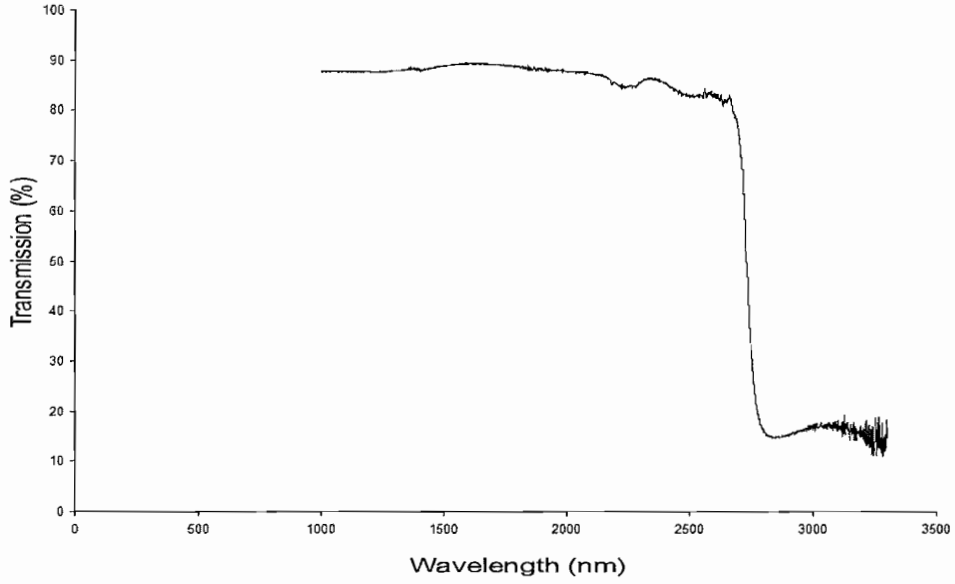

(b)

FIGURE 5.8: The transmission spectrum of the a) Borosilicate glass with 1.75 mm thickness and b) AR-glass with 15 mm focal length. Both transmission spectra are obtained by using Cary 500 UV-VIS-NIR spectrophotometer.

A silicon wafer slice can be used as a beam splitter due to its' high refractive index, which is on average 3.5 for a wide infrared range. According to the Fresnel equation, the high refractive index of optical components will result in a high reflection fraction. In addition, since the incident light makes a large angle with the optical components, the fraction of light reflected is much greater and Fresnel equations are no longer true. It is found that from measurement, silicon wafers with 400 μm thicknesses show almost half the fraction of reflected light. Figure 5.9 shows the external optical transmission of silicon wafers with 400 μm thickness.

However, multi-reflection of light is a minor problem associated with the use of high refractive index materials. A fraction of transmitted light will reflect for a second time at the interface of material and air and this, reduces the transmitted optical power received at the measurement detector.

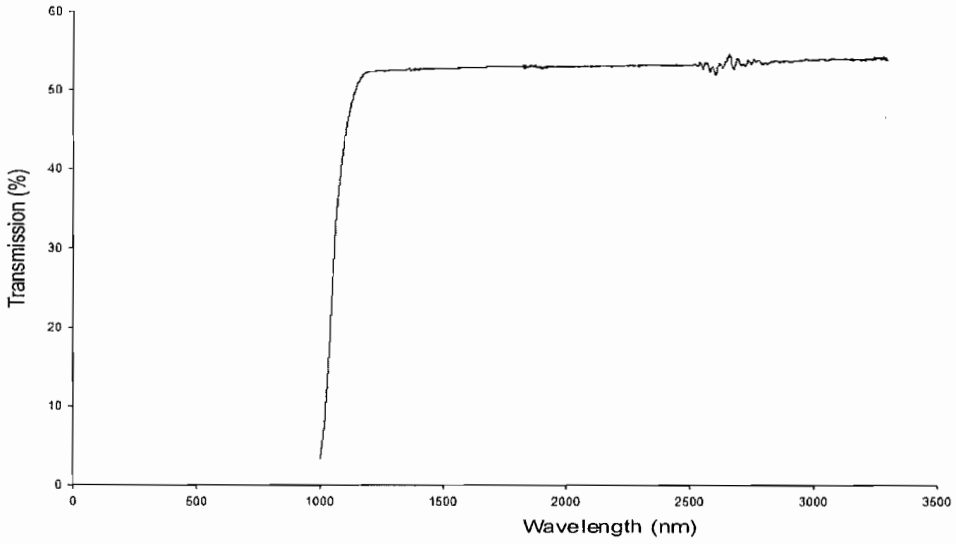

FIGURE 5.9: The external transmission spectrum of double side polished silicon wafer slices with 400 μm thickness. This transmission spectrum is obtained by using Cary 500 UV-VIS-NIR spectrophotometer.

In addition, the transmission of weaker light power from multi-reflections of reflected light will form an interference pattern at the measurement detector. The formation of that interference will increase the noise level, thus reducing the sensitivity of gas detection. This problem can be minimized by using a thin double sided polished silicon wafer slice.

5.7 SENSOR DESIGN

The basic design of the handheld gas sensor is shown in Figure 5.10. The 104 mm x 40 mm x 60 mm gas chamber is connected with four 'Top-hats'. Two of the 'Top-hats' are mounted with optical detectors and the other two are fitted with LEDs. There are overall four parts in the gas cell which are the gas chamber, beam splitter / combiner, 'Top-hat' and ferrule.

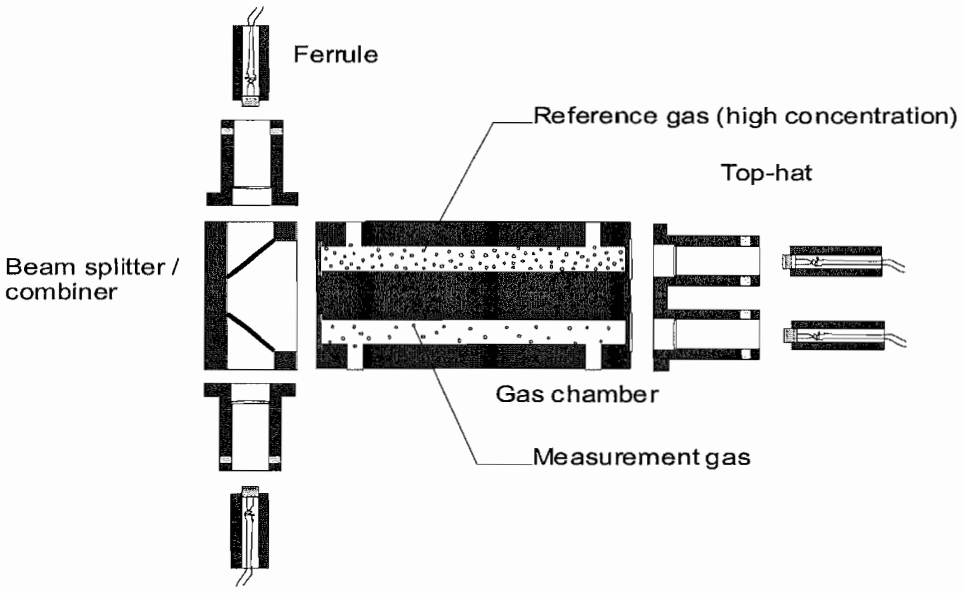

FIGURE 5.10: A cross-section diagram of the handheld gas sensor design with four 'Top-hats'. There are four separate parts; the gas chamber, beam splitter / combiner, 'Top-hat', and ferrule.

5.7.1 GAS CHAMBER

The gas chamber is made from solid aluminium and consists of two isolated gas cells; a reference cell and a measurement cell which is 100 millimetres in length and 10 millimetres in diameter. Both gas cells are sealed by optical windows at one of the ends and the other end is sealed with Viton O-rings and a lens with a 15 mm effective focal length. The use of optical windows, and lenses, seals the gas cells and can prevent interference patterns caused by parallel optics [26]. There are two connectors on each gas cell to allow gas filling and discharge from the gas cells. Figure 5.11 shows a cross-section diagram of the gas chamber. The full dimensions of the gas chamber engineering drawing are given in Appendix B (a).

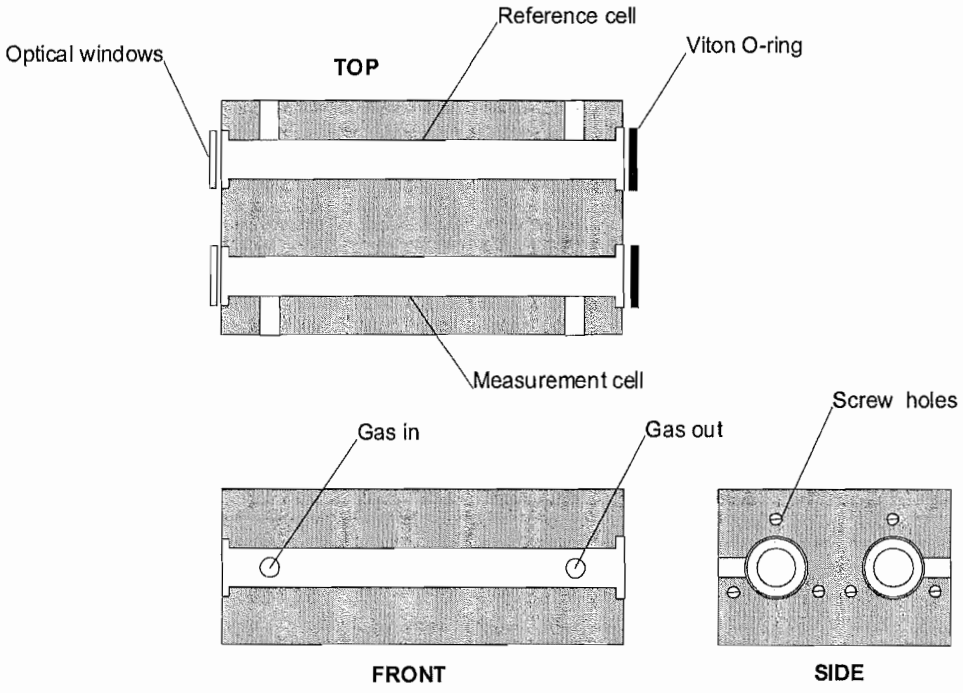

FIGURE 5.11: A cross-section diagram of the gas chamber. This diagram shows that the gas chamber consists of two separate gas cells; the reference and measurement cells.

5.7.2 BEAM SPLITTER / BEAM COMBINER

The two polished silicon wafer slices can be used as beam splitters or combiners in this design. They are fitted in the machined solid aluminium block at 45° to the light beams. Figure 5.12 shows a cross-section diagram of the light beam splitter / combiner. The full dimensions of the beam splitter / combiner engineering drawing is given in Appendix B (b).

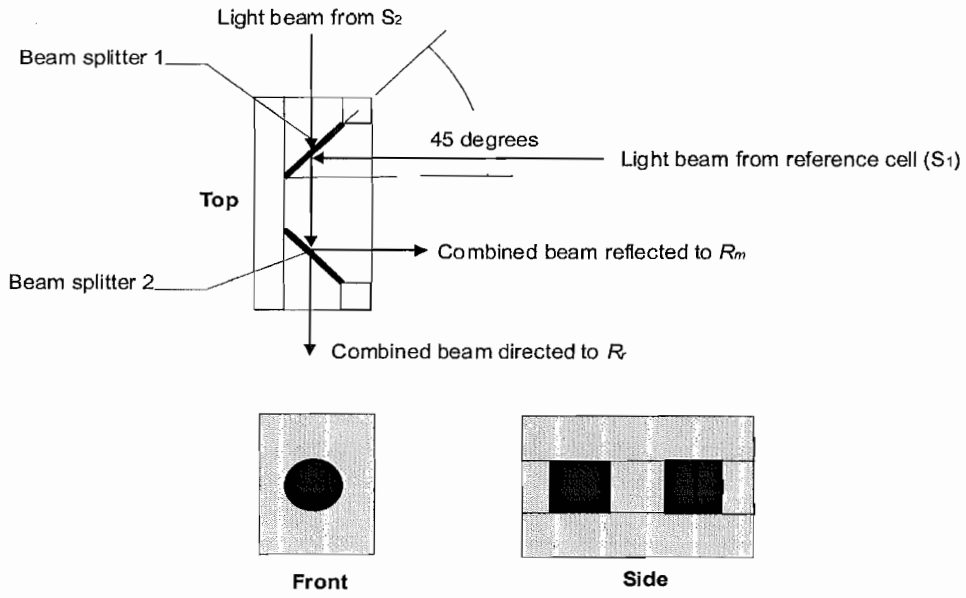

FIGURE 5.12: A cross-section diagram of the beam splitter / combiner part. Two parallel beam splitters can be used to split and combine the light beam from two optical sources.

The position of the parallel beam splitter must be exactly at 45°, as shown in Figure 5.12, to avoid the beam diverting from its actual path. The diverted beam will hit the

wall of the gas cells and produce a multi-reflection light beam and be received as an interference signal at the measurement detector.

Basically, the combination of two silicon wafer slices can be used to split S_1 and S_2 into two portions; the first portion will be reflected and the other one is transmitted at beam splitter 1. The reflected beam of S_1 will combine with the transmitted beam of S_2 and the combination of those beams will split into two portions at beam splitter 2; the transmitted beam will be directed to the reference detector, R_r and the reflected beam is directed to the measurement detector, R_m. The silicon wafer slice makes a beam splitter that will be close to 50% splitting ratio, but has disadvantage because it polarizes the light. This is will be discussed in Chapter 6 (section 6.2.1).

5.7.3 'TOP-HAT' AND FERRULE

Four ferrules are used to mount two LEDs and two optical detectors, respectively. Then, the ferrules are fitted in the 'Top-hat' which functions as the holder for connecting the LEDs and detectors to the gas chamber, as shown in the Figure 5.13. The full dimensions of the ferrule engineering drawing are given in Appendix B (c).

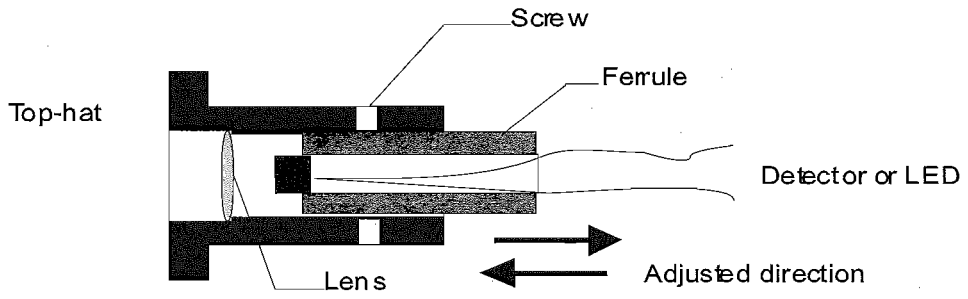

FIGURE 5.13: A cross-section diagram of the 'Top-hat' as a holder of the ferrule. The ferrule can be adjusted in its position to match with the focal length of the lens.

The position of ferrule can be adjusted forward and backward to match with the focal length of the lens. It is important to design the ferrule with an ability to be adjusted as the accurate positioning of the LED at the rear of the lens is necessary to obtain a well collimated beam. For a similar reason, the right positioning of the detector at in front of the lens will result in the better re-focussing of the light beam. Once the right position is achieved, the position of the ferrule will be fixed by a special designated screw.

Figure 5.14 shows the cross-section diagram of the 'Top-hat' and the ferrule. The full dimensions of the 'Top-hat' engineering drawing are given in Appendix B (d). In that figure, the soft silicone rubber or polymer can be used to overcome the angle dependency of the reflected light beam since two parallel beam splitters are used to reflect and combine the light beam.

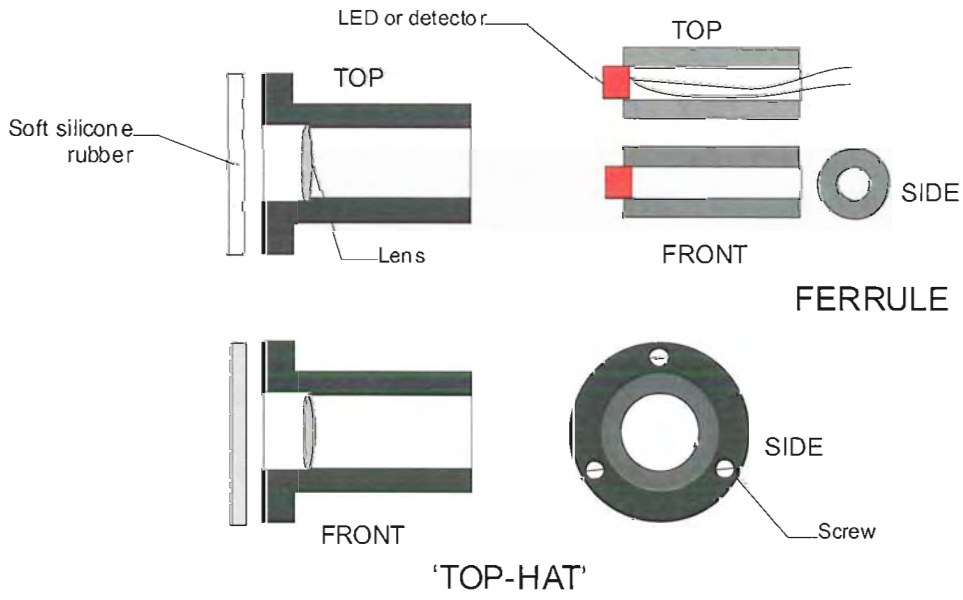

FIGURE 5.14: A cross-section diagram of the 'Top-hat' and ferrule. LEDs and optical detectors are fitted into the ferrule and 'Top-hat' is used to connect the ferrule into the optical detection system. A piece of soft silicone rubber or polymer is placed between the 'Top-hat' and the gas cell as a washer to allow the 'Top-hat' to have some movement.

The light beam path can be controlled by placing a piece of soft silicone rubber or polymer as a washer between the interface of the 'Top-hat' and the gas chamber. By adjusting the different levels of tightening of screws at the 'Top-hat', the different level of forces can be imposed at every screw. Thus, the soft silicone rubber or polymers will crush at the part at which the screw is most tight and allows the 'Top-hat' to be a little bit tilted at its position. This process will be clearly described in the section 5.8.4.

5.7.4 SENSOR SETUP AND ITS OPERATION

The optical design for a handheld methane gas sensor, which was previously presented, is proposed to operate by using a correlation spectroscopy technique. The implementation of that technique to detect the presence of methane, with an unknown concentration contained in the measurement cell, can be described by reference to Figure 5.15. This figure shows a cross-section diagram of the sensor setup consisting of two optical sources and two detectors as required to modulate the received signal by using complementary source modulation (CoSM).

The light beam in this sensor setup is guided by using two lenses to collimate the light beam from S_1 and S_2 and another two lenses to re-focus the light beam to be received at the detector R_r and R_m. Two parallel beam splitters are used to combine and split the light beam. In addition, a piece of soft silicone rubber can be used to control the deviated light path to be at its right position as presented by the straight lines in the Figure 5.15. By that, the deviation of the light beam due to a little bit of inaccuracy of the parallel beam splitter at 45° position can be minimized by an ability to control that light beam path. In a similar way, the deviation of the light beam path due to the possibility of the optical sources emitting the light beam at a very small angle can be corrected.

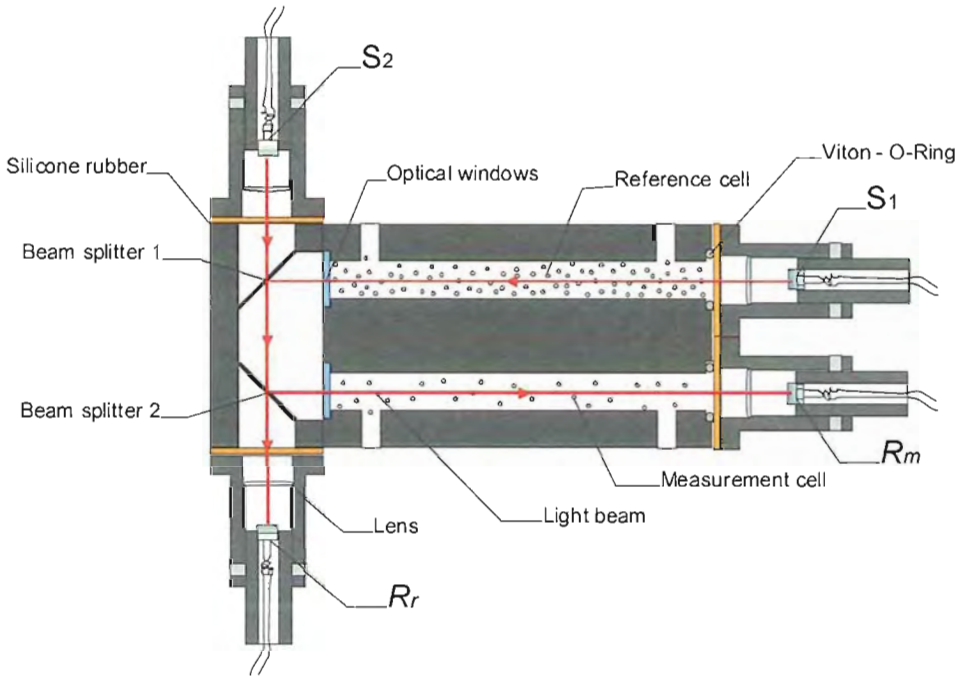

FIGURE 5.15: A cross-section diagram of the sensor setup and the light beam guidance system.

The detection system is operated by alternately on / off switching S_1 and S_2 in anti-phase in which the light beam from S_1 will pass through the reference cell that contains the sample of the target gas with 100% concentration. Then, when the light beam from S_1 reaches the beam splitter 1, a portion of the beam will be transmitted and the other one is reflected. In a similar way, the light beam from S_2 will be transmitted and at the beam splitter 1 the light beam will divide into two portions; a portion is transmitted and the other one is reflected. The reflected portion of the light beam from S_1 will combine with the transmitted light beam from S_2 and be directed to the second beam splitter. Then, the combined beam will divide into two portions of which the transmitted portion will be directed to the reference detector, R_r and the reflected portion is directed to the measurement cell and received as a final signal output at the measurement detector, R_m.

5.8 CONCLUSION

In this chapter, the design of a handheld gas sensor and the experimental setup for methane working at the 2.3 μm absorption band has been presented. It is intuitively predicted that the designated sensor that operates with a correlation spectroscopy technique can result in excellent selectivity. An appreciable sensitivity is predicted even when the short gas cells are employed, as this sensor is working at the 2.3 μm band which offers 220% stronger absorption cross-section than at 1.67 μm band.

CHAPTER 6
OPTICAL SYSTEM PERFORMANCE EVALUATION

6.1 INTRODUCTION

In this chapter, the optical system performance of the handheld sensor which was previously presented in Chapter 5 will be evaluated. The evaluation on the optical system will be carried out to investigate the effect of polarization on the sensor response and optical losses in the handheld sensor.

6.2 OPTICAL SYSTEM PERFORMANCE EVALUATION

There are two aspects that will be evaluated on the optical system of the handheld sensor which was fabricated as presented its design previously in Chapter 5. The first one is about polarization effects and multiple reflections effect due to the use of silicon wafer slices as the beam splitter / beam combiner in the handheld gas sensor design. Then, optical losses in the handheld gas sensor system will be evaluated.

6.2.1 POLARIZATION AND MULTIPLE REFLECTIONS EFFECT

The use of inclined (45^0) silicon slices as beam-splitters for the near infrared region is extremely convenient. These are readily available, low cost and have close to 50% reflection and transmission over a wide spectral band from 1100nm to well beyond 3000nm. However, like most beam-splitters, they are polarisation sensitive, having

different reflections for the two principal polarisation directions. This means that the light reaching the second beam-splitter has already been partially polarised by the first one.

This polarisation will be different for the light beam components received from each of the light sources, as one (the reference-cell beam) was reflected off the first beam-splitter, whilst the other was transmitted by it. Therefore, when we attempt to balance the beam intensities on our first reference detector, to give equal received signals from the two source LEDs at this point, the measurement-cell beam, which is reflected from the last silicon slice, will contain a small residual modulation, due to the polarisation-dependent properties of the second beam splitter. Thus, even when no gas is present in the measurement cell, a small residual modulation would be present. This is not a major problem in practice, as we can take one of two possible corrective measures.

1. We can measure this modulation, with no gas in the measurement cell, and then correct for it in the computer-based signal processing of results.
2. We can adjust the light intensities from the sources to give no modulation index on the second detector, instead of the first, and then monitor the signal intensity ratio on the first detector. We then always adjust the signals on the first detector to be in this ratio. This will be discussed deeply in section 6.2.3.

However, because of the importance of the polarisation by the beam-splitters, it is necessary to calculate the polarisation that we expect to arise. We shall do this by considering the Fresnel refraction and reflection at each surface of the silicon slices, and also take into account all significant multiple reflections from these surfaces. This analysis can be done by considering the polarization effect which resulted when the light beam hits the dielectric medium at a certain angle.

6.2.2 POLARIZATION AND MULTIPLE REFLECTIONS EFFECT ANALYSIS

Light can be polarized or partially polarized by reflection when the light beam hits a dielectric medium. A degree of the polarization depends upon the angle made by the incident light and the refractive index of the medium in which light is transmitted (normally air) and the refraction index of the dielectric medium. Theoretically, an incident light is partially polarized into s-polarized and p-polarized components when the light beam hits and is reflected by a dielectric medium. At a certain incident angle the light beam will be completely polarized and that angle known as polarization angle, θ_p. This angle is given as [92];

$$\tan\theta_p = \frac{n_t}{n_i} \tag{6.1}$$

Where n_t and n_i represent the refractive index of dielectric medium and the medium in which the incident light is transmitted (normally air, $n_i = 1$), respectively. Equation (6.1) is also known as Brewster's law.

Consider that the beam splitter is a silicon wafer slice which has a constant index of refraction 3.5 at the wavelength of the broadband light radiation source. Thus, in considering $n_t = 3.5$ and $n_i = 1$, the polarization angle of the silicon wafer slice can be calculated by using Equation (6.1) and it is found that it occurs at approximately 74°. The fraction of s-polarized and p-polarized of the reflected beam at a particular angle can be determined by using equation (6.2) and (6.3) [92];

$$p-polarized = \frac{\tan^2\left(\theta_i - \theta_t\right)}{\tan^2\left(\theta_i + \theta_t\right)} \tag{6.2}$$

$$s - polarized = \frac{\sin^2(\theta_i - \theta_t)}{\sin^2(\theta_i + \theta_t)} \tag{6.3}$$

where θ_i and θ_t are representing the incident and refraction angle, respectively. Table 6.1 shows the fraction of the *s*-polarized and *p*-polarized and the average value of the polarization fractions at the different angles. Data in the Table 6.1 can be plotted and presented in a graph as shown in Figure 6.1.

TABLE 6.1: Data in the table shows the fraction of the partially polarized light of silicon with refractive index equal to 3.5; *s*-polarized and *p*-polarized at different incident angles. The average of the partially polarized light is given in the column *s*+*p*.

Incident angle	***s*-polarized**	***p*-polarized**	***s* + *p***
10.0	0.3144	0.3037	0.3091
20.0	0.3306	0.2864	0.3085
30.0	0.3602	0.2579	0.3091
40.0	0.4043	0.2148	0.3096
45.0	0.4328	0.1873	0.3101
50.0	0.4668	0.1561	0.3114
60.0	0.5520	0.0824	0.3172
70.0	0.6656	0.0117	0.3387
74.0	0.7201	0.2822×10^{-05}	0.3601
80.0	0.8131	0.0504	0.4317
90.0	1.000	1.000	1.000

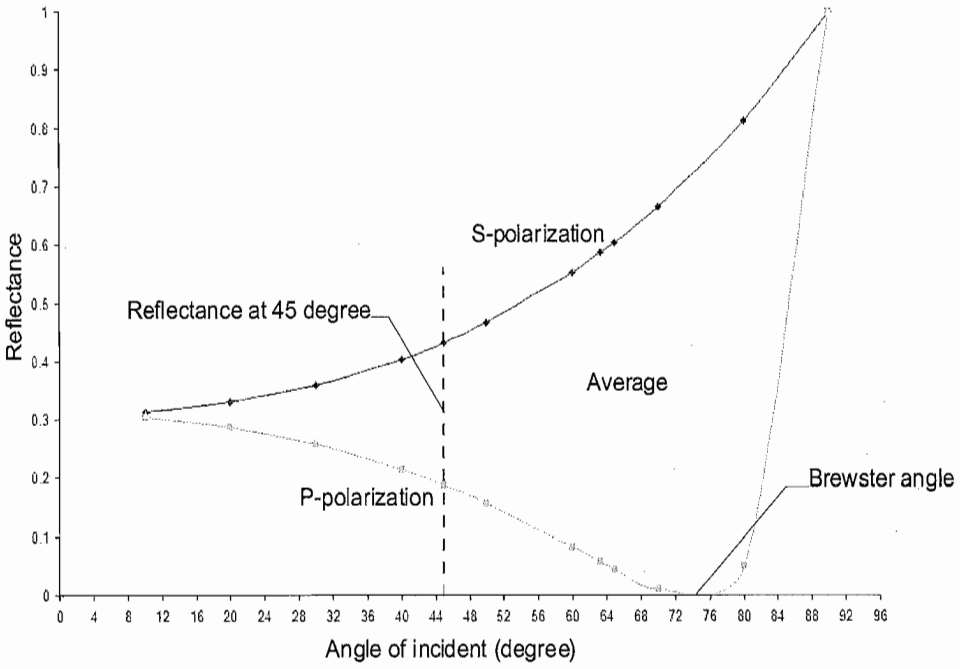

FIGURE 6.1: The graph shows the fraction of partially polarized light beam of the silicon with refractive index equal to 3.5. The fraction of the average of *s*-polarized and *p*-polarized at 45° is approximately 0.3101. The light beam is totally polarized at approximately 74° (Brewster angle) at which only *s*-polarized will be reflected.

The effect of the polarization due to the use of silicon wafer slices as the beam splitter / beam combiner in the handheld sensor system can be examined by considering Figure 6.1 and Figure 6.2.

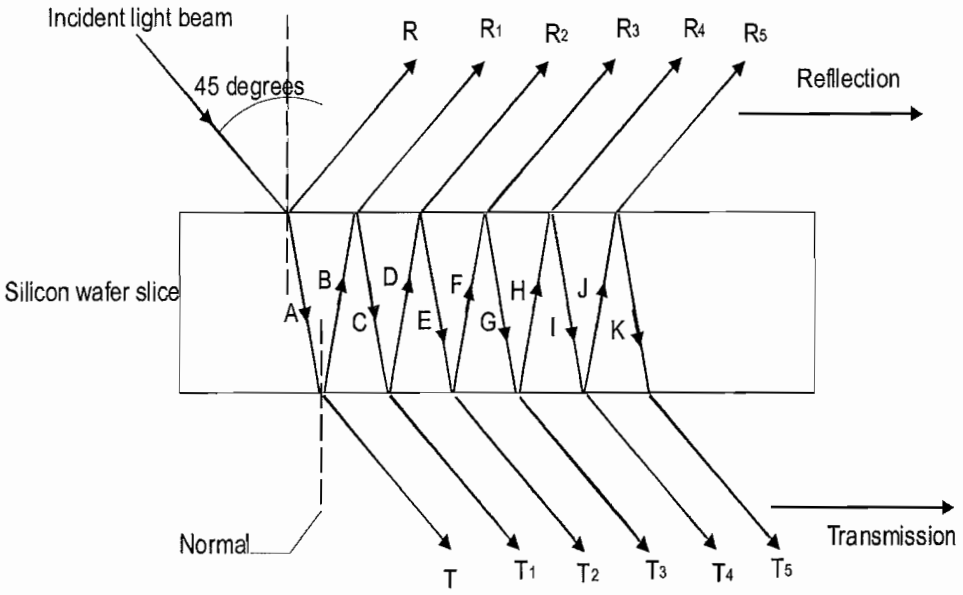

FIGURE 6.2: The diagram shows the phenomena of multiple reflections because of the beam splitter which is used in the handheld sensor has a high refractive index. The multiple reflections became weaker in their light intensities as the number of reflections increases.

The incident light of S_1 or S_2 (refer to Figure 5.6) hits the first air - silicon wafer interface at 45°, as illustrated in Figure 6.2 in which a portion of light beam will refract (indicated as A) and transmit at the other side (indicated as T) whereas the other portion is reflected (indicated as R) at the same angle as the incident angle. Because the silicon wafer has a high refractive index, the refracted light beam, A, will reflect again at the second interface (silicon wafer – air) and then form multiple reflections of the light beam, as depicted in the Figure 6.2.

In that figure, notation 1, 2, 3, 4, 5 and so on represents the number of times a light beam will be reflected and transmitted, and notation B, C... K and so on refers to the reflected and refracted light beam in the silicon wafer slice. The fraction of transmitted and reflected beam can be determined by using Fresnel formulas as given in Equation (5.1) and (5.2) or can be referred to Table 6.1 (s+p) at incident angle = 45°) and it was

found that the fraction of reflection at the first air – silicon wafer slice, R was 0.3086 and for transmission (indicated as A), was 0.6913. These figures are obtained assuming that no energy was lost or, in other words, no light was absorbed because the silicon wafer which was used was very thin. As a consequence of that assumption, the fraction of transmitted light beam (*s*-polarized and *p*-polarized), τ, can be determined more simply as;

$$\tau = 1 - r \tag{6.4}$$

However, in considering the multiple reflection effects, the fraction of the reflected and transmitted light beam, as given by the Equations (5.1) and (5.2), needs to be expanded, giving total reflection fraction, r_{total} and total transmission fraction, τ_{total} as;

$$r_{total} = R + R_1 + R_2 + R_3 + R_4 + R_5 + ...R_n \tag{6.5}$$

$$\tau_{total} = T + T_1 + T_2 + T_3 + T_4 + T_5 + ...T_n \tag{6.6}$$

where R = r, $R_1 = r\tau^2$, $R_1 = r^3\tau^2$, $R_2 = r^5\tau^2$, $R_3 = r^7\tau^2$, $R_4 = r^9\tau^2$, $R_5 = r^{11}\tau^2$, and so on whereas $T = \tau^2$, $T_1 = r^2\tau^2$, $T_2 = r^4\tau^2$, $T_3 = r^6\tau^2$, $T_4 = r^8\tau^2$, $T_5 = r^{10}\tau^2$, and so on. Figure 6.3 (a) and (b) shows the fraction of reflectance and transmittance at the first air – silicon wafer slice interface by increasing the number of reflections and transmissions.

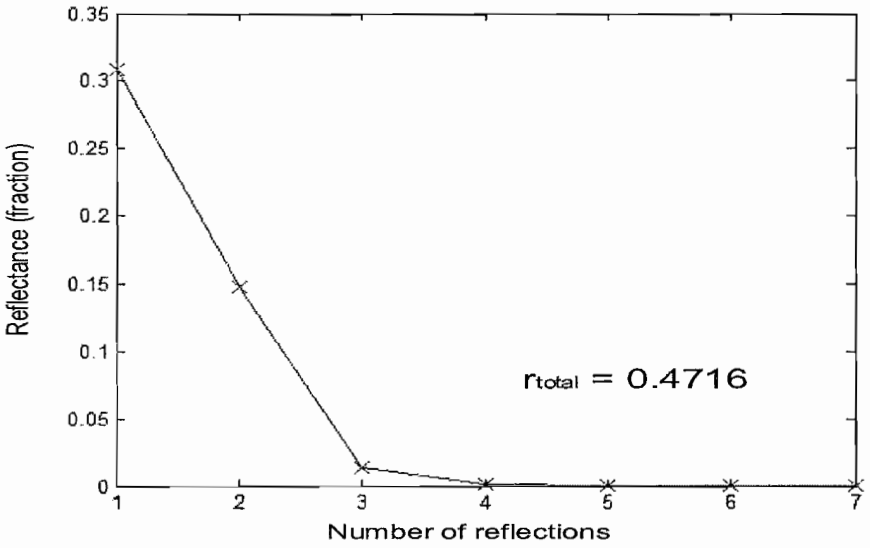

(a)

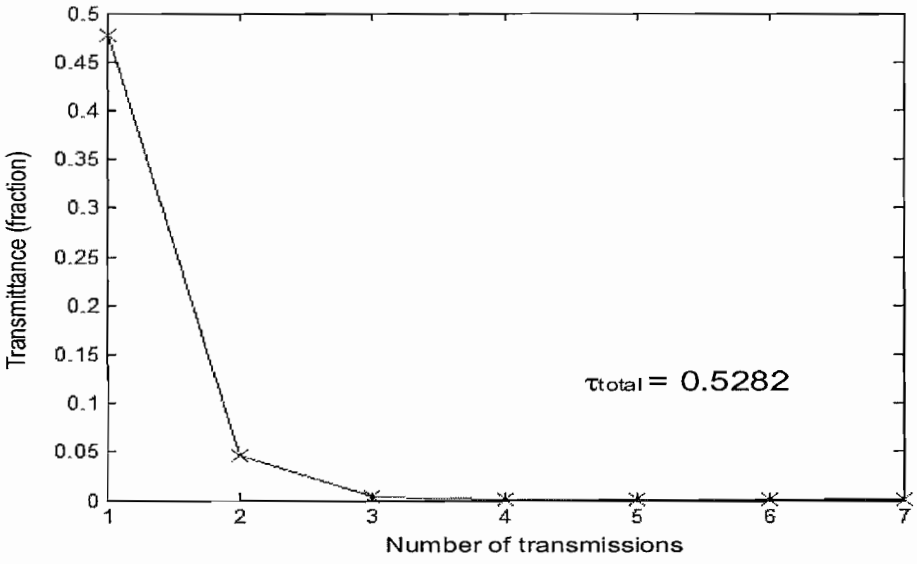

(b)

FIGURE 6.3: Figures show (a) that the fraction of reflection decreases as the number of reflections increases and (b) the fraction of transmission decreases as the number of transmissions increases at the first beam splitter. In both cases, the decreasing pattern shows drastic changes.

By using Equation (6.5) and (6.6), r_{total} and τ_{total} for both S_1 and S_2 at the first beam splitter are found to be 0.4716 and 0.5282, respectively. These figures are obtained based on calculations for only seven times multiple reflections as it is considered that after seven times, the fraction of the reflected light beam is down to almost zero. Both of the r_{total} and τ_{total} values obtained agree well with the value obtained from the spectrophotometer measurement, which was given in Figure 5.14 as 0.5313 at the average for the transmission fraction or 0.4687 for the reflection fraction. The ratio of reflectance to transmittance, r_{total} / τ_{total} at the first beam splitter can be calculated and is found to be 0.8928. This is illustrated in the Figure 6.4.

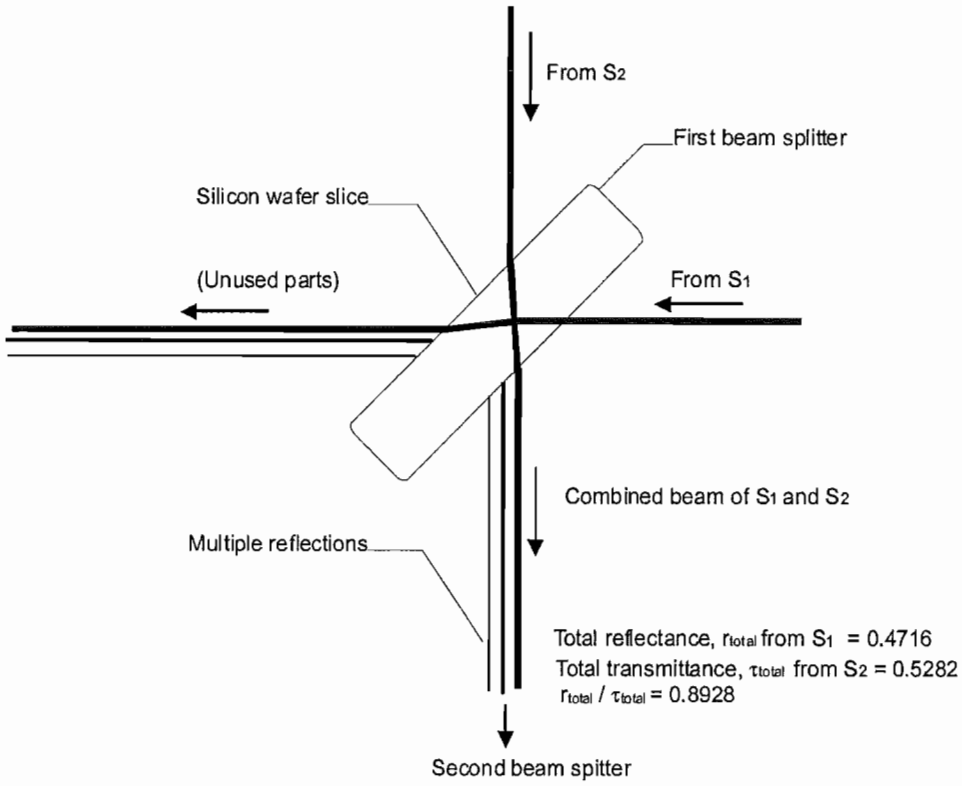

FIGURE 6.4: The fraction of light beam for both the optical sources, S_1 and S_2 reflected and transmitted at the first beam splitter.

In a similar way, the fraction of reflectance and transmittance at the second beam splitter can be determined. In this case, the fraction of reflection and transmission light beam at the beam splitter one is considered as a new incident light beam which will hit the second beam splitter. Previously, the fraction of light beam that will be reflected and transmitted when it hits the first air – silicon wafer slice has been calculated giving r = 0.3086 and τ = 0.6913. Thus, the fraction of both light beam S_1 and S_2 that will be reflected and transmitted at the second beam splitter can be calculated as;

1) The total reflected light beam of S_1 will be divided into two components, one component will be reflected again and directed to the measurement detector and the other components will be transmitted and directed to the reference detector. The new fraction of reflected light beam at the second beam splitter r_1, and transmitted, τ_1 are calculated as in the equations below;

$$r_1 = r_{total} \times r = 0.4716 \times 0.3086 = 0.1455 \tag{6.7}$$

$$\tau_1 = r_{total} \times \tau = 0.4716 \times 0.6913 = 0.3260 \tag{6.8}$$

2) The transmitted light beam of S_2 is divided into two components, one component will be reflected and directed to the measurement detector and the other components will be transmitted and directed to the reference detector. The fraction of reflected light beam at the second beam splitter r_2, and transmitted, τ_2 are calculated in the equations as;

$$r_2 = \tau_{total} \times r = 0.5282 \times 0.3086 = 0.1630 \tag{6.9}$$

$$\tau_2 = \tau_{total} \times \tau = 0.5282 \times 0.6913 = 0.3651 \tag{6.10}$$

Now, considering that the effect of multiple reflections occurs at the beam splitter two, the total fraction of light beam that will be reflected and transmitted at the second beam splitter can be calculated by using Equation (6.5) and (6.6) and considering the first seven reflections as shown in Figure 6.5. All calculations can be summarized as;

1. The total fractions of transmitted light beam at the second beam splitter, $\tau_{1\text{-total}}$ and $\tau_{2\text{-total}}$ that will be received at the reference detector are;

$$\tau_{1-total} = 0.1086 \tag{6.11}$$

$$\tau_{2-total} = 0.1369 \tag{6.12}$$

2. The total fractions of reflected light beam, $r_{1\text{-total}}$ and $r_{2\text{-total}}$ that will be received at the measurement detector are;

$$r_{1-total} = 0.1613 \tag{6.13}$$

$$r_{2-total} = 0.1853 \tag{6.14}$$

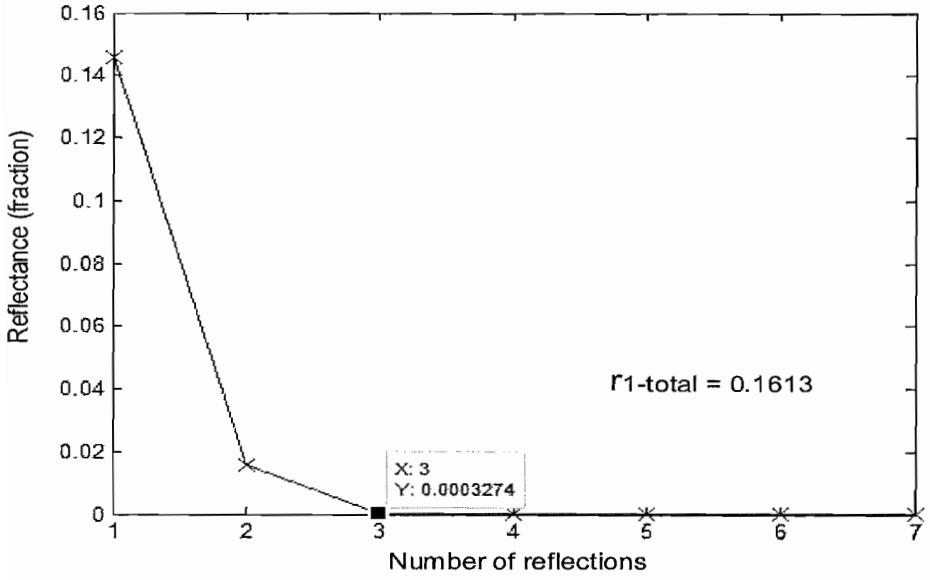
Reflectance (fraction)
Number of reflections
r1-total = 0.1613
X: 3
Y: 0.0003274

(a)

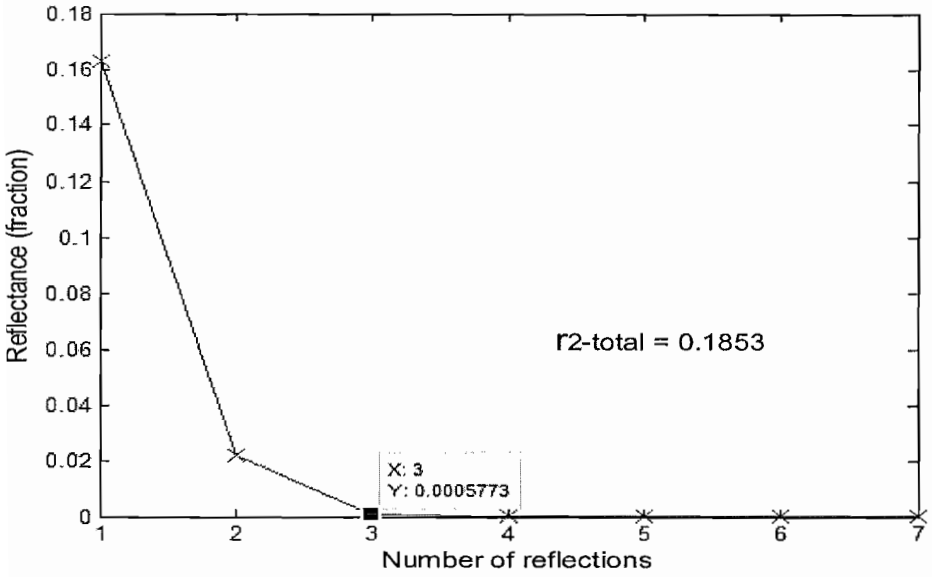
Reflectance (fraction)
Number of reflections
r2-total = 0.1853
X: 3
Y: 0.0005773

(b)

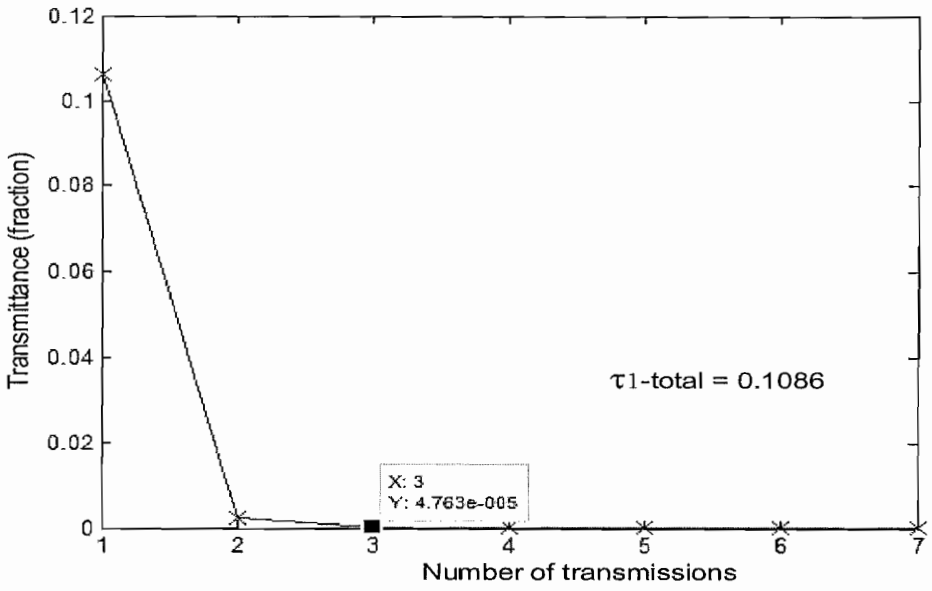

(c)

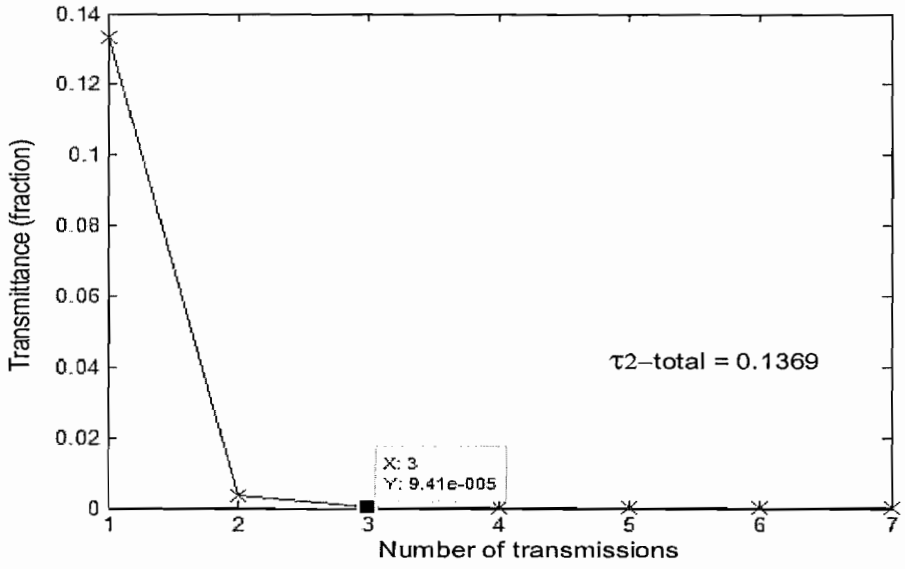

(d)

FIGURE 6.5: Figures show (a) and (b), the fraction of reflection decreases as the number of reflection increases and for both the sources; (c) and (d), the fraction of transmission decreases as the number of transmissions increases for both sources at the second beam splitter.

The fraction of reflected and transmitted light beam from S_1 and S_2 which passed through at both beam splitters and was received at both detectors can be simplified by reference to Figure 6.6.

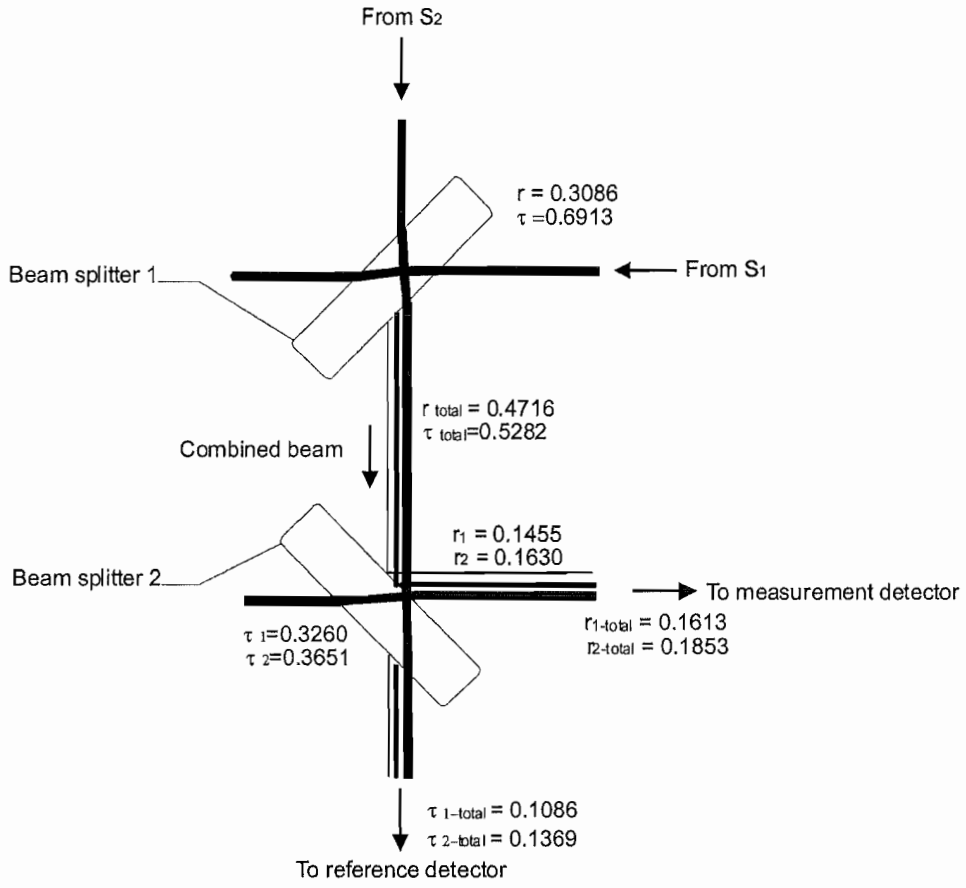

FIGURE 6.6: The fraction of light beam for both optical sources, S_1 and S_2 reflected and transmitted at the first and second beam splitter. The total fraction of the reflectance ($r_{1\text{-total}}$ and $r_{2\text{-total}}$) and transmittance ($\tau_{1\text{-total}}$ and $\tau_{2\text{-total}}$) for both sources, S_1 and S_2 are the final fraction of light beam that will be detected at the measurement and reference detector, respectively.

From Figure 6.6, there are two important points that need to be highlighted which are;

1. The total fraction of transmitted light beam at the first and second beam splitters is found to be reduced because of Fresnel loss contributed by the multiple reflections effect.
2. It is found that the fraction of the light beam received at the reference and measurement detector is not equal and the fraction of light beam originating from S_1 and S_2, received at both detectors, is also not equal. In the case of S_1, the ratio of light beam that is reflected to that transmitted is found to be 1.4853 ($r_{1\text{-total}}$ / $\tau_{1\text{-total}}$) and the ratio of light beam S_2 that is reflected to that transmitted is found to be 1.3535 ($r_{2\text{-total}}$ / $\tau_{2\text{-total}}$). Whereas, the ratio of light beam originating from S_2 to S_1 received at the reference detector is 1.2606 ($\tau_{2\text{-total}}$ / $\tau_{1\text{-total}}$) and the ratio of light beam originating from S_2 to S_1 received at the measurement detector is 1.1488 ($r_{2\text{-total}}$ / $r_{1\text{-total}}$).

6.2.3 THE POLARIZATION AND THE MULTIPLE REFLECTION EFFECT ON THE SENSOR RESPONSE

In Chapter 4, the derivation of the sensor response (modulation index) for the correlation spectroscopy system was presented by using numerical analysis and it is given by Equation (4.10). The constant k in the Equation (4.10) is the factor that is needed to balance the optical intensities of the S_1 and S_2 at the reference detector, as required in the CoSM approach.

The unbalanced optical intensity received at the reference detector is due to the fact that the light path passed through the reference cell is absorbed by gas molecules in the reference cell whereas the light path S_2 is not. In practice, even in the case where the reference cell is empty and two exactly identical light sources are used, it is intuitively predicted that the balancing between S_1 and S_2 will be slightly different. There are a few factors such as improper collimating of the light beam which is passing through the handheld gas sensor system that can contribute to the unbalancing of the optical intensities between S_1 and S_2 at both detectors. The polarization and multiple reflections

effect, as discussed previously and simplified in Figure 6.8, for instance are found to significantly contribute to that problem.

However, the modulation index (sensor response), as derived in Chapter 4 and given by Equation (4.10), is not affected by any factors which are causing the intensities of S_1 and S_2 to vary at both detectors. This is because in the CoSM system, any changes between both light sources which are passing through the measurement cell will be corrected first, prior to the combination of the light beam that will be used for probing the gas of interest in that cell. This is achieved as the CoSM system is designed and equipped with a feedback system for self referencing the sensing system.

The feedback system functions by adjusting the current level which is supplied to the optical sources. By adjusting the supply current to a certain level, the intensities of S_1 and S_2, received at the measurement detector, can be equalized. Any changes of the S_1 and S_2, after signal equalization at the reference detector, can be corrected as a PC controller is used to monitor any possible changes in the output signal received at the measurement detector.

Then, the equalized combined beams are prepared to interrogate an unknown concentration of the gas of interest. In the case where the reference cell is filled with a 100% concentration of the target gas and the measurement cell is empty, the light intensity for both light sources will be similar. If the measurement cell is filled with the gas of interest, then S_2 will be absorbed by gas molecules, whereas S_1 is not affected as it has less available energy over the wavelength which matches the absorption spectrum of the sample gas in the reference cell (as previously discussed in Chapter 4). Therefore, the gas response (modulation index) is only the differential between S_1 and S_2.

Obviously, the effects of polarization and multiple reflections on the modulation index (sensor response) were corrected by the feedback system. In a similar way, this system (the feedback) is able to correct any other factors which could give an effect of varying the intensities of both LEDs.

6.2.4 OPTICAL LOSS MEASUREMENT

The optical losses in the handheld sensor can be evaluated by measuring the optical signal received in the direct measurement and in the handheld sensor system. Direct measurement is referred to the measurement of optical signal at the optical detector by directly measuring the light radiation from the optical source (LED) as is depicted in Figure 6.7.

In that figure, V refers to the voltmeter, V_s and I_s represent voltage and current supply, respectively. A precision current source (LDX – 3412, ILX Lightwave) is used to supply a stable current for operating the LED. The photocurrent developed at the optical detector (G5853-01 - Hamamatsu) is converted to voltage and amplified by using a transimpedance amplifier with a 100 KΩ resistor. Heat produced at the LED and detector is removed by heat sinks. Data is collected by measuring S_1 and S_2 at the reference (R_r) and measurement (R_m) detector

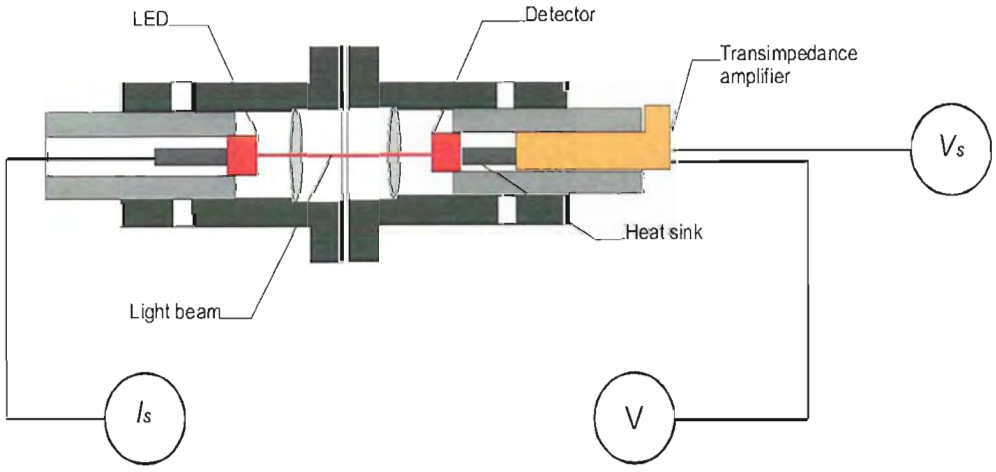

FIGURE 6.7: The diagram shows a direct measurement setup of the light radiation from the LED that is detected by the optical detector. The light beam from the LED is collimated and then focussed onto the small active area of the optical detector.

Basically, the position of both the LED's and detector's ferrules are adjusted to their best position, at the rear of the lens, before the optical system can be evaluated, to minimize the optical loss due to a poorly collimated light beam. In a similar way, the correct position of the optical detector can maximize the detecting signal as a result of the better re-focussing of the light beam on the small active detector area. The measuring data of the received optical signal, in the direct measurement, at both detectors is shown in Table 6.2.

TABLE 6.2: The received signal, detected by the reference and measurement detector, in the direct measurement.

DETECTORs / LEDs	***S1***	***S2***
R_m (Volt)	2.210	1.936
R_r (Volt)	2.180	1.945

By a similar approach, optical signals received in the handheld sensor system can be measured. The light beam from S_1 will pass through the reference cell and will be reflected when it hits the first silicon slice (beam splitter) as depicted by arrows in Figure 6.8. Then the reflected light beam will hit the second beam splitter where a portion will be transmitted and received by the reference detector, R_r, whereas the other portion will be reflected again and received by the measurement detector, R_m.

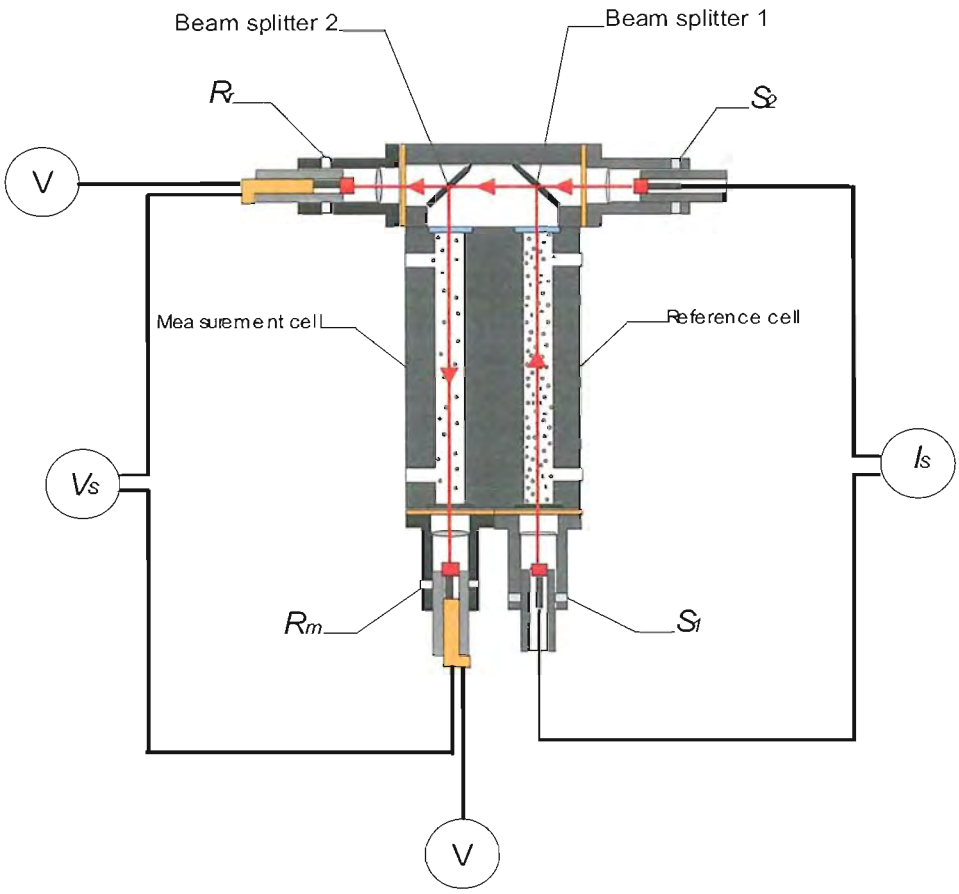

FIGURE 6.8: The diagram shows the setup for measuring the received optical signal in the handheld sensor system. The light beam from S_1 and S_2 will hit the first and second beam splitter and then be received by R_r and R_m. V_s and I_s represent the voltage supply and current source, respectively.

In a similar way, the light beam from S_2 will hit the first beam splitter and be transmitted until reaching the second beam splitter. At the second beam splitter, a portion of light beam will be transmitted and received by R_r whereas the other portion will be reflected and directed to R_m. The received optical signal at R_r and R_m from both the light sources are given in Table 6.3.

TABLE 6.3: The received signal detected by the reference and measurement detector in the handheld sensor system.

DETECTORs / LEDs	***S1***	***S2***
R_m (Volt)	0.194	0.281
R_r (Volt)	0.333	0.715

Optical losses in decibel (dB) of the received optical signal at R_r and R_m in the handheld sensor system can be calculated by using the equation below;

$$Loss(dB) = 10\log_{10}\left(\frac{P_{system}}{P_{direct}}\right) \tag{6.15}$$

where P_{system} refers to the optical power received at the optical detector (reference or measurement detector) in the handheld sensor system and P_{direct} represents the optical power received at the optical detectors in the direct measurement. Equation (6.15) can be re-written in the form of voltage as the photocurrent (the received optical signal at the optical detector) was converted to voltage by the transimpedance amplifier. It is given as;

$$Loss(dB) = 10\log_{10}\left(\frac{V_m}{V_r}\right)^2 \tag{6.16}$$

where V_m and V_r refer to the amplified voltage from R_m and R_r, respectively. Based on data in Tables 6.2 and 6.3, optical loss for each measurement can be calculated and is

given in Table 6.4 (a) in decibel units (dB) and Table 6.4 (b) gives the received optical signal as a percentage (%).

TABLE 6.4: (a) Optical losses in the handheld sensor system are obtained by using Equation (6.2) and given in decibel (dB) units and (b) the received optical signal in the handheld sensor system as percentage (%) relative to the received optical signal in the direct measurement.

(a)

DETECTORs / LEDs	**S_1**	**S_2**
Rm (dB)	-21.1	-16.8
Rr (dB)	-16.3	-8.7

(b)

DETECTORs / LEDs	**S_1**	**S_2**
Rm (%)	8.8	14.5
Rr (%)	15.3	36.8

From Table 6.4 (a) and (b), the light path from S_1 to R_m shows the biggest loss which dropped 21.1 dB or only 8.8% was received at R_m. This is because the light path from S_1 passed through two lenses, two optical windows, two beam splitters and the longest distance before being received by R_m. The light paths from S_1 to R_r and S_2 to R_r show nearly equivalent optical losses at around 16.5 dB or received signal around 15% at R_r as in both measurements a similar distance and similar number of optical components (two lenses, two beam splitter, and one window) were involved prior to being received at R_r. Finally, the light path from S_2 to R_r shows the lowest optical losses which, at

around 9 dB, or received at R_r around 37%, as the distance of the light path in that measurement is the shorter and it only passed through two lenses and 2 beam splitters. From all of the figures which are given, it is predicted that the optical system is working well and has a sufficient light transmission received at both the reference, R_r and measurement, R_m detectors.

6.3 CONCLUSION

There are two important outcomes which were extracted from the evaluation carried out on the optical system of the handheld sensor. The first one was that it was found that the signals received from S_1 and S_2 at the reference and measurement detectors are not equal. This is because of the effects of polarization and multiple reflections of the light, as silicon wafer slices were used as the beam splitter / beam combiner. However, these effects do not affect the sensor response. This is because the CoSM system of the CoSp was designed to be a self referencing system. In practice, this is important to equalize the feedback residual before any measurement is done. The second one, results from measuring the optical losses in the optical system it was found that the handheld sensor shows a good optical system. Nevertheless, as predicted the received signal at both detectors shows big losses as silicon wafer slices were used as beam splitter / combiner.

CHAPTER 7

SENSOR PERFORMANCE AND RESULTS DISCUSSION

7.1 INTRODUCTION

In this chapter, performance of the handheld sensor in detecting methane will be evaluated. Firstly, the experimental setup of the handheld methane sensor is presented. Then, results from simulation are generated to predict the sensor response (modulation index) when methane with an unknown concentration is introduced into the measurement cell. The cross-sensitivity of a few selected gases, which might be present as contaminants and influence the sensor response, will be determined. Then, results which are obtained from theoretical calculations and measurement will be discussed and compared. Finally, the sensitivity of the sensor will be calculated.

7.2 THE EXPERIMENTAL SETUP

The experimental setup consists of two main parts which are the gas sensor and signal processing unit, as illustrated in Figure 7.1. The operation of the sensor has been discussed in the previous section and in Figure 7.1 it is shown that the sensor is equipped with Personal Computer (PC) controller.

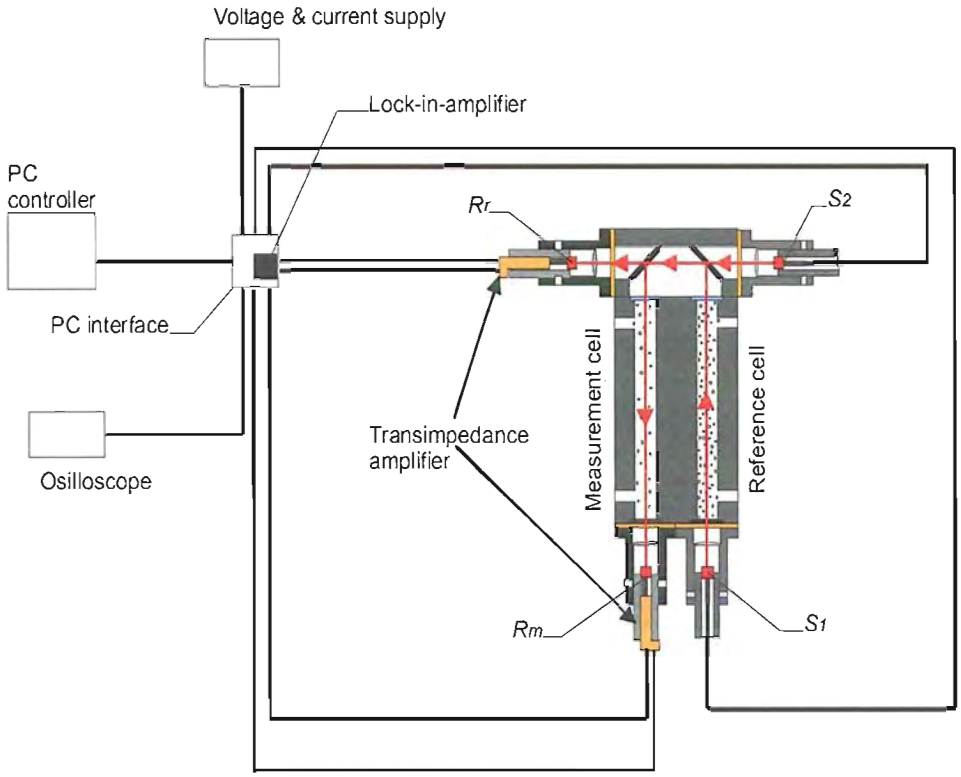

FIGURE 7.1: A schematic of the experimental setup of the gas sensing system. A PC controller is used in the sensing system for processing the measurement signal to become the final output of the sensor response (modulation index).

The PC controller is used to drive an alternating on / off hence switching the light sources S_1 and S_2 in anti-phase, and also to adjust the current level supplied to the optical sources. By these functions, the feedback system can be simply controlled by changing the feedback residual function (to adjust the residual current) at the computer display. In addition, an integration time can be changed depending upon the conditions in which the response time is required.

Basically, the photocurrent developed at the reference and measurement detector, resulting from measuring the concentration of the unknown gas in the measurement cell, will be amplified and converted into voltage. For that purpose, a transimpedance

amplifier with 100KΩ impedance is used. Then, the amplified voltage will be processed by using a lock-in-amplifier (AD820, www.analog.com) to reduce the associated noise in the measurement, thus increasing the SNR of the received signal.

A triple output DC power supply (E3631A Hewlett Packard) is used to supply a stable current source to operate the LEDs and to supply voltage to operate both the detectors. An oscilloscope is used to observe the process of balancing the intensities of both LEDs at the reference detector. The sensor response (modulation index) is processed by programming the computer to directly calculate and display the final results at the PC screen.

7.3 THE THEORETICAL MODEL

The theoretical model of the CoSM method of the CoSp system has been developed by using a numerical analysis approach as proposed by Chambers et al. [67] to predict the sensor response (modulation index) and the selectivity of our sensor. A few modifications to that model (proposed by Chambers et al.) are made to fit in with the developed handheld gas sensor, as was previously discussed in section 4.4. The gas spectrum which was used to simulate the theoretical results was generated from HITRAN database. Equation (4.10), which was derived previously, will be used to calculate the modulation index (m); a gas response parameter which is proportional to the concentration of target gas to be determined in the measurement cell.

This theoretical model, which was developed based on Equation (4.10), can be graphically illustrated by plotting the transmission spectrum of methane, all the optical components' transmission spectra, and the responsivity spectra of the reference and measurement detectors and the emission spectra of LEDs, S_1 and S_2, as shown in the Figure 7.2. In that figure, the transmission spectrum of the methane centred at 2.3 μm is generated by using the HITRAN database which assumes the presence of 100% vol / vol, the path length of interaction is 0.1 m, at a temperature of 296 K and at a pressure of 1.013 bar. The emission spectra of the LEDs and responsivity of the detectors are

obtained from manufacturer's datasheets and all the transmission spectra of the optical components are measured by using a spectrophotometer (Cary 500 UV-VIS-NIR). All data was interpolated by using MATLAB to have a similar interval between 1950 nm and 2600 nm as shown in Figure 7.2.

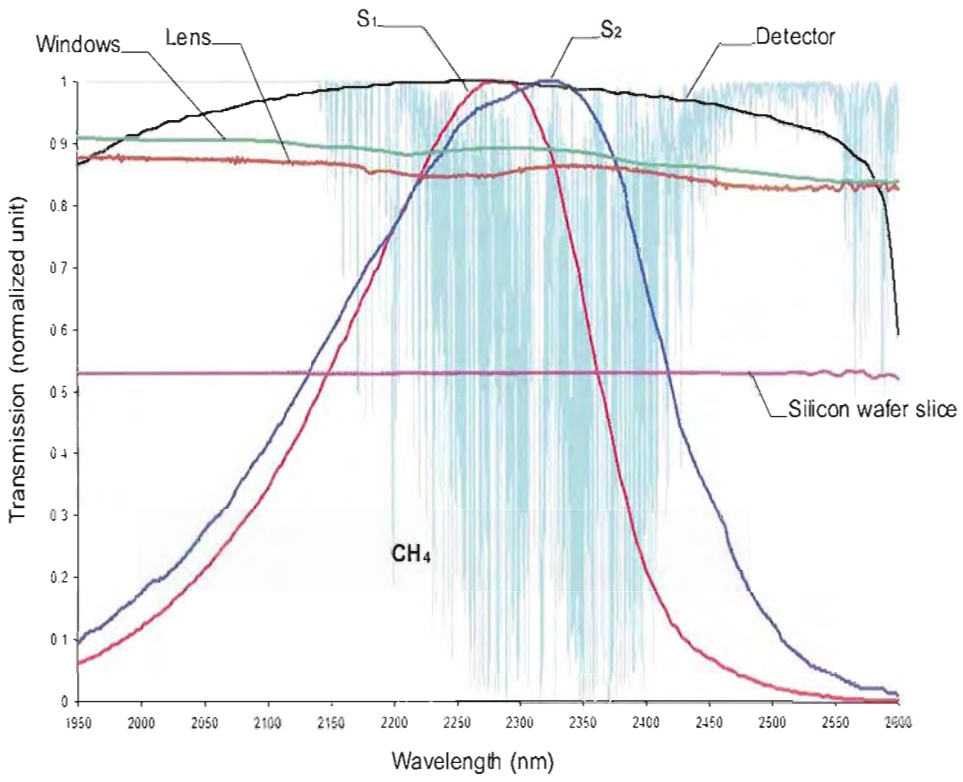

FIGURE 7.2: A graphical illustration of the numerical model of the sensor. S_2 and S_1 represent the spectral emission of the LEDs which are used to probe the presence of unknown methane concentrations in the measurement cell. The optical detectors and optical components which are used in the sensing system show a flat characteristic over the range of the light sources spectra. Both the LEDs' emission spectra and the detector responsivity spectra are obtained from manufacturer's datasheets whereas for all the optical components the data is measured by using a spectrophotometer.

According to the manufacturer's datasheet, the spectral emissions of S_1 and S_2, which are used in the handheld sensor, have a similar Full Width at Half Maximum (FWHM) of 220 nm. They show a non-identical emission spectrum and have a different emission peak (S_1-peak = 2.35 μm and S_2-peak = 2.31 μm) and spectral distribution shape, as shown in Figure 7.2. The reference and measurement detector are assumed to have a similar responsivity spectrum.

Apparently, from Figure 7.2, the detector responsivity and all the optical components' transmission spectra are approximately flat over the range of the interaction regions thus they can be considered as constant. By considering the given characteristics of S_1, S_2 and that 100% vol / vol methane is filled in the reference cell, the value of the feedback constant, k, as given in Equation (4.7), can be calculated and was found to be 0.6150. Therefore, Equation (4.10) can be re-written as;

$$m = 2\left\{\frac{\int S_1(\lambda).T_r(\lambda).T_m(\lambda).d\lambda - 0.6150\int S_2(\lambda).T_m(\lambda).d\lambda}{\int S_1(\lambda).T_r(\lambda).T_m(\lambda).d\lambda + 0.6150\int S_2(\lambda).T_m(\lambda).d\lambda}\right\} \tag{7.1}$$

Now this equation can be used to calculate the resulting modulation index when unknown methane concentrations are introduced into the measurement cell.

7.3.1 Results on Varying Methane Concentrations

By generating (HITRAN database) a set of methane spectra for different concentrations, a set of modulation indices can be calculated by using Equation (7.1). The set of modulation indices which were calculated represent the concentrations of the 100%, 80%, 50%, 25%, 4%, and 0% methane as given in Table 7.1. All figures shown in Table 7.1 were obtained by putting the transmission spectra of the measured concentrations, as $T_m(\lambda)$ and the transmission spectrum of 100% vol / vol methane as, $T_r(\lambda)$ in the

Equation (7.1). Calculations are made based on the assumption that the transmission spectra of the optical sources and methane samples are generated with 0.1 m path length at 296 K and a total pressure of 1.013 bar. Then, a graph to describe the relation between modulation indices and methane concentrations was plotted as depicted in Figure 7.3.

TABLE 7.1: Data showing a set of simulation results which was generated by using Equation (4.10) for methane with 100%, 80%, 50%, 25%, 4%, and 0% volume / volume concentration.

Methane concentration (% vol/vol) (% vol/vol)	**Modulation index (m)**
0	0
4	0.0119
25	0.0544
50	0.0828
80	0.1037
100	0.1136

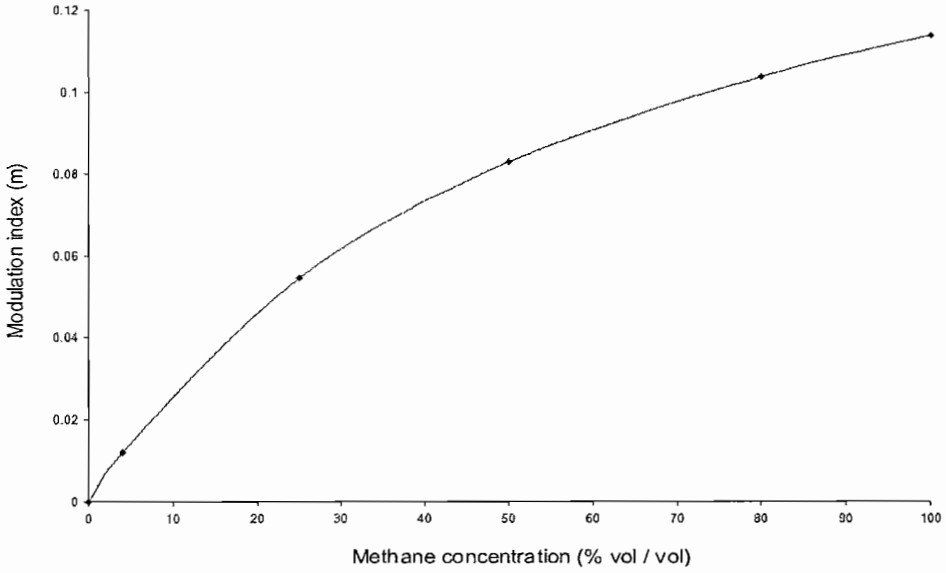

FIGURE 7.3: A set of modulation indices as the sensor response represent the concentration of the 100%, 80%, 50%, 25%, 4%, and 0% methane. All results are calculated by using Equation (4.10).

The graph in Figure 7.3 shows a linear relation between the modulation index and methane concentration at low methane concentrations and it becomes nonlinear at higher concentrations. A similar pattern was presented by Kebabian et al. [44] in their experimental results which measured nitrogen dioxide (NO_2), Crowder et al. [93] in their experiments measuring NO_2, Chambers et al. [67] in their theoretical results for methane, and Cheung et al. [68] in both their theoretical and experimental results measuring acetylene (C_2H_2).

This pattern can be explained by reference to the Beer-Lambert's law which was discussed in section 3.3. Basically, the Beer-Lambert's law shows a linear relation for the absorbance increase obtained by increasing the absorber concentration. However, this law does not apply at higher concentrations of absorbing species as absorption at high

concentrations no longer obeys Beer-Lambert's law. This is due to the fact that at high concentration the light is more strongly absorbed by absorber species.

7.3.2 RESULTS ON MEASURING CROSS-SENSITIVITY

A few available gas species in the HITRAN database are chosen to investigate their tendency to act as contaminants in the methane measurement. Commonly, the contaminant, or influences by other gases in the measurement, is referred to as crosstalk or cross-sensitivity measurement. It is defined as the measured values generated by gases other than the gas of interest [94].

Water vapour is one of the selected gases as it shows a significant absorption spectrum in the infrared regions. In addition, carbon dioxide (CO_2) and acetylene (C_2H_2) are two common gases that will be examined for their influence on the methane measurement. Figure 7.4 graphically shows the presence of H_2O, CO_2, and C_2H_2 as contaminants in the region of methane – light radiation interaction. All the gas transmission spectra were generated by considering the path length to be equal to 0.1 m, at 296 K / 23° C, at a pressure of 1.013 bar and by assuming all of those gases to have 100% vol/vol concentration. Then, all transmission spectra were equalized for their wavelength interval by interpolating the generated data in MATLAB.

In Figure 7.4, it can be seen that the presence of the H_2O absorption spectrum is the most significant contaminant which is present in the region of the methane – optical source interaction (between 1950 nm and 2600 nm). compared with CO_2 and C_2H_2. The C_2H_2 transmission spectrum is not included in the interaction region as the interaction region is limited by the bandwidth of both LEDs.

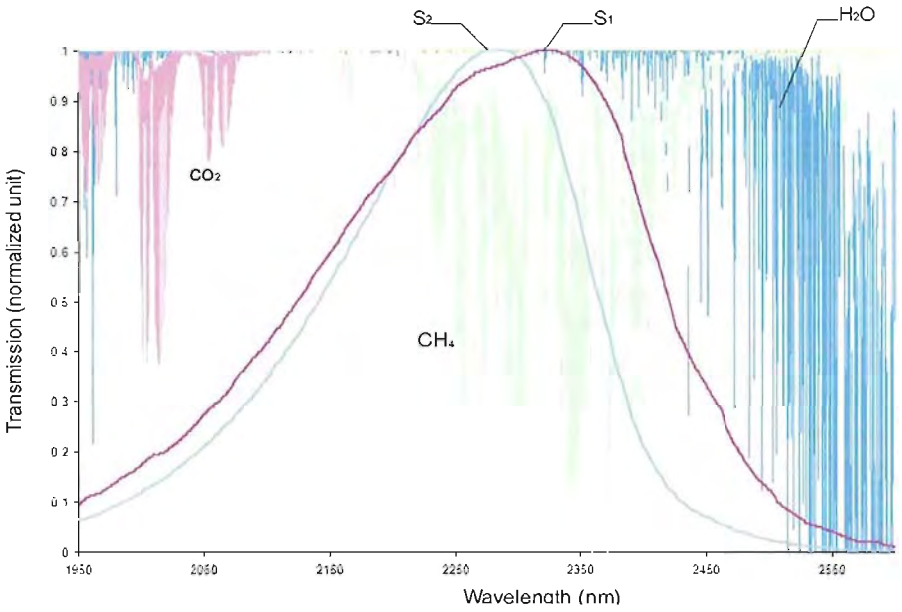

FIGURE 7.4: The graph shows a few selected gases present as contaminants in the methane transmission region, centred at 2.3 μm. The presence of those gases will influence the sensor response (modulation index) and can be measured by putting their transmission spectra as the target gas which is present in the measurement cell in Equation (4.10).

It is predicted that the cross-sensitivity of H_2O will be the highest, and followed by CO_2, whereas no cross-sensitivity by C_2H_2 is expected. This prediction was made by considering the results obtained from numerical analysis on the evaluation of the presence of contaminant gases, T_c within the emission spectrum of the S_1 and S_2. Mathematically, this analysis is given as a function of wavelength, λ as:-

$$C = \int S(\lambda) T_c(\lambda) d\lambda \tag{7.2}$$

where C is the absorbance due to the presence of contaminant gases and S represents S_1 or S_2. The presence of the transmission spectra of H_2O and CO_2 within the emission

spectrum (the contaminant gases which are absorbing the light radiation) of S_1 and S_2 as given by Equation (7.2) are shown in Figure 7.5.

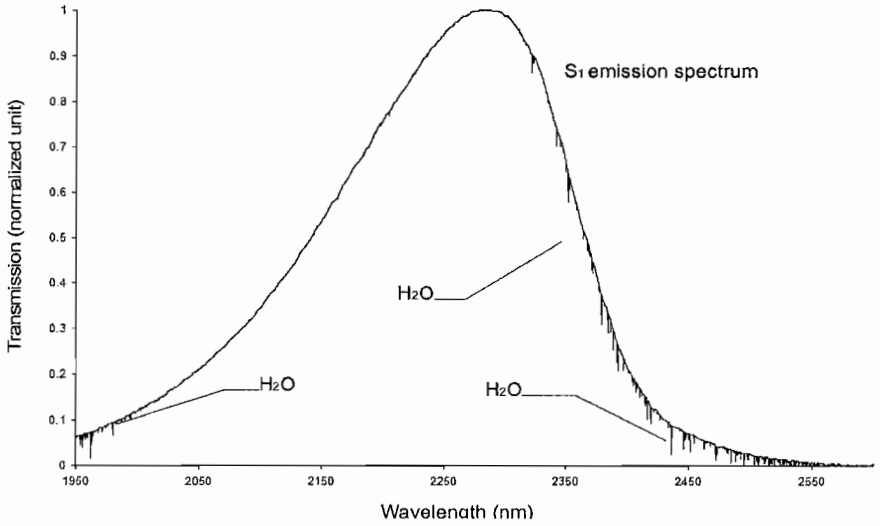

(a)

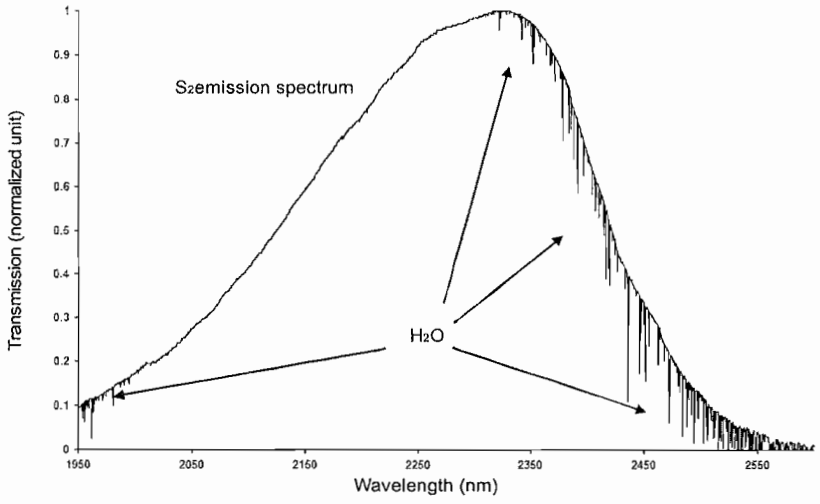

(b)

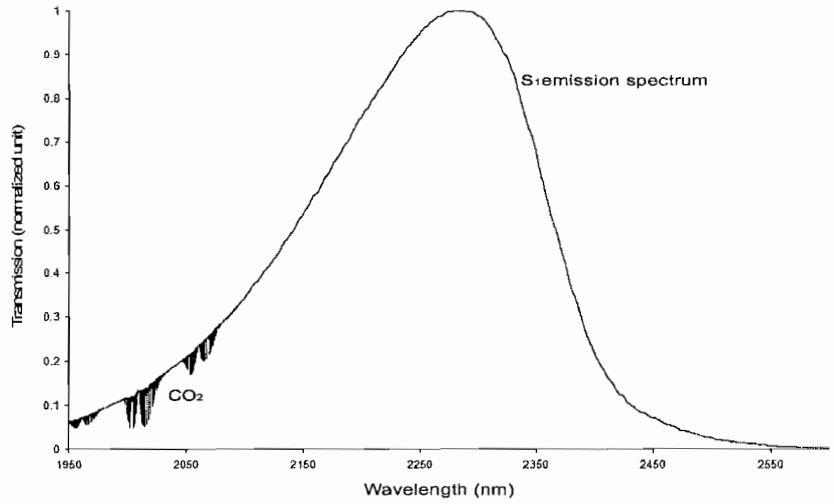

(c)

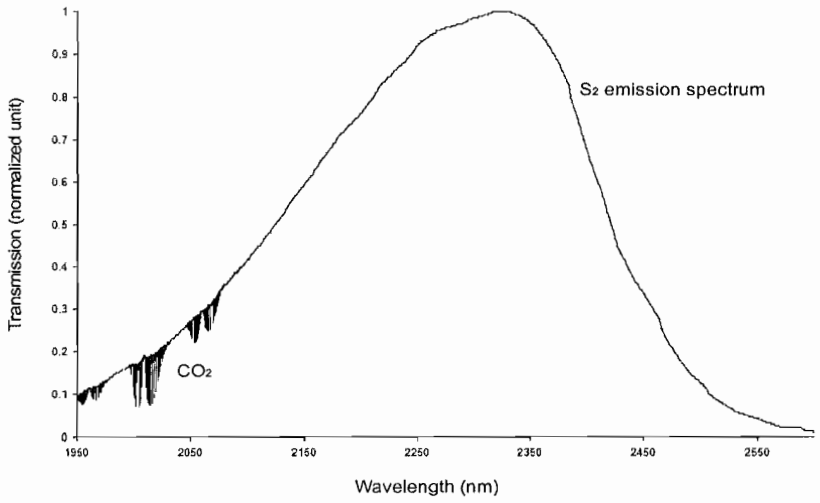

(d)

FIGURE 7.5: The influences of contaminant gases is shown graphically as their transmission spectra within the emission spectrum of the light source in which a) and b) shows the influence of H_2O on S_1 and S_2, respectively, c) and d) the influence of CO_2 on S_1 and S_2, respectively.

As predicted, the cross – sensitivity of H_2O is the biggest, followed by CO_2, whereas C_2H_2 is found not to influence the methane measurement for the optical system centred at 2.3 μm, as given in Table 7.2.

TABLE 7.2: The data show a set of simulation results which were generated by using Equation (4.10) for methane with 100%, 80%, 50%, 25%, 4%, and 0% volume / volume concentration.

Gas	**Water vapour (H_2O)**	**Carbon dioxide (CO_2)**	**Acetylene (C_2H_2)**
Modulation index (m)	0.00501	- 0.000622	~ 0
Crosstalk (%)	6.86	0.85	~ 0

Two interesting results are obtained from calculating the cross-sensitivity of H_2O and CO_2 as listed in Table 7.2. In the first one, it is found that the cross-sensitivity of H_2O showed a positive modulation index whereas for CO_2 it was negative. According to Chambers et al. [67], the negative modulation index is generated due to the presence of interleaving absorption lines between the absorption lines which were absorbed in the reference cell and the absorption lines absorbed in the measurement cell. In contrast, the positive modulation index results when the absorption lines which were absorbed in the reference cell are comparable or overlap with the absorption lines absorbed in the measurement cell.

In the second result, it is intuitively believed that the cross-sensitivity of H_2O and CO_2 can be reduced by changing S_2 for a light source which has a more identical emission spectrum shape to S_1. There are two reasons for this, which are;

1. In CoSp, a higher selectivity of gas of interest is obtained by matching the optical characteristics between the light sources which pass through the reference cell compared with the light source passing through the measurement cell, as previously discussed in section 4.2.1. Therefore, when the light sources are not identical is will contribute to some of absorption lines being absorbed in a condition with unmatched characteristics. This can be seen in Figure 7.2 in which S_1 is the light source passed through the reference cell and its spectrum does not match with the entire absorption lines absorbed by S_2. As a consequence of this, the advantages of CoSp technique do not apply for the part in which there is a mismatch, S_2 is unmatched with the absorption lines for S_1, thus possibly increasing the cross-sensitivity measurement.

2. In addition, the shape of the emission spectrum of S_2 which is centred at 2.35 μm is little bit shifted to the higher wavelength region compared to the centre of the optical system at 2.3 μm. Thus, as shown in Figure 7.5 (b), S_2 has been more affected by H_2O compared with S_1 as shown in Figure 7.5 (a) in which its emission spectrum is centred at 2.31 μm.

This problem can be solved by using an optical filter with a suitable bandwidth, and centred at 2.3 μm, to narrow the optical sources spectra. In this way, the possibility of the contaminant gases being absorbed will be reduced.

7.4 EXPERIMENTAL RESULTS

Experiments have been conducted by measuring methane gas for a set of concentrations (% vol / vol) which are 100%, 80%, 50%, 25%, and 4%. The samples of 100% and 4% have a purity 99.94% and 3.99% methane respectively, as given by the manufacturer, whereas, for the others, concentrations are prepared by mixing a methane sample (purity 99.94%) with dry nitrogen . The samples are prepared on the basis of the volume ratio of methane and nitrogen in millilitre (ml). For example, 80% vol /vol methane was prepared by mixing 50 ml methane (purity 99.94%) with 50% ml dry nitrogen. Then, a

50 ml 100% vol / vol methane sample is filled into the reference cell and 50 ml of a known concentration sample gas will be filled into the measurement cell to be measured.

7.4.1 RESULTS OF VARYING THE GAS CONCENTRATION

The modulation index (m) that resulted when the samples of methane with 100%, alternately 100% and 4%, 80%, 50%, 25%, and 4% were introduced into the measurement cell, are shown in Figure 7.6 to 7.11.

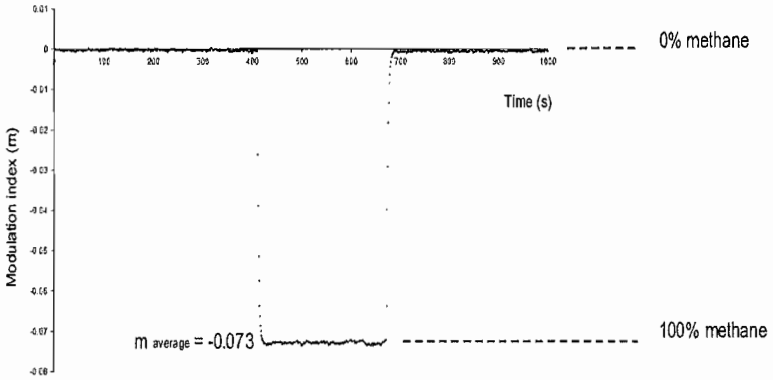

FIGURE 7.6: The modulation index, equal to – 0.073 resulting, when 100% vol/vol methane is introduced into the measurement cell. The measurement was conducted at 20° C and 1.013 bar.

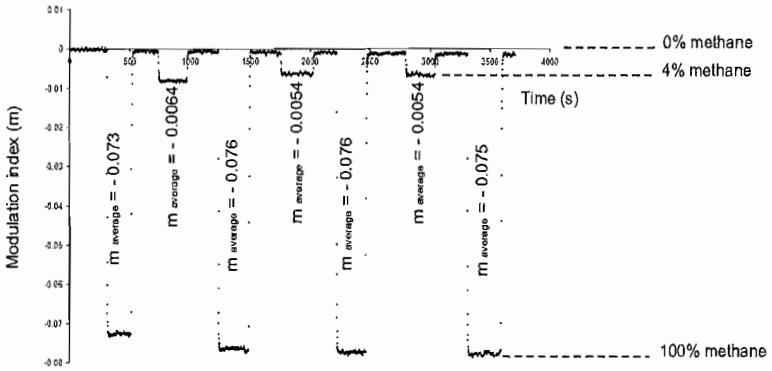

FIGURE 7.7: The modulation index, an average equal to – 0.075 and – 0.0054, resulting when alternately 100% and 4% vol/vol methane is introduced into the measurement cell. The measurement was conducted at 20° C and 1.013 bar.

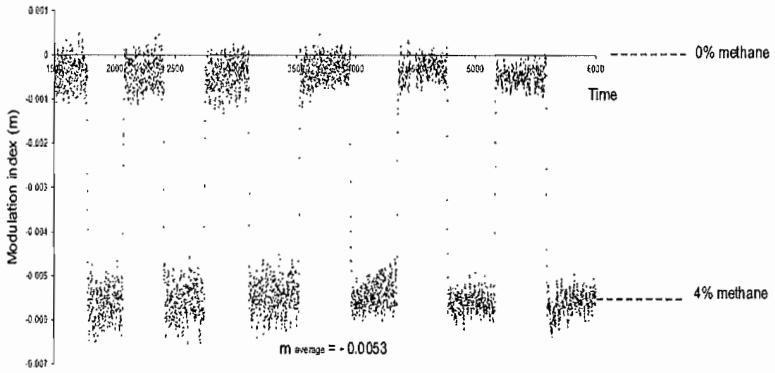

FIGURE 7.8: The modulation index, an average equal to – 0.0053 resulting, when 4% vol/vol methane is introduced into the measurement cell. The measurement was conducted at 20° C and 1.013 bar.

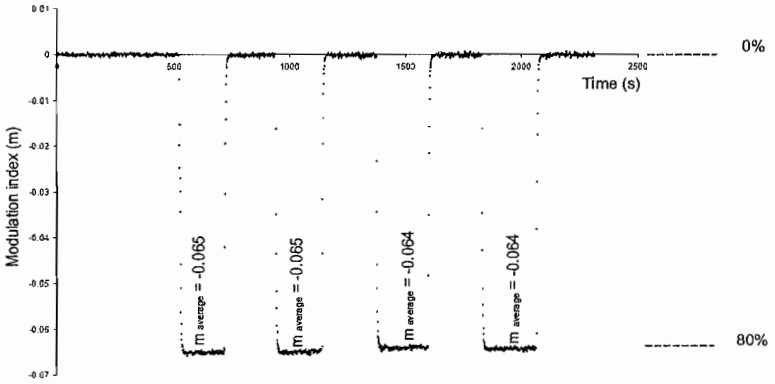

FIGURE 7.9: The modulation index, an average for a few measurement cycles, is equal to – 0.065 when 80% vol/vol methane is introduced into the measurement cell. The measurement was conducted at 20° C and 1.013 bar.

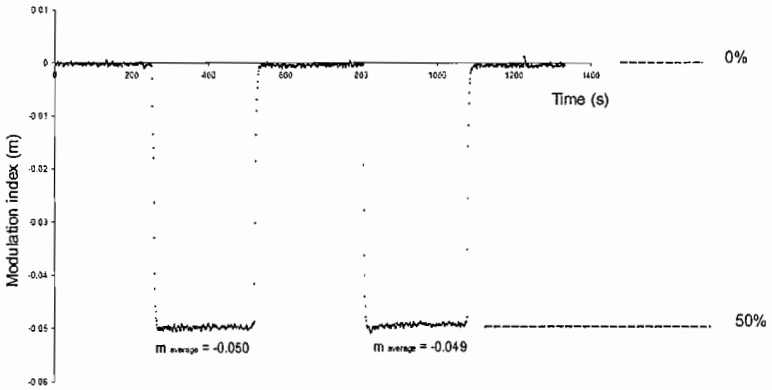

(a)

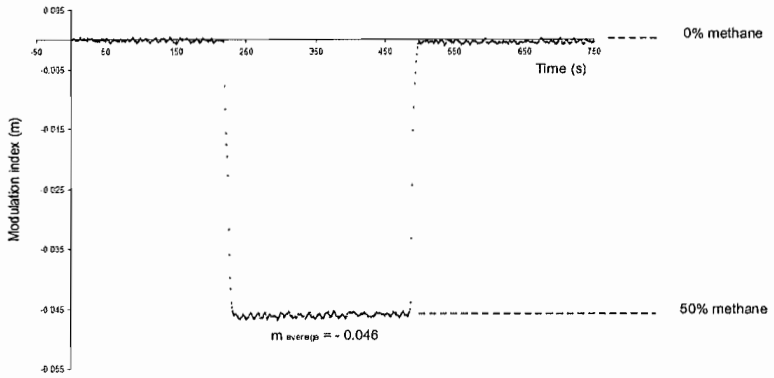

(b)

FIGURE 7.10: The modulation index is equal to a) an average – 0.0495 when 50% vol / vol methane is introduced and b) the modulation index is equal to -0.047 when the measurement of 50% vol / vol is repeated. The measurement was conducted at 20° C and 1.013 bar.

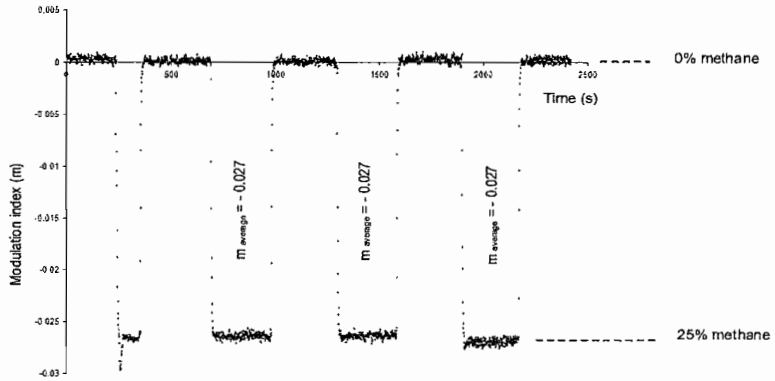

FIGURE 7.11: The modulation index, an average for a few measurement cycles, is equal to – 0.027 when 25% vol/vol methane is introduced into the measurement cell. The measurement was conducted at 20° C and 1.013 bar.

All results illustrated in Figure 7.6 to 7.11 are summarized in Table 7.3.

TABLE 7.3: The data shows a set of modulation indices which were obtained from experiments when a sample of methane with 100%, 80%, 50%, 25%, 4%, and 0% volume / volume concentration was introduced into the measurement cell.

Methane concentration (% vol/vol) (% vol/vol)	**Modulation index (m)**
0	0
4	- 0.0054
25	- 0.027
50	- 0.046
80	- 0.065
100	- 0.073

7.4.2 THE CHARACTERISTICS OF THE SENSOR RESPONSE

In general, data from experiments show that the handheld sensor gives significant response changes when the sample of methane is filled into the measurement cell. This showed that the handheld sensor which was constructed to be able to give a fast response, performed as required. The response time of this sensor depends upon the integration time which is setup in the experiment. In all of our measurements, the integration time was setup at 0.1 s.

The observation of the experimental results, as shown in Figure 7.6 to 7.11, found that the sensor response formed a curve pattern at every concentration transition of alternately methane filling / discharge into / from the measurement cell. This characteristic is caused by the delay time due to fill / discharge of the methane sample completely into / from the measurement cell.

In the other observations, as shown in Figure 7.9, the measurement of 80% vol / vol methane for the first two cycles gives the modulation index as – 0.065 whereas for the last two measurements it is found to be slightly lower at – 0.064. This gives approximately 1.5% differences in the measurement modulation index probably contributed to by imprecisely mixing the concentration of the gas samples. A similar behaviour can be seen in Figure 7.10 (a) in which a modulation index equal to – 0.049 and – 0.050 were obtained when 50% vol / vol methane is introduced into the measurement cell. When the measurement is repeated a few times with a more careful sample preparation, it is found that the actual modulation index that resulted by introducing 50% methane vol / vol into the measurement cell was around – 0.046 to – 0.047 or 2% error.

Other factors that need to be considered are the uniformity of the gas sample as samples were prepared by simply mixing methane and dry nitrogen in a syringe container. It is possible to obtain more uniform samples by leaving the gas samples for a duration of time to allow both gases to completely diffuse. However, in that way the gas samples are exposed to the factors which result in varying their absorption lines' characteristics. For example, the total pressure of the gas sample in the syringe can change as the temperature increases. This will result in a broadening of the bandwidth of the gas absorption lines, thus more light will be absorbed.

Even in the case where measurement is carried out on a standard sample (standard refers to sample provided by manufacturer i.e 100% and 4 % methane); the modulation index for that measurement also varies as shown in Figure 7.7. For 100% vol / vol methane, an error of approximately 4.1% is observed. This error possibly arises due to a variation in the emission spectrum of the light sources. To overcome this problem, it is

necessary to switch on the light source for a period of time before the experiment can be done. In this way the constant emission spectrum can be obtained.

In a few measurements, a drift pattern was observed as shown in Figure 7.7. The presence of a drift pattern possibly results from improper balancing of the residual feedback (the residual current level) in the equalizing of S_1 and S_2 at the reference detector. This problem does not affect the sensor response (the modulation index value) because the modulation index is only a difference value between two different concentrations. However, it will shift the modulation index value which is initially setup at zero before the measurement is done.

The relation between the sensor response (modulation index) and methane concentration, as summarized in Table 7.3, can be illustrated by plotting a graph of the modulation index versus methane concentration, and it is given in Figure 7.12. The graph shows that at lower concentration the modulation index changes in a linear pattern as the methane concentration increases, whereas at higher concentration the non-linearity pattern becomes significantly apparent. This pattern agreed well with that predicted previously by a theoretical model. However, the negative modulation index which was obtained from experiment is totally opposed to the theoretical prediction which shows positive value, as given in Table 7.1 and illustrated in Figure 7.3. The explanation of this behaviour (negative modulation index) will be discussed later in section 7.4.

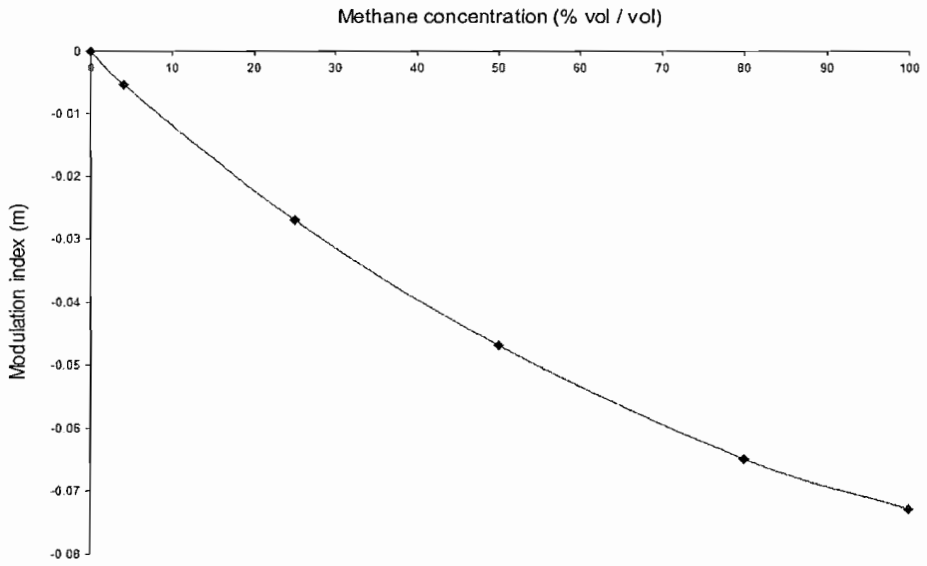

FIGURE 7.12: A set of modulation indices which were obtained from measuring 100%, 80%, 50%, 25%, and 4% vol / vol methane. All measurements were conducted at 20°C and 1.013 bar.

7.4.3 RESULTS ON MEASURING THE CROSS-SENSITIVITY

Two experiments were conducted to measure the cross-sensitivity of a few selected contaminant gases. The first experiment was conducted to measure cross-sensitivity by directly measuring the contaminant gas which is filled in the single gas cell. The second measurement measured the cross-sensitivity by our handheld sensor which was working by a correlation spectroscopy technique. In this way, the selectivity of our sensor can be compared and it is intuitively predicted that the correlation spectroscopy will show improved selectivity compared to the direct measurement.

The first experiment is made by modifying our sensor, in which the reference detector is set to measure the initial intensity of the light beam, I_0, before that beam is used to

probe the contaminant gas in the measurement cell. Then, as the light beam is passed through the gas cell containing contaminant gas (methane also will be measured as a reference value), the absorbed light beam will be detected at the measurement detector as, I. By using the Beer-Lambert's law, as given in section 3.3, absorbance, A, can be calculated, as both parameter I and I_0 are known. The results on measuring 100% vol / vol methane gives absorption equal to – 0.073 and results for a few selected contaminant gases are summarized in Table 7.4.

TABLE 7.4: The approximations for the cross-sensitivity of each contaminant gas are calculated by taking the absorbance of 100% vol / vol methane as a reference value.

Gas	**Propane + Butane (30% + 70%)**	**Carbon dioxide (CO_2)**	**Acetylene (C_2H_2)**
Absorbance (normalized unit)	- 0.00901	- 0.003	- 0.00447
Cross-sensitivity (%)	12.35	4.11	6.13

The second measurement is carried out by measuring the contaminant gases in the correlation spectroscopy system. The measurements are taken by filling 50 ml 100% vol / vol methane in the reference cell and a 50 ml contaminant gas sample is filled into the measurement cell. All results are show in Table 7.5.

TABLE 7.5: The approximation for the cross-sensitivity of each of the contaminant gases which was obtained in the CoSp system.

Gas	Propane + Butane (30% + 70%)	Carbon dioxide (CO_2)	Acetylene (C_2H_2)	Water vapour* (H_2O)
Modulation index (m)	- 0.0064	0.00038	- 0.0014	0. 0019
Cross-sensitivity (%)	8.10	0.48	1.77	2.40

*Humidity at 94 % and was measured by using TESTO 625 (www.testo.co.uk)

As predicted, the cross-sensitivity which was obtained in the correlation spectroscopy system was found to be smaller than the cross-sensitivity which was obtained from measuring by the direct measurement as shown in Table 7.6.

TABLE 7.6: The cross-sensitivity comparison between the results obtained from the direct measurement and CoSp system.

Gas	Propane + Butane (30% + 70%)	Carbon dioxide (CO_2)	Acetylene (C_2H_2)	Water vapour* (H_2O)
Cross-sensitivity in CoSp (%)	8.06	0.48	1.71	2.35
Cross-sensitivity in direct measurement (%)	12.35	4.11	6.13	Not available

*Humidity at 94 % and was measured by using TESTO 625 (www.testo.co.uk)

It is intuitively predicted that the cross-sensitivity in the correlation spectroscopy system might be of the order ten times better than the cross-sensitivity obtained in the direct measurement. Nevertheless, data from experiments show that the cross-sensitivity of the correlation spectroscopy system is only approximately 1.5 to 8.6 times better than the direct measurement and this varies depending upon the species of contaminant gases. It is believed that, the use of two optical sources with non - identical emission spectra contributes to the lowering of the selectivity of the measurement.

The advantages of correlation spectroscopy as a high selectivity technique are not totally manifest when two non – identical optical sources are employed in the complementary source modulation technique. As discussed previously, in section 4.2.1, a high selectivity is achieved when the light source which is passed through the reference cell (S_1) is matched by optical filtering to sweep a similar absorption characteristic in the measurement cell. However, as S_2 is really not identical with S_1, a small difference in absorption characteristics, which are not comparable with the matched optical filter, will affect the modulation index (possibly increasing the cross-sensitivity). For example, as shown in Figure 7.5 (a) and (b), it is obvious that S_2 is relatively more affected by H_2O compared to S_1. Thus, the cross-sensitivity of H_2O in the correlation spectroscopy technique, which is 2.35% as given in Table 7.6, might be less if an identical optical source were used. Unfortunately, results from direct measurement for H_2O are not available, thus the comparison with the correlation spectroscopy system cannot be done.

The direct measurement on a sample which contains 30% propane and 70% butane and acetylene gives 12.35% and 6.13% for their cross-sensitivity, whereas in correlation spectroscopy the result is 8.06% and 1.71%, respectively. There are two important points from these results. The first is that, it is surprising to obtain a high value of cross-sensitivity for both gases. Acetylene, for example, does not show an absorption band within the region of both optical sources' emission spectrum. It appears as a strong absorption band centred at around 3.04 μm [95], as shown in Figure 7.13.

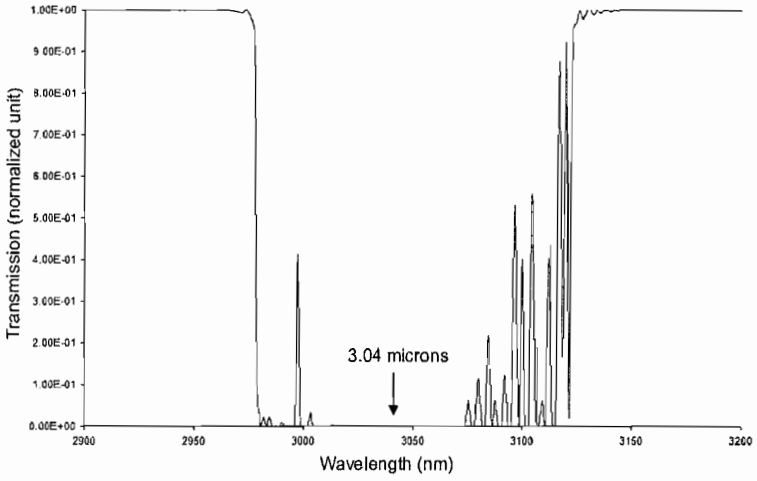

FIGURE 7.13: The graph shows a transmission spectrum of C_2H_2 centred at 3.04 μm. This graph is obtained by using HITRAN database for 100% concentration of C_2H_2 with a path length 0.1 m, at 1.013 bar and 296 K.

This gives the possibility that the emission spectrum of either one or both optical sources is wider than the datasheet given by the manufacturer. The consequence of this, is that some of the C_2H_2 absorption lines possibly absorb the light beam. For a similar reason, for the mixed sample of 30% propane and 70% butane, the high cross-sensitivity is possibly contributed to by the presence of an absorption band of propane centred at 2.98 μm [96].

In the other measurement, the cross-sensitivity of CO_2 which is obtained from correlation spectroscopy is 8.5 times better than the cross-sensitivity obtained by the direct measurement. As shown in Figure 7.5 (c) and (d), the absorption spectrum of CO_2 is found to be within the emission spectrum of both optical sources, thus the advantages of correlation spectroscopy are totally applied for CO_2, and this was proved by a better selectivity, which is 8.5 times better than the direct measurement.

7.4.4 RESULTS ON VARYING SENSOR TEMPERATURE

To investigate the effects of temperature on the modulation index, experiments were conducted by measuring 100% vol / vol methane at 20° C, 25° C, 30° C, 39° C, and 43° C. A thermostatically controlled bath (Clifton 8 from Bennett Scientific Ltd.) was used to heat water. Then, the hot water is flowed into the water channel of a heat exchanger plate via a rubber tube, and circulated back into the water bath as shown in Figure 7.14. The temperature of the sensor is increased correspondently with the increment of plate's temperature. In order to maintain the required temperature, a heat insulator is used to cover the sensor.

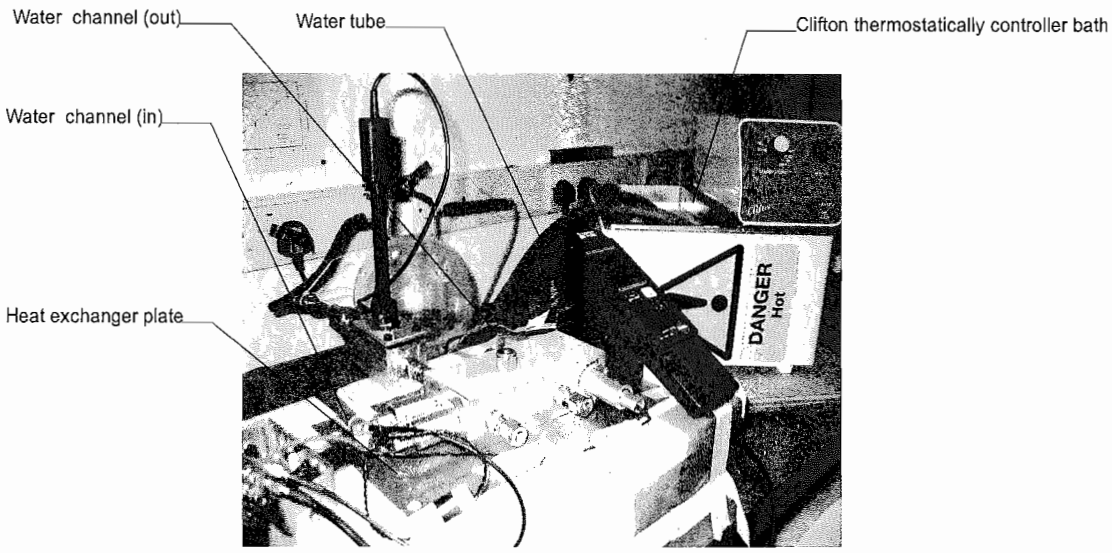

FIGURE 7.14: The experimental setup for evaluating temperature effects on the sensor response (modulation index).

All the results are shown in Table 7.7 and, Figure 7.15 shows the effects of increasing the sensor temperature on the modulation index.

TABLE 7.7: The modulation index of 100% vol / vol methane which is obtained by varying the sensor temperature.

Temperature (° C)	**Modulation index (m)**
20	- 0.073
25	- 0.079
30	- 0.084
39	- 0.092
43	- 0.093

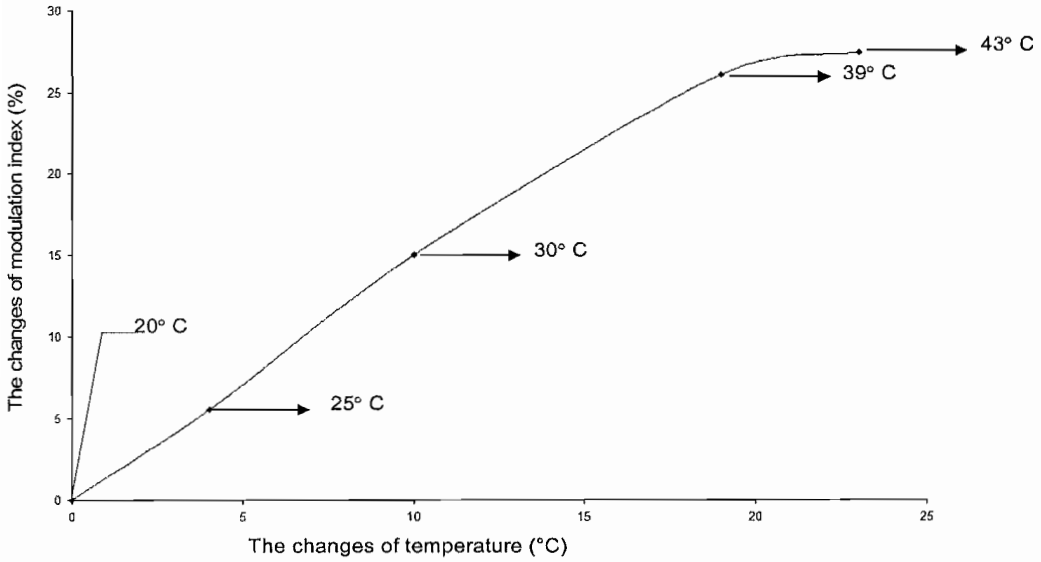

FIGURE 7.15: The graph shows the changes of modulation index caused by increasing the sensor temperature between 20° C and 43° C.

The graph in Figure 7.15 shows a linear relation between the changes of modulation index by increasing the changes of temperature between 20° C and 39° C before starting to become non-linear at around 40° C. However, there is no further data to predict the behaviour of our sensor at higher temperature.

Theoretically, at a particular gas concentration, modulation index is not affected by temperature variation if the path length of the gas cell and total pressure is constant. In the case of our sensor, it is found that the modulation index increases as the temperature is increased. This is because by increasing the temperature of the sensor the pressure of the reference cell will increase as it is sealed. The pressure of the measurement cell does not change as it is stabilized to be at atmosphere pressure. In addition, as the modulation index is very dependent on the characteristics of the light sources, any changes in the peak emission of the LEDs will affect its value. According to the manufacturer's datasheet, it is found that the peak emission of the LEDs typically will shift to the longer wavelength region by approximately 1 to 1.5 nm for every 1 K change.

7.4.5 RESULTS ON VARYING GAS SAMPLE VOLUMES

Ideally, the modulation index should be independent from the changes of the sample volume. Thus, it is important to investigate the effect on the modulation index caused by varying the volume of the gas sample. This investigation is carried out by measuring 100% vol / vol methane with a 50 ml, 30 ml, and 20 ml gas sample volume. The results from the experiments are illustrated in Figure 7.16.

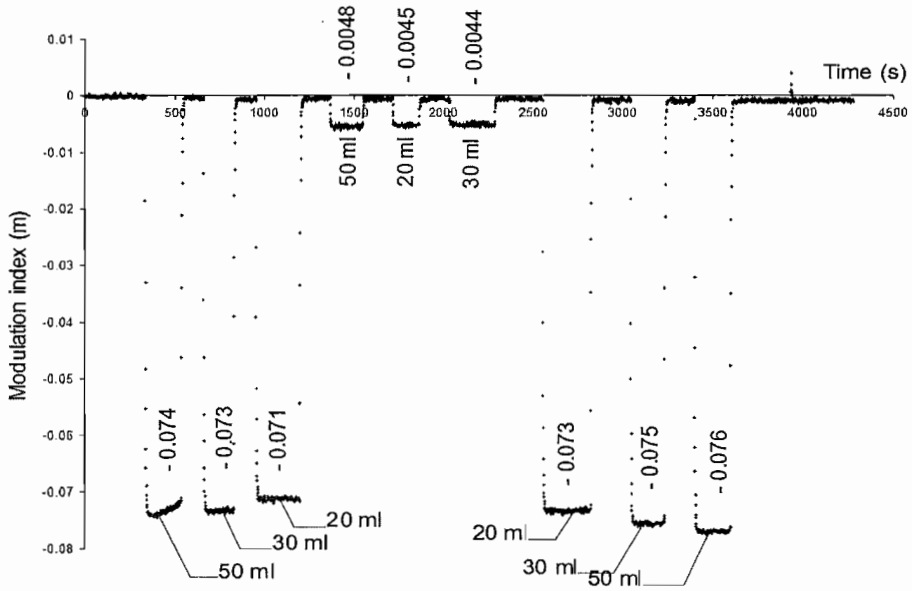

FIGURE 7.16: The graph shows a variation of the modulation index when a varying gas sample volume is filled in the measurement cell.

In general, the graph in Figure 7.16 shows that the modulation index decreases as the gas sample volume decreases. For 100% vol / vol methane, it is found that the modulation index varies between – 0.071 and – 0.076 whereas for 4% vol / vol methane it varies between – 0.0048 and – 0.0044. The variation of the modulation index is probably due to the variation of total pressure in the gas cell. The variation in the gas

pressure might result from frequent gas molecule collisions particularly at high gas volumes in the sealed gas chamber.

7.5 THE COMPARISON BETWEEN THEORETICAL AND EXPERIMENTAL RESULTS

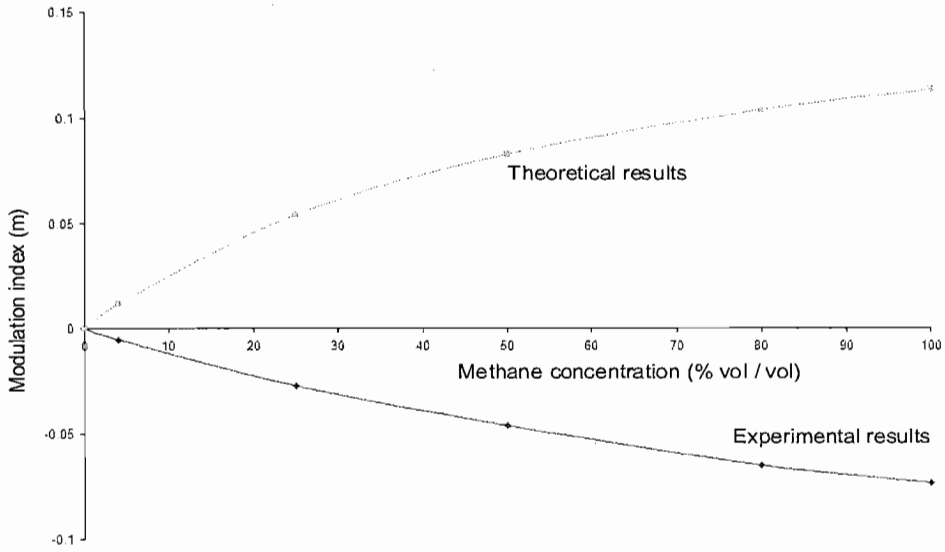

FIGURE 7.17: The graph shows a comparison between the results obtained from theory and by experiment.

The first comparison is of the modulation index versus gas concentration. The graph is shown in Figure 7.3 (theoretical results) and 7.12 (experimental results). Both graphs can be re-plotted as given in Figure 7.17. The modulation index was obtained from our theoretical results and gives a negative value as shown in Figure 7.17. This is in totally contrast with the theoretical model which gives a positive response. Chambers et al. [67] conclude that the response of modulation index being either negative or positive is dependent on the degree of overlap between the reference and measurement absorption

spectra and he reported that methane shows a positive value and for water vapour it is negative. In this case, water vapour is considered as a contaminant gas which does not overlap the absorption spectra.

In our theoretical model, the modulation index of methane gives a positive value and for water vapour it is also positive. This is because the absorption spectrum of methane, centred at 2.3 μm, is found to overlap with the absorption spectrum of water. However, results from experiments show an opposite pattern, which is a negative modulation index for methane and as well as for water vapour. This unexpected observation is not able to be explained by our proposed theoretical model.

However, the opposite values of theoretical and experimental results does not affect the actual modulation index value because the modulation index is only a normalized value resulting from a difference between two light paths, A and B, as described in Figure 7.18.

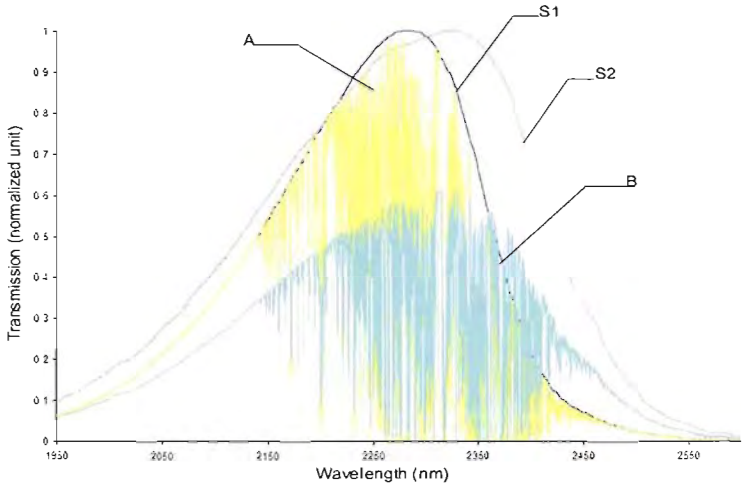

FIGURE 7.18: The modulation index can be graphically described as a difference between A and B. In that graph A and B are referred to as the absorbed light by S_1 and S_2, respectively.

As the graph in Figure 7.18 illustrates; A represents the integration of $\int S_1(\lambda).T_r(\lambda).T_m(\lambda).d\lambda$ whereas B represents the integration of $0.6150\int S_2(\lambda).T_m(\lambda).d\lambda$, as given in Equation (7.1). Thus, the positive or negative sign is only important in the prediction of the characteristics of the contaminant gas in which either the absorption spectrum of the contaminant gas overlaps or does not overlap with the absorption spectrum of the reference gas. Therefore, the graph in Figure 7.17 can be re-plotted by assuming that both theoretical and experimental results have a negative value, as illustrated in Figure 7.19.

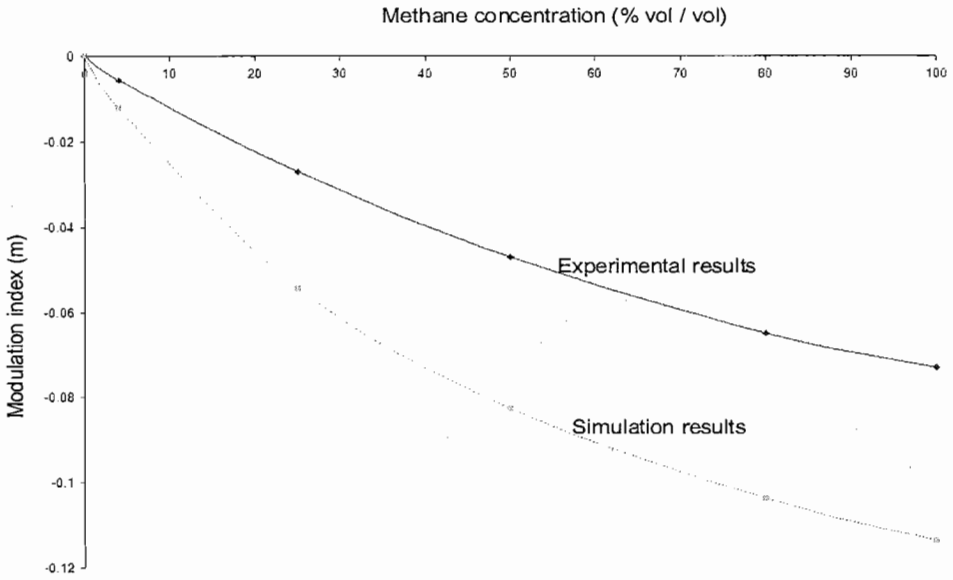

FIGURE 7.19: The comparison between experimental and theoretical results considering that both results are only a difference value between two optical path lengths.

The second comparison between theoretical and experimental results is made on the big difference between the modulation indices. Even though the pattern of both theoretical and experimental results is similar, the modulation index which is obtained by theoretical calculations is bigger than by experimental results. There are two main possible factors which contribute to this result. The first factor might be caused because

the actual emission spectra of both optical sources are different which we assumed for calculating our theoretical model. The second factor is that the theoretical model which was developed is totally dependent on the absorption spectra which are generated from the HITRAN database. Both of these factors will determine the value of the modulation index. Therefore, in any circumstances in which there is any difference between the actual optical sources emission spectra and the absorption spectrum of the gas this will significantly influence the obtained modulation index. For example, as reported by Narendran et al. [97], in their investigation of the characteristics of white LEDs' emission spectrum, the peak emission of the LED shifted to the longer wavelength region by increasing the drive current. Thus, it is possible that the LEDs which are used as optical sources in this sensor have a change in their emission peak position as different drive currents were operated, particularly in this process, to equalize the intensity of S_1 and S_2 at the reference detector.

For a similar reason, the comparison between theoretical and experimental cross-sensitivity, as shown in Table 7.8, also gives a similar pattern in which the theoretical result is bigger than the experiment value. In addition, the cross-sensitivity of C_2H_2 is not zero, as calculated and this gives significant evidence that the emission spectrum of S_1 or S_2, or both, are wider than was assumed in our theoretical model, hence possibly absorbing a few C_2H_2 absorption lines centred at 3.04 μm.

TABLE 7.8: The comparison between the cross-sensitivity in the theoretical and measurement results.

Gas	**Water vapour (H_2O)**	**Carbon dioxide (CO_2)**	**Acetylene (C_2H_2)**
Cross-sensitivity (%) (Theoretical result)	6.86	0.85	0
Cross-sensitivity (%) (Experimental result)	2.35	0.48	1.7

7.6 SENSOR SENSITIVITY

The sensitivity of our sensor is limited by the presence of noise in the measurement. The noise arising predominantly from shot noise, which arises from the nature of random photon arrival at the optical detector and thermal noise origins from the optical receiver circuit. The sources of shot noise and thermal noise can be expressed in terms of B which is the post-detection electronic processor bandwidth that limits the noise contribution by averaging the signal, as given in Equation (7.3) and (7.4), respectively. I_S refers to the shot noise current, I_T is thermal noise current, q is the electronic charge, I_{Sig} refers to the dc output current of the output detector, $R_{Feedback}$ is the feedback resistor (transimpedance amplifier) which is set at 10 MΩ, and k is the Boltzman constant.

$$I_S = \sqrt{2qI_{Sig}B} \tag{7.3}$$

$$I_T = \sqrt{\frac{4kTB}{R_{Feedback}}} \tag{7.4}$$

From the calculation, it is found that the noise which limited methane detection was 3.085 x 10^{-4} per root square frequency or equivalent to 0.21% of methane concentration or 2100 part per million (ppm). This calculation is made by assuming that the graph in Figure 7.12 is linear within the range from 0% methane to 4% methane. When considering the standard of IDHL (Immediately Dangerous for Health of Life) in which the safety level of gases was set as 10%, the value of 2100 ppm is less than half the IDHL for methane, as the LEL for methane is 5000 ppm.

7.7 CONCLUSIONS

In this chapter, we presented our sensor performance from theoretical and experimental results. It is found that our handheld gas sensor is able to give a fast response, a high selectivity and an appreciable sensitivity in the detection of methane for the optical system working at 2.3 μm.

CHAPTER 8
CONCLUSIONS

8.1 INTRODUCTION

There were two aims for this project, the first to evaluate the most convenient absorption band of methane to determine in which wavelength region the sensor will be operated. Theoretically, the selection of the best methane absorption band should consider the absorption band cross-section, as the selection of a stronger absorption band (larger cross-section means stronger absorption) will improve the sensor performance. The selected absorption band also needs to be isolated or minimized from the effects of the presence of the contaminants' gas spectrum at the region of the selected absorption band. The presence of contaminant gases will increase the cross-sensitivity measurement and this will affect the reliability of the sensor. The practicality to construct the optical system in the region of the selected absorption band is also important particularly in selecting the suitable optical components.

The second aim is to design a miniature of the correlation spectroscopy for a handheld methane gas sensor, at a reasonable cost while still able to give a highly selective technique and appreciable sensitivity. To be a handheld sensor, a few parameters which theoretically influence the performance of the sensor need to be understood before the sensor can be designed. Then, the compromises between each parameter will be considered, particularly considering the practicality of the sensor being constructed. A theoretical model is developed to predict the sensor response (modulation index) and an experiment is carried out to evaluate the sensor performance.

8.2 THE ANALYSIS OF ABSORPTION BAND OF METHANE AT 2.3 μm

In our analysis, we found that the most convenient methane absorption band to be used is an absorption band centred at 2.3 μm. This band was selected as an 'exclusive' because of its location which is in between the near-infrared and mid-infrared region. Although this band is not as strong as the absorption band centred at 3.31 μm, it offers a band approximately two and a half times stronger than the absorption of most common methane sensors working in a region which is centred at 1.67 μm.

This 2.3 μm band is classified into an octad system and comprises 8 vibrational bands split into 24 sub bands. There are three stronger band cross-sections of methane vibrational bands centred at 2.3 μm which are $v_3 + v_4$ at 2.3233 μm to 2.3152 μm, $v_1 + v_4$ at 2.3677 μm, and $v_2 + v_3$ at 2.2 μm. Although this band is not as strong as v_3 of the methane fundamental absorption band centred at 3.31 μm, due to the practical limitation to develop an optical system working in the mid-infrared region, the selection of 2.3 μm has advantages as a few available optical components show a sufficient transmission in this region.

It was found that the presence of the water vapour absorption spectrum centred at 2.3 μm had the biggest effect compared with at 1.67 μm and 3.31 μm. However, as the LEDs which were used have a bandwidth of 220 nm, thus the influence of water vapour can be minimized. In addition, the presence of the water vapour absorption spectrum is centred at approximately 3.04 μm, thus it does not have too significant an affect on the absorption band at 2.3 μm as the region of interaction between light and methane is limited by the bandwidth of the LEDs. In conclusion, we found that the 2.3 μm absorption band of methane is the most convenient band, which is practical, and we believe it can improve our sensor performance.

8.3 THE HANDHELD SENSOR

In this project we present a miniature of the correlation spectroscopy handheld sensor. The miniature is a compact folded-path arrangement, designed to achieve a Complementary Source Modulation (CoSM) gas detection system. This sensor with dimensions 104 mm x 40 mm x 60 mm for its gas chamber was constructed for working with optical system centred at 2.3 μm.

The sensor consists of two parallel gas cells, the reference and measurement cell, both having overall 100 mm of efficient interaction length of light path with gas molecules. A 'Top-hat' is a special part which was designed to fit in the optical sources and optical detectors. It also functions as a beam controller in which the light beam passing through the optical system can be controlled to have the right propagation path. This function is important to avoid any possibility of stray light due to imprecise machining of the gas chamber, or imprecise positioning of the LEDs, or the positioning of the optical detectors in the ferrules.

Two silicon wafer slices were used as beam splitter / beam combiner. The use of silicon wafer slices is more important to cut the cost of the sensor as it is cheaper relative to an infrared cube beam splitter. Nevertheless, it has several disadvantages such as high optical loss due to Fresnel reflections and multiple reflections and is affected by polarization effects. To reduce the optical loss, a thin double sided polished silicon wafer slice is used. Fortunately, the effect of polarization cannot affect the sensor response as correlation spectroscopy is designed to be a self referencing system.

A low-cost collimator lens of technical glass (Schott AR-Glass) was used to collimate the light beam emitted from the infrared LED and it re-focussed the light beam onto a small active surface of the detector. Two low-cost borosilicate windows were used to seal one end of each gas cell. Both the lens and the optical window are made of a common material, are readily available and show a sufficient optical transmission at 2.3 μm. This selection (lens and optical window) can avoid the use of common infrared based optical materials because infrared optical components are often relatively expensive and need to be custom ordered.

In conclusion, we have presented a simple design and constructed a prototype of the correlation spectroscopy handheld sensor for the methane absorption band working at 2.3 μm. From our theoretical and experimental results we found that our sensor shows a fast response and appreciable sensitivity which is approximately 0.2% vol / vol of methane. However, the selectivity of our sensor depends upon the species of contaminant gases. We believe that, by improving a few aspects, a highly selective performance of our sensor can be achieved. Therefore, a few studies should be continued in the future to improve all aspects of the sensor performance.

8.4 FUTURE WORK

Both aims of the project have reached definite conclusions; we showed that our miniature correlation spectroscopy sensor was a compact and handheld sensor. This sensor showed an ability to give a fast response, good selectivity and an appreciable sensitivity in detecting methane gas. However, many aspects still need to be improved and a few observations need to be explained. These include:

- LEDs with more identical emission spectra should be used so as to take advantage of the fact that correlation spectroscopy is a highly selective gas sensor technique.

- An optical filter should be used to narrow the bandwidth of the LEDs. A suitable bandwidth of the optical filter and the centre of its wavelength should match, as well as possible, the gas absorption band and at the same time it can eliminate the contaminant gas effects.

- A Complementary Source Modulation technique to achieve a gas detection system can possibly be changed to a new technique which only uses one optical source, thus the non-identical optical spectrum can be overcome. Of course, in that way the cost of sensor also can be reduced.

- A better theoretical model needs to be developed. A study of the optical emission spectrum characteristics such as the influence of drive current and temperature on the emission spectrum shape is really important as it significantly influences the prediction of results. This model should explain the negative value of the modulation index which was obtained in our experimental results. The development of that model should consider the effect of temperature on the sensor response.

There are a few interesting ideas which can be explored in order to obtain a better performance for the miniature correlation spectroscopy sensor. These include:

- The sensitivity of our sensor can be improved by using a longer gas cell. We suggest that the reference cell (measurement cell still as previous) can be replaced with Photonic Band Gap fibres (PBGs) [49] as the ability of this type of fibre to give longer interactions between light and gas molecules, thus increases the absorption of light radiation by gas molecules. The problem associated with long filling times in our technique does not affect the sensor response as the sample gas only needs to be filled one time or after a period of time in case of the sample gas leakage from the PBGs. Therefore, the delay in the response time only depends upon the filling time of the gas in the measurement cell.

- Our sensor also can be used to detect the absorption spectrum of carbon dioxide (CO_2) centred at 2.01 μm as the optical system has a sufficient transmission spectrum at that region. For that purpose, new LEDs centred at 2.01 μm are needed to match with the CO_2 absorption spectrum.

- Our sensor design probably can be applied to a laser technique (tunable diode laser) in the case when a LED at the desired wavelength is not available (in an application to measure other gases).

The above suggestions only cover a part of the possible future studies that could be done within the aims of our project. We believe that the future research on the

correlation spectroscopy should be expanded in terms of commercial products as this technique shows a highly selective technique and is able to give an appreciable sensitivity even when the compact sensor is constructed.

BIBLIOGRAPHY

[1] HITRAN Database (2000). [CD-ROM] University of Florida. Available: http://www.HITRAN.com.

[2] Banwell, C. N., McCash, E. M. (1994). *Fundamentals of Molecular Spectroscopy (Fourth Edition)*, McGraw-Hill, pp. 57.

[3] Sigist, M. W. (1994). Introduction to Environmental Sensing. In *Air Monitoring by Spectroscopic Techniques*, edited by Sigist, M. W., Wiley, New York, pp. 19.

[4] Barrow, G. M. (1962). *Introduction to Molecular Spectroscopy (International Student Edition)*, McGraw-Hill, Kogakusha Ltd., chap. 4.

[5] Banwell, C. N., McCash, E. M. (1994). *Fundamentals of Molecular Spectroscopy (Fourth Edition)*, McGraw-Hill, chap. 3.

[6] Banwell, C. N., McCash, E. M. (1994). *Fundamentals of Molecular Spectroscopy (Fourth Edition)*, McGraw-Hill, pp. 61.

[7] Hollas, J. M. (1996). *Modern Spectroscopy (Third Edition)*, Wiley, pp. 93.

[8] Banwell, C. N., McCash, E. M. (1994). *Fundamentals of Molecular Spectroscopy (Fourth Edition)*, McGraw-Hill, chap. 2.

[9] Banwell, C. N., McCash, E. M. (1994). *Fundamentals of Molecular Spectroscopy (Fourth Edition)*, McGraw-Hill, pp. 45.

[10] Banwell, C. N., McCash, E. M. (1994). *Fundamentals of Molecular Spectroscopy (Fourth Edition)*, McGraw-Hill, pp. 63.

[11] Banwell, C. N., McCash, E. M. (1994). *Fundamentals of Molecular Spectroscopy (Fourth Edition)*, McGraw-Hill, pp. 66.

[12] Herzberg, G. (1966). *Molecular Spectra and Molecular Structure*, D. Van Nostrand Company, Inc., Princeton, pp. 38.

[13] Herzberg, G. (1966). *Molecular Spectra and Molecular Structure*, D. Van Nostrand Company, Inc., Princeton, pp. 100.

[14] Herzberg, G. (1966). *Molecular Spectra and Molecular Structure*, D. Van Nostrand Company, Inc., Princeton, pp. 447.

[15] Herzberg, G. (1966). *Molecular Spectra and Molecular Structure*, D. Van Nostrand Company, Inc., Princeton, pp. 454.

[16] Werle, P., Slemr, F., et al. (2002). Near and mid-infrared laser-optical sensors for gas analysis, *Optics and Laser Engineering* 37, 101 – 114.

[17] Flammable limits. Retrieved from the World Wide Web: http://www.ilpi.com/msds/ref/flammablelimits.html.

[18] Gases-explosive and flammability concentration limits. Retrieved from the World Wide Web: http://www.engineeringtoolbox.com/explosive-concentration-limits-22- 423.html.

[19] Wilson, D. M., Hoyt, S. et al. (2001). Chemical sensors for portable, handheld field instruments. *IEEE Sensors Journal*, Vol. 1, No. 4, 256 – 274.

[20] Sigist, M. W. (1994). Introduction to Environmental Sensing. In *Air Monitoring by Spectroscopic Techniques*, edited by Sigist, M. W., Wiley, New York, pp. 19.

[21] Martin, P. A. (2002). Near-infrared diode laser spectroscopy in chemical process and environmental air monitoring. *Chemical Society Review*, 31, 201 – 210.

[22] Banwell, C. N., McCash, E. M. (1994). *Fundamentals of Molecular Spectroscopy (Fourth Edition)*, McGraw-Hill, pp. 58 - 59.

[23] Sigist, M. W. (1994). Introduction to Environmental Sensing. In *Air Monitoring by Spectroscopic Techniques*, edited by Sigist, M. W., Wiley, New York, pp. 20.

[24] Platt, U. (1994). Differential Optical Absorption Spectroscopy (DOAS). In *Air Monitoring by Spectroscopic Techniques*, edited by Sigist, M. W., Wiley, New York, pp. 46.

[25] Anderson, T. N., Lucht, R. P., et al. (2005). Combustion exhaust measurements of nitric oxide with an ultraviolet diode-laser-based absorption sensor. *Applied Optics*, Vol. 44, No. 8, 1491 – 1502.

[26] Hennig, O., Strzoda, R., et al. (2003). Handheld unit for simultaneous detection of methane and ethane based on NIR-absorption spectroscopy. *Sensors and Actuators B*, 95, 151 – 156.

[27] Dakin, J. P., Gunning, M. J., et al. (2003). Detection of gases by correlation spectroscopy. *Sensors and Actuators B*, 90,124 - 131.

[28] White, J. U., (1942). Long optical paths of large aperture (Cross Reference). *Journal Optical Society of America*, 32, 285 – 288.

[29] Melendez, J., de Castro, A. J., et al. (1995). Spectrally selective gas cell for electrooptical infrared compact multigas sensor. *Sensors and Actuators A*, 46-47, 417- 421.

[30] Galle, B. O., Samuelsson, J., et al. (2001). Measurement of methane emissions from landfills using a time correlation tracer method based on FTIR absorption spectroscopy. *Environmental Science Technology*, 35, 21 – 25.

[31] Kobayasi, T., Hirama, M., et al. (1981). Remote monitoring of NO_2 by differential absorption using optical fiber link. *Applied Optics*, Vol. 20, No. 19, 3279.

[32] Schiff, H. I., Mackay, G. I., et al. (1994). The use of tunable diode laser absorption spectroscopy for atmospheric measurements. In *Air Monitoring by Spectroscopic Techniques*, edited by Sigist, M. W., Wiley, New York, pp. 20.

[33] Hants, P. L., Hants, S. T. (1994). Gas measurement in the fundamental infrared region. . In *Air Monitoring by Spectroscopic Techniques*, edited by Sigist, M. W., Wiley, New York, pp. 459 – 461.

[34] Schiff, H. I., Mackay, G. I., et al. (1994). The use of tunable diode laser absorption spectroscopy for atmospheric measurements. In *Air Monitoring by Spectroscopic Techniques*, edited by Sigist, M. W., Wiley, New York, pp. 265.

[35] Hants, P. L., Hants, S. T. (1994). Gas measurement in the fundamental infrared region. . In *Air Monitoring by Spectroscopic Techniques*, edited by Sigist, M. W., Wiley, New York, pp. 370 – 371.

[36] Tittle, F. K., Lancaster, D. G., et al. (1999). Laser based absorption sensors for trace gas monitoring in a spacecraft habitat. *Society of Automotive Engineers*, Inc., 99ES-102.

[37] Platt, U. (1994). Differential Optical Absorption Spectroscopy (DOAS). *In Air Monitoring by Spectroscopic Techniques*, edited by Sigist, M. W., Wiley, New York, pp. 47.

[38] Tranchart, S., Bachir, I. H., et al. (1996). Sensitive trace gas detection with near-infrared laser diodes and an integrating sphere. *Applied Optics*, Vol. 35, No. 36, 7070 – 7074.

[39] Culshaw, B. January (2004). Optical fibre sensor technologies: Opportunities and-perhaps-pitfalls. *Journal of Lightwave Technology*, Vol. 22, No.1, 39.

[40] Lackner, M., Totsching, G., et al. (2003). Demonstration of methane spectroscopy using a vertical cavity surface-emitting laser at 1.68 μm with up to 5 MHz repetition rate. *Measurement Science Technology*, 14, 101-106.

[41] Monro, T. M., Belardi, W., et al. (2001). Sensing with microstructured optical fibres. *Measurement Science Technology*, 12, 854-858.

[42] Steawart, G., Mencaglia, A., et al. January (1998). Interferometric signals in fiber optic methane sensors with wavelength modulation of the DFB laser source. *Journal of Lightwave Technology*, Vol. 16, No.1, 43.

[43] Edwards, H. O., Dakin, J. P. (1993). Gas sensors using correlation spectroscopy compatible with fiber-optic operation. *Sensors and actuators B*, 11, 9 -19.

[44] Kebabian, P. L., Annen, K. D., et al. (2000). Nitrogen dioxide sensing using a novel gas correlation detector. *Measurement Science Technology*, 11, 499-503.

[45] Hordvick, A., Berg, A., et al. (1983). A fibre optic gas detection system. *Proceedings, 9th. European Conference on Optical Communication*, pp. 317. Geneva.

[46] Chan, K., Ito, H., et al. (1984). An optical-fibre-based gas sensor for remote absorption measurement of low –level CH_4 gas in the near-infrared region. *Journal of Lightwave Technology*, Vol. LT-2, NO.3, 234.

[47] Stueflotten, G., Christensen, T., et al. (1987). An infrared fibre optic gas detection system. *Proceedings, Optical Fibres Sensor 94*, pp. 87. Stuggart.

[48] Dakin, J. P., Culshaw, B. (1997). *Optical Fibre Sensors (Vol. 4)*, Artech House, pp. 9.

[49] Ritari, T., Tuominen, J., et al. (2004). Gas sensing using air-guiding photonic bandgap fibers. *Optics express*, Vol. 12, No. 17, 4080-4087.

[50] Hansen, T. P., Broeng, J., et al. (2004). Air-guiding photonic bandgap fibers: Spectral properties, macrobending loss and practical handling. *Journal Lightwave Technology*, 22, 11-15.

[51] Monro, T. M., West, Y. D., et al. (2000). Chalcogenide holey fibres. *Electronic Letters*, 36, 1998–2000.

[52] Herzberg, G. (1966). *Molecular Spectra and Molecular Structure*, D. Van Nostrand Company, Inc., Princeton, pp. 272 - 274.

[53] Herzberg, G. (1966). *Molecular Spectra and Molecular Structure*, D. Van Nostrand Company, Inc., Princeton, pp. 294 - 295.

[54] Herzberg, G. (1966). *Molecular Spectra and Molecular Structure*, D. Van Nostrand Company, Inc., Princeton, pp. 288 - 289.

[55] Allen, M. G. (1998). Review article - Diode laser absorption sensors for gas-dynamic and combustion lows. *Measurement Science Technology*, 9, 545-562.

[56] Klein, D., Dahnke, H., et al. (2000). Real-time detection of $^{13}CH_4$ in ambient air by use of mid-infrared cavity leak-out spectroscopy. *Optics letter*, Vol. 25, No. 21.

[57] Schiff, H. I., Mackay, G. I., et al. (1994). The use of tunable diode laser absorption spectroscopy for atmospheric measurements. In *Air Monitoring by Spectroscopic Techniques*, edited by Sigist, M. W., Wiley, New York, pp. 244 - 250.

[58] Iseki, T., Tai, H., et al. (2000). A portable remote methane sensor using a tunable diode laser. *Measurement Science Technology*, 11, 594-602.

[59] Thomas, D. (February 10, 2005). Trace gas detection by tunable diode laser absorption spectroscopy. [on – line magazine]. Discovery, The science & technology journal of AWE.
Available: http://www.awe.co.uk/Images/Tunable%20Diode_tcm6-3411.pdf.

[60] Goody, R. (1968). Cross-correlating spectrometer. *Journal Optical Society America*, 58, 900 – 9008.

[61] Taylor, F. W., Houghton, J. T., et al. (1972). Radiometer for remote sounding of the upper atmosphere. *Applied optics*, 11, 135.

[62] Edwards, H. O. (1991). *A study of techniques for optical fibre sensors.* PhD thesis. University of Southampton.

[63] Dakin, J. P., Edwards, H. O. (1992). Progress in fibre-remoted gas correlation spectroscopy. *Optical Engineering*, 31(special issue), 1616-1620.

[64] Dakin, J. P., Edwards, H. O., et al. (1995). Progress with optical gas sensor using correlation spectroscopy. *Sensors and Actuators B*, 29, 87.

[65] Dakin, J. P. (1998). Evolution of highly-selective gas sensing methods using correlation spectroscopy. *Invited papers, Advances in optoelectronics for environmental monitoring.* Erice, Sicily.

[66] Chambers, P., Austin, E. D., et al. (2004). Model to predict the response of correlation spectroscopy gas detection system for CH_4. *Proceedings, 16th international Conference on Optical Fibre Sensors*, 738 – 41. Nara, Japan.

[67] Chambers, P., Austin, E. D., et al. (2004). Theoretical analysis of a methane gas detection system using the complementary source modulation method of correlation spectroscopy. *Measurement Science Technology*, 15, 1-8.

[68] Cheung, A., Johnstone, W., et al. (2004). Detection of acetylene gas using optical correlation spectroscopy. *Proceedings, 17th International Conference on Optical Fibre Sensors*, Bruges, Belgium.

[69] Krier, A., Sherstnev, V. V. (2000). Powerful interface light emitting diodes for methane gas detection. *Journal Physics D*: Applied physics, 33, 101-106.

[70] Hamamatsu Photonics UK Limited, Hertfordshire, UK. Homepage: http://www.hamamatsu.com.

[71] ISBG CO., Ltd. St. Petersburg, Russia. Homepage: http://www.ibsg-st-petersburg.com.

[72] Johnson, S. F. (1992). Gas monitors employing infrared LEDs. *Measurement Science Technology*, 3, 191-195.

[73] William, L.W. (1991). Optical Material for Infrared. In *Infrared Optical Design and Fabrication*, edited by Hartmann, R., Smith, W. J., SPIE Optical Engineering Press, Washington, pp. 58 - 59.

[74] Welford, W. T., Winston, R. (1978). *Optics of nonimaging concentrators – Light and solar energy*. Academic press.

[75] Herzberg, G. (1966). *Molecular Spectra and Molecular Structure*, D. Van Nostrand Company, Inc., Princeton, pp. 306 - 307.

[76] Ouardi, O., Hilico, J. C., et al. (1996). The hot bands of methane between 5 and 10 μm. *Journal of Molecular Spectroscopy*, 180, 311-322, Article No. 0254.

[77] Rothman, L. S., Gamache, R. R., et al. (1983). AFGL atmospheric absorption line parameters compilation. *Applied Optics*, Vol. 22, No.15, 2247 – 2256.

[78] Brown, L. R., Margolis, J. S., et al. (1992). Methane and its isotopes: Current status and prospect for improvement. *Journal Quantum Spectroscopic Radiation Transfer*, Vol. 48 No. 5/6, 617 – 628.

[79] Hilico, J. C., Champion, J. P., et al. (1994). New analysis on the pentad system of methane and prediction of the (pentad-pentad) spectrum. *Journal Molecular Spectroscopy*, 168, 455-476.

[80] Hilico, J. C., Robert, O., et al. (2001). Analysis of the interacting octad system of $^{12}CH_4$. *Journal Molecular Spectroscopy*, 208, 1-13.

[81] Brown, L. R., Benner, D. C., et al. (2003). Methane line parameters in HITRAN. *Journal Quantum Spectroscopic Radiation Transfer*, Vol. 82, 219 – 238.

[82] Nielsen, A. H., Nielsen, H. H. (1935). The infrared absorption bands of methane. *Physical Review*, Vol.48, 864 – 867.

[83] Mihalcea, R. M., Baer, D. S., et al. (1998). Diode-laser absorption measurement of CO_2 near 2.0 μm at elevated temperatures. *Applied Optics*, Vol. 37, No. 36.

[84] Malathy, V., Benner, D. C. et al. (1993). Measurements of air-broadening and pressure- shifting of methane lines in the 2.3 μm region. *Journal of Molecular Spectroscopy*, 157, 95 – 111.

[85] Brown, L. R. (1988). Methane line parameters from 3700 to 4136 cm^{-1}. *Applied Optics*, Vol. 27, No. 36, 3275.

[86] Material properties. Retrieved from the World Wide Web: http://www.mellesgriot.com/products/optics/toc.htm.

[87] Optical components. Retrieved from the World Wide Web: http://www.optosigma.com/miva/merchant.mv?Screen=CTGY&store_Code=OS&Category_Code=Optical+Components.

[88] Material datasheet. Retrieved from the World Wide Web: http://www.escoproducts.com/3matstech.html.

[89] Infrared material datasheet. Retrieved from the World Wide Web: http://www.crystran.co.uk/.

[90] Hackforth, H. L. (1960). *Infrared radiation.* McGraw-Hill.

[91] Dereniak, E. L., Boreman, G. D. (1996). *Infrared Detectors and System.* John Wiley & Sons, Inc.

[92] Hecht, E. (1987). *Optics (Second Edition),* Addison-Wesley Publishing Company, Inc., chap. 8.

[93] Crowder, J. G., Hardway, H. R., et al. (2002). Mid-infrared gas detection using optically immersed, room-temperature, semiconductor devices. *Measurement Science Technology,* 13, 882 - 884.

[94] Dillig, B., Drager Review. Retrieved from the World Wide Web: http://www.draegerriview.com.

[95] Herzberg, G. (1966). *Molecular Spectra and Molecular Structure,* D. Van Nostrand Company, Inc., Princeton, pp. 196.

[96] Herzberg, G. (1966). *Molecular Spectra and Molecular Structure,* D. Van Nostrand Company, Inc., Princeton, pp. 361.

[97] Narendran, N., Maliyagoda, N., et al. (January 2000). Characterizing white LEDs for general illumination applications. *Proceedings, SPIE's photonics west conference,* 3938 – 39, San Jose, SPIE.

APPENDIX A: REFRACTIVE INDEX OF COMMON INFRARED MATERIALS

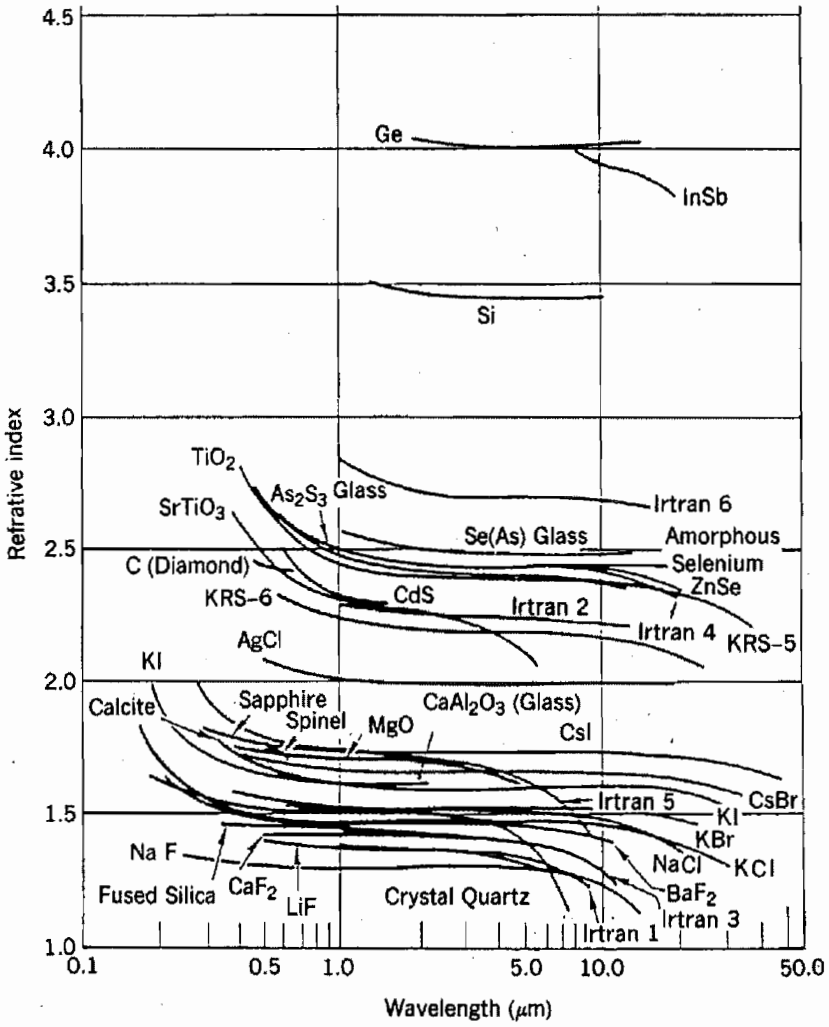

SOURCE: Dereniak, E. L., Boreman, G. D. (1996). Infrared Detectors and System. John Wiley & Sons, Inc., pp. 30.

APPENDIX B: GAS CELL DESIGN

B (a) Gas chamber

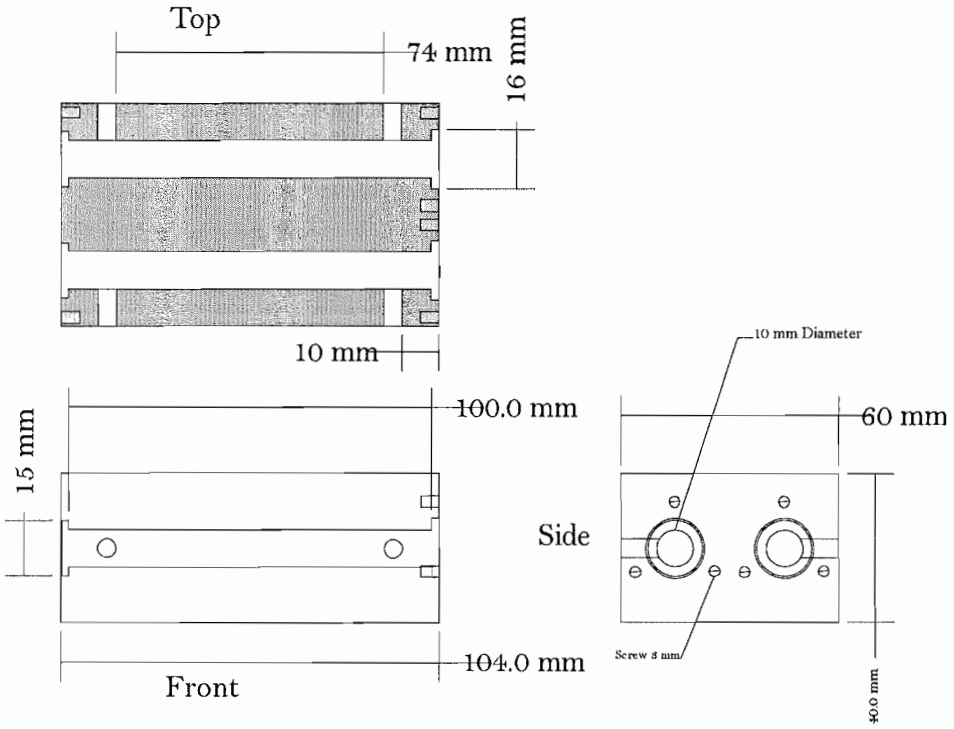

B (b) Beam splitter / combiner

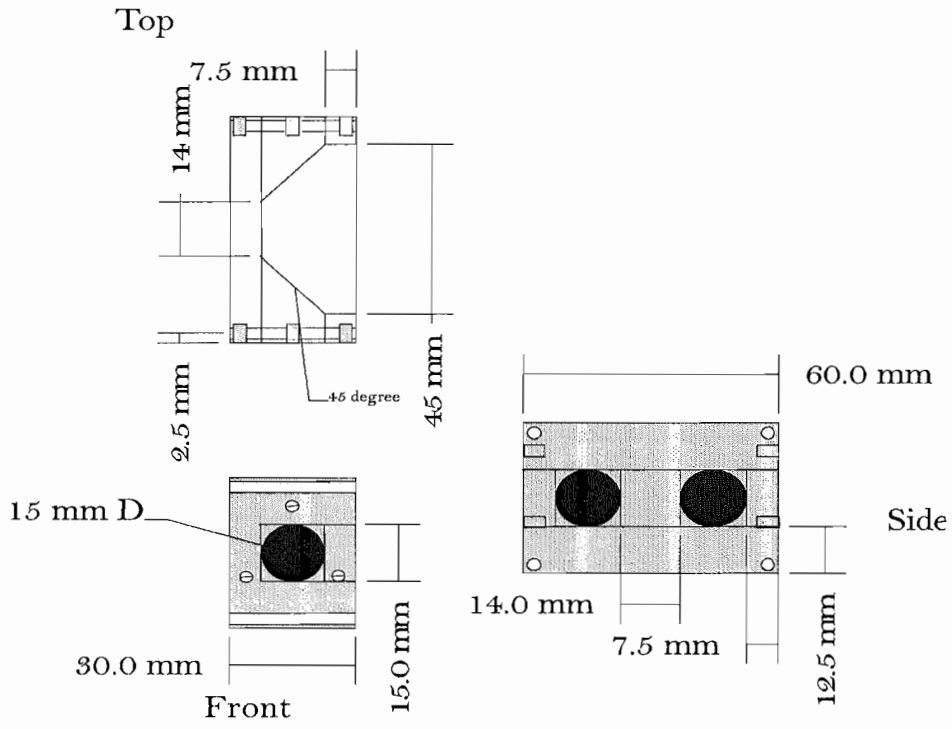

B (c) Beam splitter / combiner

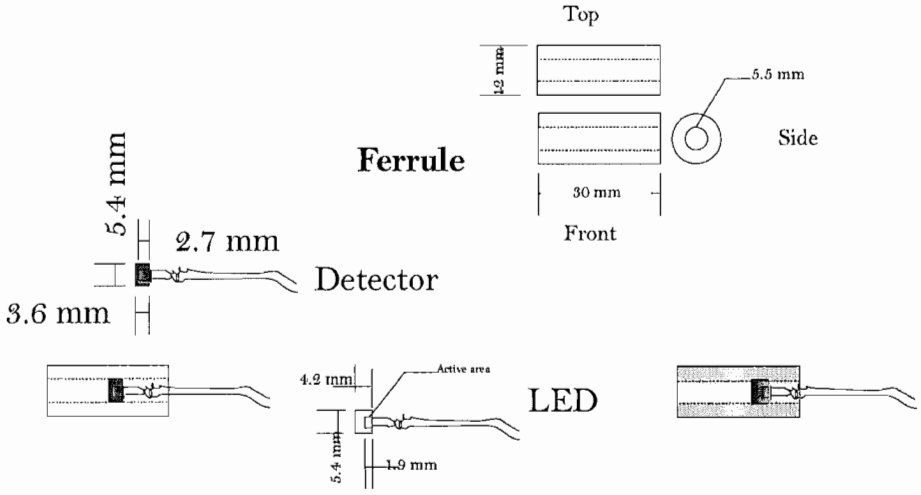

B (d) Beam splitter / combiner